

**PSYCHOPHYSICAL EVALUATION OF A SENSORY
FEEDBACK SYSTEM FOR PROSTHETIC HANDS**

by

İpek Karakuş

B.S., in Electrical and Electronics Engineering, Erciyes University, 2010

M.S., in Biomedical Engineering, Istanbul Technical University, 2013

Submitted to the Institute of Biomedical Engineering

in partial fulfillment of the requirements

for the degree of

Doctor

of

Philosophy

Boğaziçi University

2020

To Yavuzer...

ACKNOWLEDGMENTS

It has been a long journey for me through which I learned lots of things, gained invaluable experience and got support from a lot of nice people. First of all, I would like to thank to my advisor, Prof. Burak Güçlü, for his guidance and support throughout this PhD work. I also thank to Prof. Çağatay Başdoğan, Assoc. Prof. Esin Öztürk Işık, Prof. Ahmet Ademoğlu, Assoc. Prof. Erkan Kaplanoğlu for their valuable comments during my progress and being members of my thesis committee.

I am thankful to all former and current members of Tactile Research Laboratory for their support in seven years. Special thanks goes to Deniz Kılınç Bülbül, Sedef Yusufogulları and Begüm Devlet Kılıçkap for their friendship, kindness and encouragement. I also express my gratitude to all participants for their patience during experiments. I thank to Ahmet Atasoy and Hasan Şahin for their help with the design and modification of the robotic hand; Erhan Uyanık and Ahmet Turan Talaş for manufacturing the required equipments.

I would like to express my deepest gratitude to my husband, Yavuzer Karakuş, for his endless love, support and patience during this period of our life. Without him, I would never find the power and motivation to complete this study.

I thank to my mother, father, sister and brother for their support during all my life. I also thank to my parents-in-law and brother-in-law for being kind and supportive. I would also like to express my gratitude to my "sister", Ebru Konuksever Polat, for her great support and friendship as in all cases. I also thank to all my friends for enjoying life together during this stressful period.

The Scientific and Technological Research Council of Turkey (TUBITAK) supported this work under Student Fellowship Program BİDEB-2211. Council of Higher Education supported this work under OYP programme. This work was also supported

by TUBITAK Grant 117F481 within European Union's FLAG-ERA JTC 2017 project GRAFIN.

ACADEMIC ETHICS AND INTEGRITY STATEMENT

I, İpek Karakuş, hereby certify that I am aware of the Academic Ethics and Integrity Policy issued by the Council of Higher Education (YÖK) and I fully acknowledge all the consequences due to its violation by plagiarism or any other way.

Name :

Signature:

Date:

ABSTRACT

PSYCHOPHYSICAL EVALUATION OF A SENSORY FEEDBACK SYSTEM FOR PROSTHETIC HANDS

In this study, a vibrotactile sensory feedback system was designed and tested in accordance with the discrete event-driven sensory feedback control paradigm. Novel approaches were applied in terms of data processing and psychophysical characterization. As the first part, the sensing and signal processing system was designed. Therefore, a robotic hand was equipped with force and bend sensors by mimicking receptors in human hand. The sensor data was recorded during a cylindrical grasping task, and classified for object type and movement phase. Among three machine learning algorithms (k-Nearest Neighbour, Multinomial Logistic Regression and Support Vector Machines), highest classification accuracy was obtained with k-nearest neighbor classifier and the results were promising for the subsequent work. In the second part, the sensory feedback system was designed using two vibrotactile actuators and a user-specific calibration method was presented. The actuators were placed on the upper arms of 10 able-bodied participants. A psychophysical characterization procedure was applied to determine the stimulation amplitudes for each participant specifically. Then, same-different discrimination and pattern recognition experiments were conducted to evaluate the discrimination and closed-set identification of stimuli with varying parameters. Finally, discrete-event driven feedback experiments were run by mapping the parameters of the stimuli to the discrete events related to class labels representing object/movement type. According to the results, the psychophysical characterization procedure was reliable. On the other hand, the performance in the complex tasks was not affected by the psychophysical variations across participants. Experimental results showed that the system can be used to provide object-type and movement-type related information in daily use of prosthetic devices.

Keywords: Somatosensory, feedback, neuroprosthesis, discrete events, machine learning, vibrotactile, psychophysics.

ÖZET

EL PROTEZLERİNDE KULLANILABİLECEK BİR DUYUSAL GERİ BESLEME SİSTEMİNİN PSİKOFİZİKSEL AÇIDAN İNCELENMESİ

Bu çalışmada, ayırık olaya dayalı duyuşal geribesleme kontrol yaklaşımına uygun şekilde bir titreşim uyaranlı duyuşal geri besleme sistemi tasarlandı ve test edildi. Veri işleme ve psikofiziksel karakterizasyon konusunda özgün yaklaşımlar uygulandı. İlk kısımda, algılama ve işaret işleme sistemi tasarlandı. Bu sebeple, bir robotik el insan elindeki reseptörleri taklit ederek kuvvet ve bükülme sensörleri ile donatıldı. Silindirik kavrama hareketi sırasında sensör verisi kaydedildi ve nesne tipi ile hareket tipi için sınıflandırıldı. Üç makine öğrenmesi algoritması arasından (k-En Yakın Komşu, Çok-sınıflı Lojistik Regresyon, Destek Vektör Makineleri), en yüksek doğruluk k-en yakın komşu sınıflayıcısı ile elde edildi ve sonuçlar sonraki çalışma için umut vericiydi. İkinci kısımda, iki titreşim uyaranlı eyleyici kullanılarak duyuşal geri besleme sistemi tasarlandı ve kullanıcıya özel bir kalibrasyon yöntemi sunuldu. Eyleyiciler 10 sağlıklı katılımcının üst kollarına yerleştirildi. Her katılımcı için uyarın genliklerini özel olarak belirlemek için bir psikofiziksel karakterizasyon protokolü uygulandı. Daha sonra, değişen parametrelere sahip uyarının ayırt edilmesi ve kapalı-set içerisinden tanınması için aynı-farklı ayırt etme ve örüntü tanıma deneyleri gerçekleştirildi. Son olarak, uyarınların parametreleri nesne/hareket tipini temsil eden sınıf etiketleriyle ilişkili olaylarla eşleştirilerek ayırık olaya dayalı geri besleme deneyleri gerçekleştirildi. Sonuçlara göre, uygulanan psikofiziksel karakterizasyon prosedürü güvenilirli. Diğer bir yandan, karmaşık görevlerdeki performans katılımcılar arasındaki psikofiziksel farklılıklardan etkilenmedi. Deneysel sonuçlar gösterdi ki bu sistem protezlerin günlük kullanımında obje tipi ve hareket tipine ilişkin bilgi sağlamak için kullanılabilir.

Anahtar Sözcükler: Beden duyusu, geri besleme, nöroprotez, ayırık olaylar, makine öğrenmesi, titreşim uyaranlı, psikofizik.

TABLE OF CONTENTS

ACKNOWLEDGMENTS	iv
ACADEMIC ETHICS AND INTEGRITY STATEMENT	vi
ABSTRACT	vii
ÖZET	viii
LIST OF FIGURES	xii
LIST OF TABLES	xv
LIST OF SYMBOLS	xvi
LIST OF ABBREVIATIONS	xvii
1. INTRODUCTION	1
1.1 Motivation and aim	1
1.2 Literature	2
1.2.1 Sensory feedback in prosthetics	2
1.2.2 Object recognition & machine learning in prosthetics	7
1.2.3 Psychophysics in prosthetics literature	8
1.3 Novelty and Contribution	9
1.4 Outline	10
2. SENSORS AND SIGNAL PROCESSING	12
2.1 Background	12
2.1.1 Hand anatomy & mechanoreceptors	12
2.1.2 Machine learning methods	13
2.1.2.1 k-nearest neighbour	14
2.1.2.2 Multinomial logistic regression	15
2.1.2.3 Support vector machines	16
2.2 Material and Methods	16
2.2.1 Robotic hand	17
2.2.2 Sensor characterization and signal conditioning	18
2.2.3 Grasping experiment and data acquisition	22
2.2.4 Data processing and classification	25
2.3 Results	28

2.3.1	Sensor characterization	28
2.3.2	Cylindrical grasping data	32
2.3.3	Classification results	34
2.4	Discussion	39
2.4.1	General conclusions	39
2.4.2	Limitations	41
2.4.3	Future improvements	42
3.	PSYCHOPHYSICAL CHARACTERIZATION AND VIBROTACTILE FEED- BACK	43
3.1	Background	43
3.1.1	Human somatosensory system	43
3.1.2	Psychophysics & tactile perception	46
3.2	Material and Methods	51
3.2.1	Participants	51
3.2.2	Vibrotactile actuators and instrumentation	52
3.2.3	Vibrotactile stimuli and the representation of discrete events . .	54
3.2.4	Psychophysical characterization of participants	56
3.2.4.1	Absolute detection thresholds	57
3.2.4.2	Psychometric functions	58
3.2.4.3	Subjective magnitude estimates	59
3.2.4.4	Equal magnitude levels	60
3.2.4.5	Re-calibration of the psychophysical model:	60
3.2.5	Same-different discrimination experiments	61
3.2.6	Vibrotactile pattern recognition experiments	62
3.2.7	Discrete event-driven feedback experiments	64
3.2.8	Statistical analyses	66
3.3	Results	67
3.3.1	Psychophysical characterization	67
3.3.2	Magnitude and frequency discrimination	75
3.3.3	Vibrotactile pattern recognition	77
3.3.4	Discrete event-driven feedback	80
3.4	Discussion	82

3.4.1	General conclusions	82
3.4.2	Previous studies with DESC policy	83
3.4.3	Technical limitations	84
3.4.4	Psychophysical issues	85
3.4.5	Future directions and practical use	86
4.	CONCLUSION	88
4.1	Overall summary	88
4.2	Limitations	89
4.3	Future work	89
	APPENDIX A. CLASSIFICATION RESULTS	90
	APPENDIX B. PSYCHOPHYSICAL CHARACTERIZATION OF PARTICIPANTS	
	100	
	APPENDIX C. INDIVIDUAL SUBJECT PERFORMANCE IN DISCRETE EVENT-	
	DRIVEN FEEDBACK EXPERIMENTS	111
	APPENDIX D. LIST OF PUBLICATIONS	119
	REFERENCES	120

LIST OF FIGURES

Figure 2.1	Hand anatomy and mechanoreceptors	13
Figure 2.2	k-nearest neighbour algorithm	15
Figure 2.3	Logistic functions	15
Figure 2.4	Support vector machines	16
Figure 2.5	3D graphical view of the "Boğaziçi Hand"	17
Figure 2.6	Sensors and sensor modifications	19
Figure 2.7	Sensor interface circuits	20
Figure 2.8	Force sensor calibration setup	21
Figure 2.9	Sensor names and locations	23
Figure 2.10	Robotic hand with force and bend sensors	23
Figure 2.11	Objects and cylindrical grasping	24
Figure 2.12	Data processing procedure blocks	25
Figure 2.13	Class labeling procedure	26
Figure 2.14	Bend sensor calibration curves	30
Figure 2.15	Force sensor calibration curves	31
Figure 2.16	Cylindrical grasping data	33
Figure 2.17	Labeled data from example bend and force sensors	34
Figure 2.18	Confusion matrices of kNN classifier for ring finger	38
Figure 3.1	Skin anatomy and mechanoreceptors	44
Figure 3.2	Physiological properties of mechanoreceptors	45
Figure 3.3	Somatosensory pathway	46
Figure 3.4	Psychometric function	47
Figure 3.5	Effect of frequency on vibrotactile thresholds	49
Figure 3.6	Effects of contactor size, stimulus duration and static indentation depth on tactile thresholds	50
Figure 3.7	Actuator characteristics	52
Figure 3.8	Actuators	53
Figure 3.9	Actuator calibration curves	54
Figure 3.10	Psychophysical characterization and experimental procedures	57

Figure 3.11	Stimulus timing diagram of two-interval forced-choice task	58
Figure 3.12	Stimulus timing diagram of magnitude estimation task	59
Figure 3.13	Stimulus timing diagram of the same-different discrimination task	61
Figure 3.14	Stimulus timing diagram of vibrotactile pattern recognition task	63
Figure 3.15	Images representing vibrotactile patterns	63
Figure 3.16	Full movement cycle of the robotic hand	64
Figure 3.17	Pictures representing discrete events	65
Figure 3.18	Stimulus timing diagram of discrete event-driven feedback experiments	65
Figure 3.19	Measurements of psychophysical characterization	68
Figure 3.20	Psychometric functions for S1	71
Figure 3.21	Magnitude estimation fits for S1	72
Figure 3.22	Results of same-different discrimination experiments	76
Figure 3.23	Confusion matrices for vibrotactile pattern recognition experiments	78
Figure 3.24	Results of vibrotactile pattern recognition experiments	79
Figure 3.25	Confusion matrix for discrete event-driven feedback experiments	80
Figure 3.26	Performance scores of discrete event-driven feedback experiments	81
Figure 3.27	Averaged performance scores for vibrotactile pattern recognition and discrete event-driven feedback experiments	82
Figure A.1	Confusion matrices - kNN classifier / Thumb	90
Figure A.2	Confusion matrices - kNN classifier / Index finger	92
Figure A.3	Confusion matrices - kNN classifier / Middle finger	94
Figure A.4	Confusion matrices - kNN classifier / Ring finger	96
Figure A.5	Confusion matrices - kNN classifier / Little finger	98
Figure B.1	S1 / Psychometric curves	100
Figure B.2	S1 / Magnitude estimation fits	101
Figure B.3	S2 / Psychometric curves	101
Figure B.4	S2 / Magnitude estimation fits	102
Figure B.5	S3 / Psychometric curves	102
Figure B.6	S3 / Magnitude estimation fits	103
Figure B.7	S4 / Psychometric curves	103
Figure B.8	S4 / Magnitude estimation fits	104

Figure B.9	S5 / Psychometric curves	104
Figure B.10	S5 / Magnitude estimation fits	105
Figure B.11	S6 / Psychometric curves	105
Figure B.12	S6 / Magnitude estimation fits	106
Figure B.13	S7 / Psychometric curves	106
Figure B.14	S7 / Magnitude estimation fits	107
Figure B.15	S8 / Psychometric curves	107
Figure B.16	S8 / Magnitude estimation fits	108
Figure B.17	S9 / Psychometric curves	108
Figure B.18	S9 / Magnitude estimation fits	109
Figure B.19	S10 / Psychometric curves	109
Figure B.20	S10 / Magnitude estimation fits	110
Figure C.1	S2 / Discrete event-driven feedback experiment	112
Figure C.2	S3 / Discrete event-driven feedback experiment	113
Figure C.3	S6 / Discrete event-driven feedback experiment	114
Figure C.4	S7 / Discrete event-driven feedback experiment	115
Figure C.5	S8 / Discrete event-driven feedback experiment	116
Figure C.6	S9 / Discrete event-driven feedback experiment	117
Figure C.7	S10 / Discrete event-driven feedback experiment	118

LIST OF TABLES

Table 1.1	Vibrotactile sensory feedback literature	4
Table 2.1	Dimensions of classification data	28
Table 2.2	Parameters of calibration equations	29
Table 2.3	Classification results-1	35
Table 2.4	Classification results-2	36
Table 2.5	Finger average of classification accuracy	37
Table 2.6	Classification results - kNN Classifier, Ring Finger	39
Table 3.1	Somatosensory receptors	43
Table 3.2	Representation of discrete events	55
Table 3.3	Average absolute detection thresholds	69
Table 3.4	Parameters of psychometric functions	70
Table 3.5	Parameters of magnitude estimation fits	73
Table 3.6	Psychophysical models	74
Table 3.7	Average accuracies for same-different discrimination experiment	75
Table 3.8	Average results of vibrotactile pattern recognition experiments	79
Table A.1	Classification results - kNN Classifier / Thumb	91
Table A.2	Classification results - kNN Classifier / Index finger	93
Table A.3	Classification results - kNN Classifier / Middle finger	95
Table A.4	Classification results - kNN Classifier / Ring finger	97
Table A.5	Classification results - kNN Classifier / Little finger	99
Table C.1	Sequence list	111
Table C.2	S2 / Discrete event-driven feedback experiment	112
Table C.3	S3 / Discrete event-driven feedback experiment	113
Table C.4	S6 / Discrete event-driven feedback experiment	114
Table C.5	S7 / Discrete event-driven feedback experiment	115
Table C.6	S8 / Discrete event-driven feedback experiment	116
Table C.7	S9 / Discrete event-driven feedback experiment	117
Table C.8	S10 / Discrete event-driven feedback experiment	118

LIST OF SYMBOLS

t	Time
f	Frequency
Hz	Hertz, unit of frequency
R^2	Coefficient of determination
$p(c)$	Probability of correct detection
a	Magnitude
A	Stimulus amplitude
dB	Decibel
k	Number of neighbors in kNN algorithm
C	Regularization parameter in SVM algorithm
Ω	Ohm, unit of resistance
α	Midpoint of the psychometric curve
β	The parameter representing the slope of the psychometric curve
γ	Exponent of power function

LIST OF ABBREVIATIONS

SF	Sensory Feedback
DOF	Degree of Freedom
DOM	Degree of Mobility
SMA	Shape-Memory Alloy
ADL	Activities of Daily Living
DESC	Discrete Event Driven Sensory Feedback Control
EMG	Electromyography
PNS	Peripheral Nervous System
CNS	Central Nervous System
MCP	Metacarpophalangeal
PIP	Proximal Interphalangeal
DIP	Distal Interphalangeal
IP	Interphalangeal
MLR	Multinomial Logistic Regression
kNN	k Nearest Neighbor
SVM	Support Vector Machines
DL	Difference Limen
JND	Just-Noticeable Difference
SL	Sensation Level
ME	Magnitude estimate
LME	Logarithm of magnitude estimate
RA	Rapidly adapting
SA	Slowly adapting

1. INTRODUCTION

1.1 Motivation and aim

Upper limb amputation causes significant impairment in sensory and motor functions which may be partially retrieved by using a prosthetic device. The traditional prosthetic designs (body-powered or myoelectric) focused on providing motor functions, however lack of somatosensory feedback causes difficulties in the control of the device because the user rely on mostly visual cues [1]. This increases cognitive load and may result in rejection of the prosthesis at one point [2]. As a matter of fact, despite the improved capabilities of myoelectric prostheses (multiple degrees of freedom), body-powered prostheses (one degree of freedom) are still preferred by amputees due to some natural feedback that is provided by transmitted reaction forces during movement [3]. Sensory feedback is also known to reduce the phantom limb pain causing discomfort for the amputees [4]. The lost sensory function of the hand may be partially compensated by a sensory feedback system integrated to the prosthetic device. By this way, in addition to the better control of the device, it can be felt as a part of body [5–10].

Despite the accepted importance and necessity, there is not a commercially available prosthetic hand with an improved sensory feedback system. To my knowledge, "Vincent Evolution 2 Hand" (Vincent Systems, Germany) is the only commercially available prosthetic hand with sensory feedback [11]. However, the detailed specifications on the feedback mechanism of that prosthesis is not reported in detail. On the other hand, numerous prosthetic hands with improved mechanical properties and embedded sensors were developed in laboratory [12–16] and there is an ongoing research in this area.

Our motivation for this PhD work is to design a sensory feedback system by adopting a biologically inspired approach in terms of sensing and signal processing mechanisms. To that end, we first placed force and bend sensors on a robotic hand

to mimic the behavior of receptors in human hand. We recorded sensor data during periodical flexion and extension movements in the form of cylindrical grasping of two objects with varying stiffness. We classified the sensor data using machine learning algorithms to extract the required information on object and movement type just as the brain does. Next, we designed the stimulation system by getting inspired from the discrete event-driven sensory feedback control (DESC) policy. Therefore, we applied the object type and movement phase related feedback as time-discrete vibrotactile stimuli mapped to the critical hypothetical transition events of the robotic hand. Considering the change in human psychophysical measures such as detection and discrimination thresholds, we performed a user-specific psychophysical characterization procedure to find the vibration amplitudes. Finally, we tested the system through a set of discrimination and closed-set identification experiments.

1.2 Literature

1.2.1 Sensory feedback in prosthetics

Sensory substitution is a technique using which a lost sensory information is regained through a different sensory channel or different modality [17]. In case of hand amputation, tactile and proprioceptive information can be substituted through auditory [18] or somatosensory [19] system. The regained sensation may be sensed as more natural if it is somatotopically- or modality-matched to lost sensory information. In somatotopical matching, the substitution signal is perceived to be applied on the same location as in the natural interaction with the environment. In modality-matched stimulation, the neural pathway of the lost sensation is stimulated [1].

The sensory feedback studies can be grouped depending on the stimulation method (i.e. invasive and non-invasive stimulation) and the conveyed information. Invasive stimulation is done by stimulating the neural tissue directly in peripheral or central nervous system [9, 20–26], requiring surgery to place the electrodes. On the other hand in non-invasive stimulation, a skin surface is stimulated by electrotactile,

vibrotactile or mechanotactile (slow or static indentation) stimulation [27–37]. Non-invasive methods have the advantage of not requiring surgery, therefore, preferable by the amputees. Detailed information on the invasive and non-invasive sensory feedback methods can be found in [1,38,39].

Electrotactile stimulation directly stimulates the afferent nerve endings in the dermis by current pulses, resulting more natural sensation compared to other methods. Stimulation electrodes are simple, light and has no moving parts. However, it may cause pain if the pain threshold is exceeded. This limits the current range to be used and decreases the sensitivity of the system. Additionally, human tactile perception thresholds vary depending on electrode location and the physical properties of the area below the electrode (such as moisture and impedance). Therefore, the system should be re-calibrated each time the electrodes are placed. Stimulation signal may also interfere with EMG signals used for control of the prosthesis. There are studies offering solution for interference but it requires extra signal processing effort [40]. ‘Mechanotactile’ stimulation refers to converting the sensory feedback signals to static indentations of the skin instead of higher-frequency mechanical vibrations, and typically it gives the best non-invasive performance since it is modality matched [32]. However, that approach requires bulky indenters or motors, and therefore, usually not preferred over small vibrotactile actuators which are easily implemented and which consume less power [39]. Additionally, there is only one parameter that can be modulated to transmit information.

Vibrotactile stimulation is applied as mechanical vibrations on the skin. Vibration frequency is generally around 250 Hz in order to activate Pacinian channel which is known to be more sensitive to high-frequency vibration. Vibrotactile stimulation is painless and the stimulation signal does not result interference with EMG signals. There are numerous vibrotactile feedback studies in the literature, varying in the type of stimulation, conveyed information and used apparatus. Since it is also the feedback method used in this study, a brief summary of the previous studies on vibrotactile sensory substitution/feedback in neuroprostheses is given in Table 1.1.

Table 1.1

A list of vibrotactile sensory feedback studies in the literature.

Authors/Year	Input	Feedback type	Equipment
Patterson and Katz/1992 [41]	Grasp force	Vibrotactile and mechanotactile	Myoelectric hand
Poveda/2002 [42]	Grasp force	Vibrotactile	Myoelectric hand
Pylatiuk et al./2006 [43]	Grasp force	Vibrotactile	Myoelectric hand
Chattarjee et al./2008 [44]	Grasp force	Vibrotactile	Myoelectric hand
Cipriani et al./2008 [45]	Grasp force	Vibrotactile	Myoelectric hand
Witteveen et al./2012 [46]	Hand opening	Vibrotactile and electrotactile	Virtual hand
Antfolk et al./2013 [32]	Finger force (passive)	Vibration and pressure	Myoelectric hand
Rombokas et al./2013 [47]	Contact force	Vibrotactile	Virtual environment
Cipriani et al./2014 [48]	Discrete events	Vibrotactile	Robotic hand
Witteveen et al./2014 [34]	Hand opening and grasping force	Vibrotactile	Virtual hand
Clemente et al./2016 [35]	Discrete events	Vibrotactile	Prosthetic hand
Markovic et al./2018 [49]	Contact, force level and prosthesis state	Vibrotactile	Myoelectric hand
Abozeria et al./2018 [37]	Grip force (cont.) and slip (discrete)	Vibrotactile	Robotic hand
Pena et al. /2019 [50]	Grasp force and hand aperture	Vibrotactile	Myoelectric hand
Engels et al. /2019 [51]	Discrete events	Vibrotactile	Prosthetic hand

Vibrotactile feedback was also used with some state-of-the-art myoelectric prostheses and its efficiency was investigated. In Markovic et al. (2018), a novel vibrotactile stimulation system was presented [49]. The system transmits multiple variables (contact, prosthesis state and level of grasping force), creating different tactile patterns by intensity and spatial modulation. They placed eight C3 tactors on the forearm. The information from sensors of Michelangelo hand was processed in real time and the corresponding vibrotactile patterns were generated. Number of pulses, the activated

factor and the vibration intensity were the adjusted parameters. They tested the effectiveness of the system on six amputee participants by the box and blocks task, the cups relocation task, the block turn task, and the clothespin relocation task. The task completion time and number of retries were used as performance metrics. They concluded that improvement due to feedback was task-dependent. The participants benefited from feedback during complex tasks (block turn, clothespin and cups relocation), and the performance remained almost same during simple tasks (box and blocks). Training had also a task-dependent effect on subject performance. According to subjective questionnaire, the feedback was considered as helpful during daily life activities.

In Pena et al. (2019), two different vibrotactile sensory substitution systems were tested [50]. In the first configuration, the burst width of a single vibrotactile actuator was modulated proportional to the grasp force or hand aperture. In the second configuration, the signal level was transmitted by activating five actuators in a spatial order. The experiments were conducted with able-bodied participants by using a ProHand myoelectric prosthesis with built in force and hand aperture sensors. The experiments were run with and without active myoelectric control of the participant. There was no difference between two stimulation configurations when the myoelectric control was absent. On the other hand, 5-actuator configuration was better than single-actuator configuration when the myoelectric control was included.

In order to provide multi-modality sensory information, some methods were also presented in the literature. Choi et al. (2017) used mixed modality stimulation method, in which the superposition of two stimulation pulse trains with different frequencies were applied [52]. D'Alonzo et al. (2014) presented a hybrid method which uses vibrotactile and electrotactile stimulation to decode two different modalities [53]. In both of studies, it was shown that the system can be used to provide multi-channel sensory information.

In noninvasive stimulation methods, the stimulation signal is often generated and applied continuously by modulating amplitude, frequency or pulse width proportional to change of a sensor output [31,44]. This increases signal processing load of the

system and cognitive load of the user. As an alternative, time-discrete feedback was tested and seemed to be promising in some studies [35,37,48,54]. This idea is based on a neuroscientific theory called Discrete Event-Driven Sensory Feedback Control (DESC) policy [55–57]. DESC policy posits that, object manipulation mostly relies on a series of events corresponding to sub-goals of a task. The brain combines the sensory signals from these events to regulate the motor control. It means that, the sensory feedback systems can be designed to transmit time-discrete signals rather than continuous stimulation, and the same task can be facilitated. Thus, both the signal processing load of the system and the attentional demands from the user may be decreased. It was shown that intermittent stimulation also prevents adaptation to sensory feedback [58].

Cipriani et al. (2014) used the DESC approach for non-invasive sensory feedback for the first time [48]. Critical discrete events (contact, lift off, release etc.) were defined for a grasp and lift task. The user controlled an apparatus to perform the task. Short-lasting mechanical vibrations were applied to user’s fingers at the beginning of the events. It was shown that users could use discrete sensory feedback for control of a prosthetic hand. In a subsequent study, Clemente et al. (2016) designed an apparatus (DESC Glove) with sensorized thimbles [35]. Contact and release events were detected and short-duration mechanical vibrations were applied on the arm. They tested the device in a virtual eggs test with upper limb amputees. According to the experimental results, the sensory feedback improved subject performance. Barone et al. (2017) designed a prosthetic digit with embedded force sensor and vibration motor by using the same approach, and tested with a user with partial hand amputation [54]. It was shown that the device provided easier control of a prosthesis.

In a recent study, Abozeria et al. (2018) compared the effects of discrete slip feedback, continuous force feedback and vision on control of a robotic hand [37]. Both feedback methods had a positive effect on subject performance compared to the vision alone. It was also shown that discrete slip feedback is sufficient to prevent object slippage with no need of learning.

In terms of the information conveyed to the user, grasp force [36], hand aper-

ture/position [34], object slippage [37, 59], EMG signal [60, 61] and acceleration signal [62, 63] feedback were used in the previous studies. Among these, the grasp force and/or hand position are used more frequent since these parameters are of high importance for object manipulation. Without sensory feedback, a user needs to control the robotic hand movements by visual cues during grasping. This results in an increase of cognitive load. Additionally, the motor response may not be fast enough and synchronized to grasp the object securely after observing contact.

1.2.2 Object recognition & machine learning in prosthetics

The object/grasp recognition studies in the literature are mostly related to robotic applications, not focused on prosthetics [64–68]. Additionally, mostly force information was used from robotic grippers with force sensors and sensorized robotic hands [64, 66]. However, combining tactile and proprioceptive information, as in object recognition by humans, is a more convenient approach to determine stiffness. Schmitz et al. (2014) used a robotic hand with embedded tactile and joint angle sensors for recognition of various objects in different orientations [65]. Higher accuracy was obtained when multimodal information was used.

Object recognition in robotic applications has been generally performed following an exploratory procedure [67, 69, 70]. However, real-time contact information is needed for precise object manipulation during usage of a prosthesis. In Chitta et al. (2010), the state of liquid containers could be discriminated (open, closed, filled level) with 94% accuracy before the object was lifted and without exploratory procedures, by using tactile and joint angle information from a mobile manipulator [68]. In Spiers et al. (2016), the same approach was used and promising results were obtained [66].

Edwards et al. (2016) used real-time machine learning for control of a myoelectric prosthesis [71]. They compared the prosthesis control performance during non-adaptive and adaptive control (with real time prediction of joint motion) procedures. They combined sensor data from the hand and the EMG signal from the user

to predict the joint activation order. They tested the system with an able-bodied and an amputee participant in a simple repetitive switching sequence task. They also conducted a more difficult task (box and blocks) with three able bodied participants. Both tasks were implemented with and without adaptive control. The mean completion time and number of switches required to complete the event were used as performance measures. The results showed a decrease in number of switches when adaptive control was implemented. They concluded that real-time prediction learning can improve the control of prosthesis and decrease the cognitive load while using a prosthetic hand.

Parker et al. (2019) presented the first study implementing machine learning to provide feedback to the user [72]. They used a custom-designed robotic arm, controlled by a joystick. The information provided by the servo motors was used as input to the feedback system consisting of four tactors. The tactors were placed on different body locations (shoulder, elbow, wrist and hand). Five subjects participated in the experiments. The robotic arm was moved in one direction (back and forth) and the participant was asked to move it from wall to wall of a box without creating excessive load on servos. The task was repeated for no feedback, reactive feedback (vibration when current load exceeds a threshold) and predictive feedback (electrical load was predicted by the system) conditions. According to the results, average load on the motors decreased with feedback and was lowest in predictive feedback condition. These results proved that machine learning can be used in feedback systems designed for prosthetic devices.

1.2.3 Psychophysics in prosthetics literature

Psychophysical procedures were previously used in the sensory feedback literature to test the system performance after design or compare the effects of various stimulation methods or parameters [63, 73–78]. For example in Geng et al. (2011), effects of different stimulation patterns on perception threshold were compared in an electrotactile stimulation system [74]. In Murray et al. (2003), psychophysical characterization and testbed validation of a vibrotactile glove was performed [73]. The

system contained miniature voice coils in order to transmit continuous force information to the user. Through the psychophysical experiments, effects of frequency and amplitude of the feedback signal and effects of amplitude and frequency modulation on people’s sensitivity were investigated. Similarly in a recent study, psychophysical principles were used to compare the sensitivities of lower and upper arm to mechanotactile sensation [77].

Geng et al. (2018) investigated the feasibility of an electrotactile stimulation system through some psychometric measures [75]. Similarly in Dong et al. (2020), the changes in psychophysical measurements were investigated and compared for subdermal and surface electrotactile stimulation [78]. Aziziaghdam et al. (2017) designed a tactor to provide real-time contact feedback and performed psychophysical evaluation of the apparatus [63]. Using well-known psychophysical procedures (absolute threshold, just-noticeable difference and magnitude estimation measurements), they tested the usability of the system in object hardness recognition. Wilke et al. (2019) compared the efficiencies of visual and auditory feedback from a prosthetic device with vibrotactile feedback through psychometric characterization [76]. To our knowledge, psychophysical procedures were not used previously in order to find user-specific stimulation amplitudes for a sensory feedback system.

1.3 Novelty and Contribution

In this PhD study, we designed a vibrotactile sensory feedback system by applying novel approaches in terms of signal processing and stimulation procedure. First of all, we implemented a biologically inspired sensorization and signal processing method by using high number of sensors and machine learning algorithms. Machine learning methods are mostly used for object recognition in robotic applications in order to improve the object manipulation performance. To my knowledge, machine learning was used in only one study for providing feedback to the user [72]. In that study, the electrical load of a robotic limb was predicted by a learner. The predictions were fed back to the user to give information on the possible interactions of the limb. We, on the

other hand, used machine learning to directly classify sensor data [79] and generate the appropriate feedback signal [80]. From this aspect, our study is the first implementation of machine learning to apply time-discrete feedback signals for easier control of a prosthesis.

In the previous DESC based vibrotactile feedback studies [35, 48, 54], the vibration parameters were adjusted once to a perceivable level and kept constant for different events. However it is known that the psychophysical measures such as detection and discrimination thresholds vary across participants [81–84] and magnitude scaling is subjective [85, 86]. These measures are also highly affected by multiple factors [87–91]. Therefore, using the same stimulation parameters would not provide the best solution, instead, user specific calibration is required. In our study, the stimulus amplitudes were calculated relative to the detection thresholds, as a result of user-specific psychophysical characterization procedure. To our knowledge, such a detailed procedure using well established psychophysical methods was not presented previously in sensory feedback literature. We also increased the amount of information transferred to the user, by changing both frequency and magnitude of the vibration for representation of discrete events. Thus, we could convey object-type and movement-type related signals together. We also tested a new actuator type with good linearity over a wide frequency range. The methods and procedures presented in this thesis may be inspiring for the new somatosensory feedback studies.

1.4 Outline

In this chapter, the motivation and aim to start this study was explained and a summary of the related studies in the literature was given. Then, the novelty and contributions of the study were summarized. In Chapter 2, the methods and results of the first part of this study were explained, including robotic hand and sensor modifications, placement of sensors on the robotic hand, processing of the sensor data and classification of object type and movement type. In Chapter 3, the design of sensory feedback procedure using vibrotactile actuators, psychophysical procedures for select-

ing the participant-specific stimulation parameters and experimental procedures for testing the system were presented. Finally in Chapter 4, a general conclusion was made with the limitations of the study and future directions. Detailed classification results, psychophysical characterization of the participants and individual participant performances in the experiments can be found in the appendices.

2. SENSORS AND SIGNAL PROCESSING

2.1 Background

2.1.1 Hand anatomy & mechanoreceptors

Human hand has a complex structure in accordance with its functions and capabilities. It has 27 bones which are grouped as carpals, metacarpals and phalanges [92,93]. Metacarpals connect the finger bones to the wrist. The bones of the fingers are called as phalanges. Each long finger has three phalanges (distal, middle and proximal) while the thumb has two (distal and proximal). The joints between metacarpals and proximal phalanges are called as metacarpophalangeal joint (MP or MCP). Similarly, the joints between the phalanges are named as distal interphalangeal (DIP, between distal and middle phalanges) and proximal interphalangeal (PIP, between middle and proximal phalanges) joints. The joint connecting phalanges of the thumb is called as interphalangeal joint (IP). Figure 2.1(a) shows the anatomy of the hand with bones and joints. The bones with the connected muscle groups and nerves, provide the motor functions of the hand [94].

The hand also has sensory functions which are mediated by various receptors and afferent nerves. Human somatosensory system consists of three subsystems namely interoception, proprioception, and exteroception [95]. Among these, proprioception and exteroception helps motor control by providing information related to the body and environment. Proprioception refers to the mechanism on posture and body movements, containing specialized structures such as receptors in muscles, joints and skin. Exteroception comprises contact, pressure, vibration, motion, stroking, pain and thermal sensations [95]. Hand is the major tool of exteroceptive and proprioceptive system. Our palms are covered with glabrous skin which has four types of mechanoreceptors namely Pacinian corpuscles, Merkel disc receptors, Meissner corpuscles and Ruffini endings (Figure 2.1(b)). In order to design a prosthetic device to replace the functions

of the lost hand, the anatomy and biomechanics of the human hand should be considered. Additionally, sensory functions of the hand should be mimicked by proper sensor integration, similar to the receptors in the hand. More detailed information on human somatosensory system and physiological properties of mechanoreceptors is given in Section 3.1.

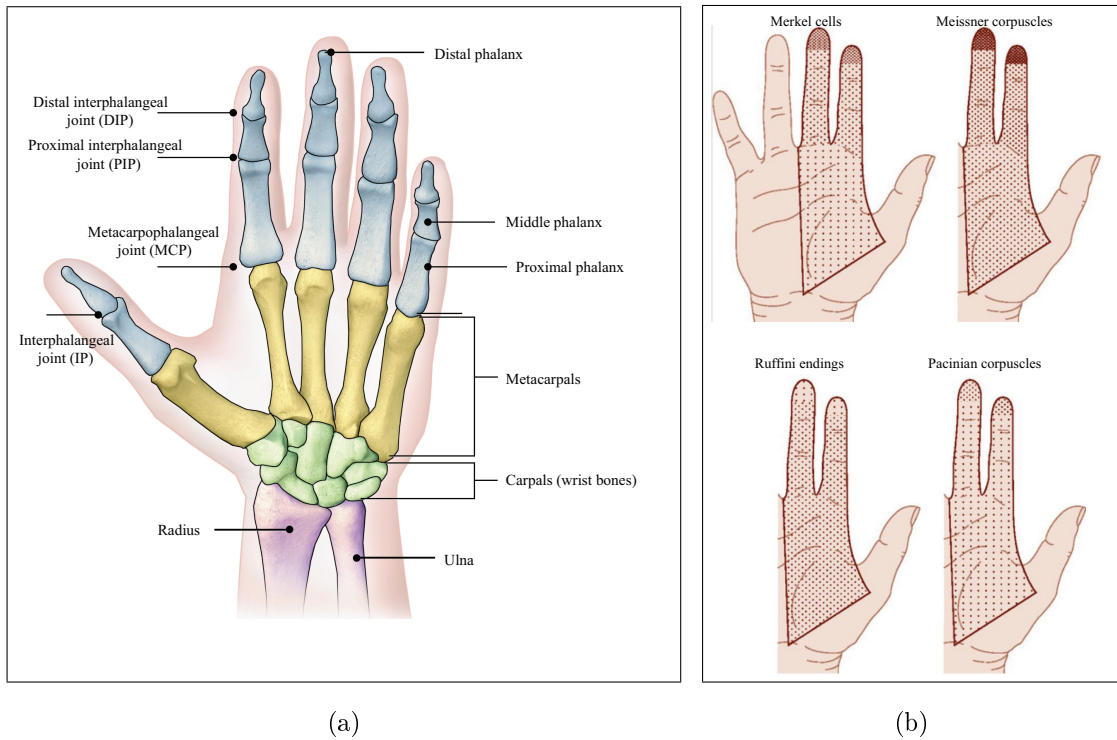


Figure 2.1 Hand anatomy and mechanoreceptors. a) Bones and joints of human hand (Modified from [96]). b) Types and distribution of mechanoreceptors (Modified from [97]).

2.1.2 Machine learning methods

Machine learning is a set of methods to generate models that can make predictions from a given dataset. It is widely used in marketing, robotics, speech recognition and medicine. The machine learning methods can be grouped as regression and classification algorithms. Regression models can be used only for numerical data, and the output is continuous. However in classification algorithms the data can be either numerical or categorical and the output is discrete [98–100].

Classification algorithms are mainly divided into three subgroups namely supervised learning methods, unsupervised learning methods and reinforcement learning methods. Supervised methods can be used if the training dataset is labeled (real classes are known). A model is generated based on the features of the training data, which has differences across different classes. In unsupervised learning the data is not labeled and those methods are based on clustering the dataset into groups according to the similarities of features. Reinforcement learning is in between supervised and unsupervised learning. The class labels are not included directly in model generation however the model is reinforced by reward and punishment based on the correct class labels. Classification algorithms can also be categorized as parametric/non-parametric methods. Parametric methods are based on the assumption that the data follows a distribution which can be summarized by a fixed number of parameters. However in non-parametric methods, no assumption is made for the distribution of the data [100].

The commonly used classification algorithms include decision trees, support vector machines, naive bayes, k-nearest neighbour, linear regression, logistic regression. I will explain the methods used in this study briefly in the following subsections. Since the theory and mathematics behind these methods are out of the scope of this study, such details are not given here.

2.1.2.1 k-nearest neighbour. k nearest neighbour (kNN) is a non-parametric, supervised classification method based on similarities between samples in a dataset. The training data (labeled data) is stored as a look-up table. In order to classify a new sample, the distance between the sample and all data points in training dataset are calculated and k nearest neighbours are selected. The class which is the most frequent in these k neighbours is assigned as the class of the new sample (Figure 2.2). Euclidian, Minkowski, Mahalanobis and Hamming distances are mostly used as distance metric. The distance metric with the parameter 'k' are effective on the classification performance [98–100].

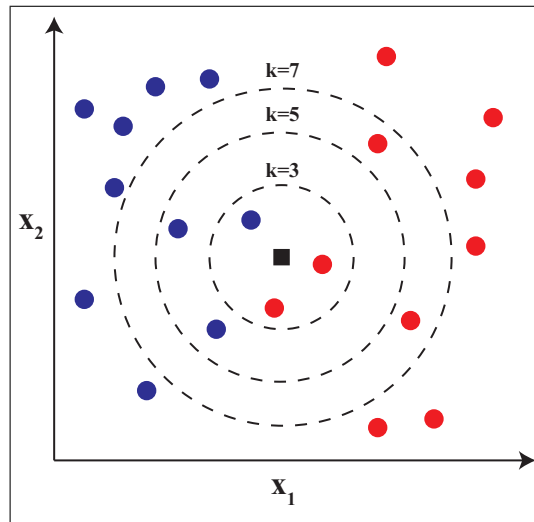


Figure 2.2 Representation of k-nearest neighbour algorithm. Blue and red circles represent two different classes, black square represents new sample. For $k=3$, $k=5$ and $k=7$ nearest neighbours (samples in dashed circles) the new sample is assigned to red, blue and red classes respectively.

2.1.2.2 Multinomial logistic regression. Despite its name, logistic regression is a regression based parametric classification algorithm. In this method, the probability of belonging to a class is defined as a logistic (sigmoid) function (Figure 2.3). By calculating the probabilities of belonging different classes and selecting the maximum probability, a decision boundary is generated. The term 'multinomial' is added for the special case of logistic regression (MLR) which is used for multiclass (more than two outcomes) problems [98–100].

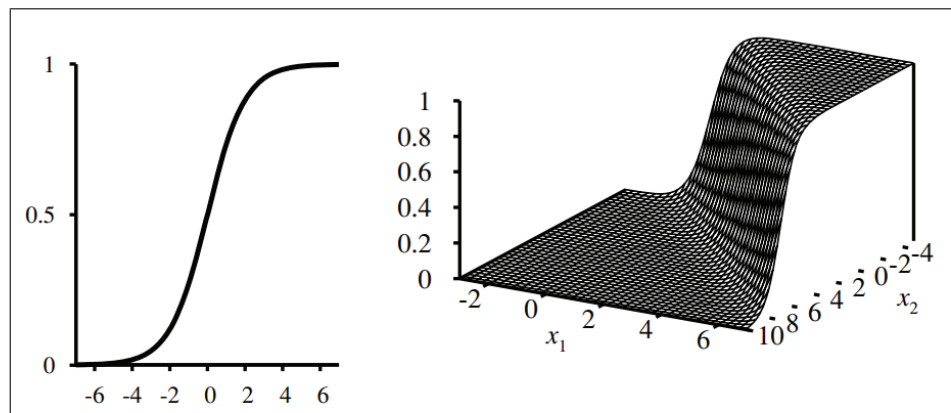


Figure 2.3 Logistics function for one-dimensional (left) and two-dimensional(right) feature spaces. y-axis shows the probability of belonging to a class [100].

2.1.2.3 Support vector machines. Support vector machines (SVM) is a non-parametric supervised learning algorithm widely used in machine learning applications. This method is based on defining a separating boundary in the data space such that the distances of closest data points (support vectors) from all classes to that boundary are maximized (Figure 2.4). For higher dimensional data, kernel functions can be used to find linear separators between different classes. The classification performance depend on the kernel function, its parameters and the regularization parameter (C) [98–100].

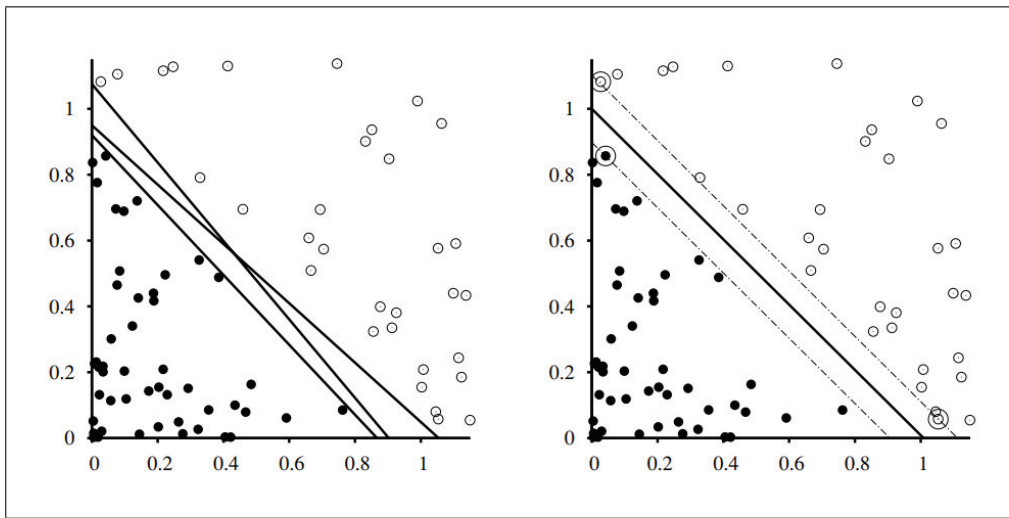


Figure 2.4 Representation of support vector machines classification. Filled and empty circles represent two different classes. On the left, various separating lines are shown. On the right, the separating boundary calculated by SVM algorithm is drawn. The samples closest to the boundary (surrounded with circles) are called as support vectors [100].

2.2 Material and Methods

The work presented here is in review as: İ. Karakuş, A. Atasoy, E. Kaplanoğlu, M. Özkan, B. Güçlü "Classification of somatosensory information from a robotic hand", *Frontiers in Neuroscience*.

Some figures were also published in: İ. Karakuş, H. Şahin, A. Atasoy, E. Kaplanoğlu, M. Özkan, B. Güçlü (2018) "Evaluation of sensory feedback from a robotic hand: A preliminary study", *EuroHaptics 2018*, in *Haptics: Science, Technology and Applications*, pp. 452-463, Springer, Pisa / Italy, June 2018.

2.2.1 Robotic hand

The underactuated robotic hand ("Boğaziçi Hand") used in this study (3D graphical view: Figure 2.5(a)) was designed and produced at Robotic Laboratory, Institute of Biomedical Engineering, Boğaziçi University. It is dimensionally similar to a human hand (with condyloid joint structures unlike most commercial products) [101]. Long fingers are formed by three phalanges; each finger has three degrees of freedom (DOF) and one degree of mobility (DOM) which is flexion/extension. The thumb has two phalanges, two DOFs and two DOMs (including abduction/adduction).

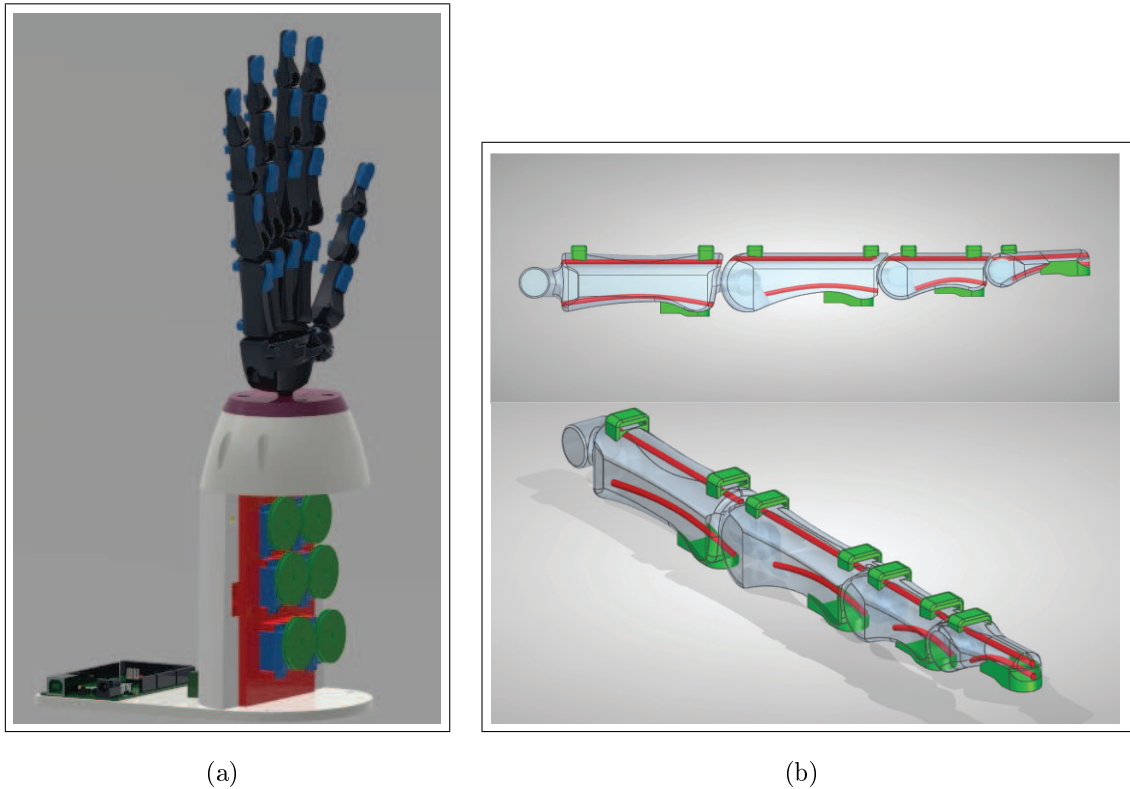


Figure 2.5 3D graphical view of the a) "Boğaziçi Hand" [79] b) index finger.

For this study, we modified the hand without changing its mechanical properties. The original hand was controlled by DC motors and shape-memory-alloy (SMA) actuators. DC motors were replaced with six servo motors (Goteck, GS-9025MG): one for each finger, one additional for thumb abduction/adduction. The motors were commanded by using Arduino Mega. Each finger is actuated through a single tendon

system. A nylon thread is attached between the tip of the finger’s distal phalanx and the motor shaft. When the motor is activated, the nylon thread wraps around the shaft and the tension flexes the finger. An elastic thread passing through the joint extends the finger to its initial position when the motor is deactivated.

We also modified the finger design for easy integration of sensors (Figure 2.5(b)). Sliding sockets were added on the dorsal surfaces of the fingers to mount the bend sensors. Additionally, flat surfaces were made on the phalanges for proper integration of force sensors.

2.2.2 Sensor characterization and signal conditioning

It is well known that sensory inputs for contact/grasp force and joint/hand position are of primary importance for object manipulation. The function of the mechanoreceptors which mediate these inputs may be mimicked by using a combination of force and bend sensors, respectively. Although the current engineering technology includes a wide range of options [102], requirements specific to prosthetic applications limit the choices. That is to say, the sensors should be light, thin, easy to mount, low-powered, and very importantly, able to accommodate large deformations. As such, piezoresistive sensors were preferred in this study (Figure 2.6(a)) which are commonly used in rehabilitation and robotic applications [103–105].

We used bend sensors (FlexSensor, SpectraSymbol) to measure joint angles. They are made of resistive carbon elements which are close to each other when the sensor is straight, with total resistance of 15 k Ω . When a bend sensor is flexed, the carbon elements are separated wider apart, so the resistance increases to 50 k Ω at 90 degrees. We modified the bend sensors to fit the desired joint lengths (Figure 2.6(b)). After they were trimmed, the continuity of the electrical traces was ensured by coating the cut end with conductive glue (Nickel Print) [79, 106]. A separate bend sensor was prepared for each joint.

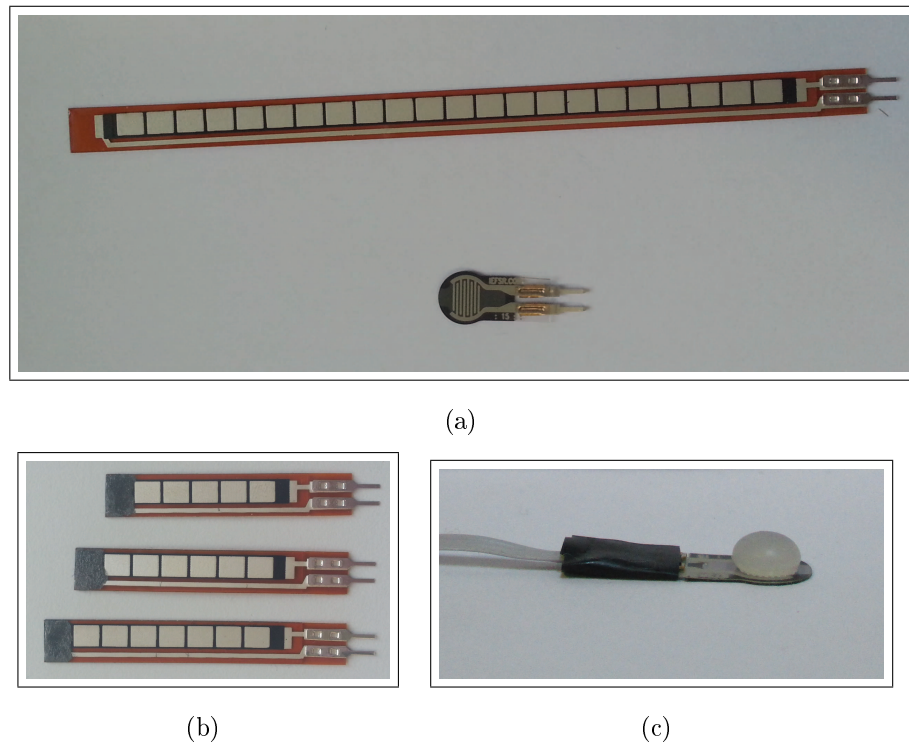
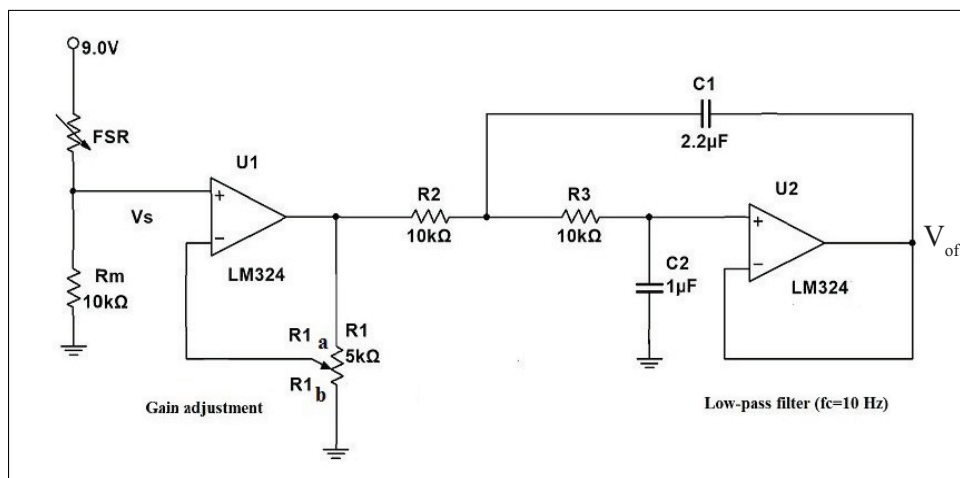


Figure 2.6 a) Force and bend sensors used in the study. b) Bend sensors were cut and the electrical traces were modified for adjusting length to each particular joint. c) Dome-shaped silicon rubber was glued on force sensors for improved contact with objects [79].

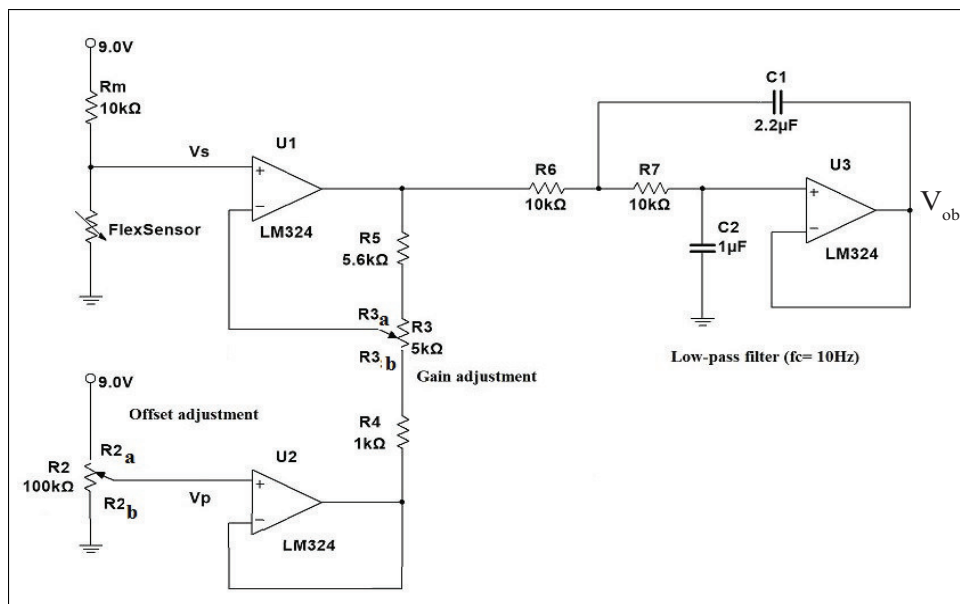
For measuring tactile contact and grasping, piezoresistive force sensors (FSR400-Short, Interlink Electronics) were used [107, 108]. These sensors consist of two flexible layers which are normally separated, resulting in a very high resistance ($\gg M\Omega$ s) without force. One of the layers has interdigitating electrodes while the other has a conductive material. When the two layers get closer with applied force, the resistance decreases, e.g. to 3-5 k Ω under 1 kgf. Since these sensors have planar active sensing areas which are not suitable for forces applied from different angles, we modified them by gluing a dome-shaped silicon rubber piece on each (Figure 2.6(c)). This also distributed the applied force more homogeneously over the active area [79, 108] and reduced the effect of the exact contact point on the grasped object.

Multi-channel op-amp circuits were constructed (LM324, a separate interface circuit for each sensor) to convert the resistance changes in sensor outputs to voltage changes (Figure 2.7). At the first stage of each channel, there is a voltage divider.

Because of the reversed direction of change, the force sensors are connected as pull-up resistors (Figure 2.7(a)), but the bend sensors are pull-down resistors (Figure 2.7(b)). Next, there is a gain adjustable amplifier stage in order to use the full span of the data acquisition card for all sensors with varying sensitivity ranges. Finally, a second-order Butterworth low-pass filter ($f_c=10$ Hz) is used at unity gain. An additional offset adjustment stage is included for bend sensors (Figure 2.7(b)) to set the initial sensor output as zero. The initial values of force sensors were always zero due to their very high nominal resistances.



(a)



(b)

Figure 2.7 Interface circuits for the a) force sensors and the b) bend sensors. Component symbols with subscripts refer to values after adjusting the multi-turn trimpots [79].

The outputs of the interface circuits can be given as in Eq. 2.1 and Eq. 2.2, respectively for the force and bend sensors:

$$V_{0f} = \frac{R_1}{R_{1b}} V_s \quad (2.1)$$

$$V_{0b} = \left(1 + \frac{R_5 + R_{3a}}{R_{3b} + R_4}\right) V_s - \left(\frac{R_5 + R_{3a}}{R_{3b} + R_4}\right) V_p \quad (2.2)$$

where V_{0f} and V_{0b} are the circuit outputs, V_s is the output of voltage divider, V_p is the output of offset adjustment stage and subscripts refer to resistance values after adjusting the multi-turn trim pots.

The sensors were calibrated according to the outputs of the interface circuits in Figure 2.7 (see Section 2.3.1 for the calibration curves). A digital precision balance was used for the calibration of force sensors (Figure 2.8). The sensor was fixed on the scale and the force was changed gradually using a micromanipulator. The gain of the interface circuit was adjusted to span the calibration range (up to 0.5 kgf). The lower limit of the calibration range was determined by the sensor threshold below which it did not respond. The calibration was done both for loading and unloading cycles.

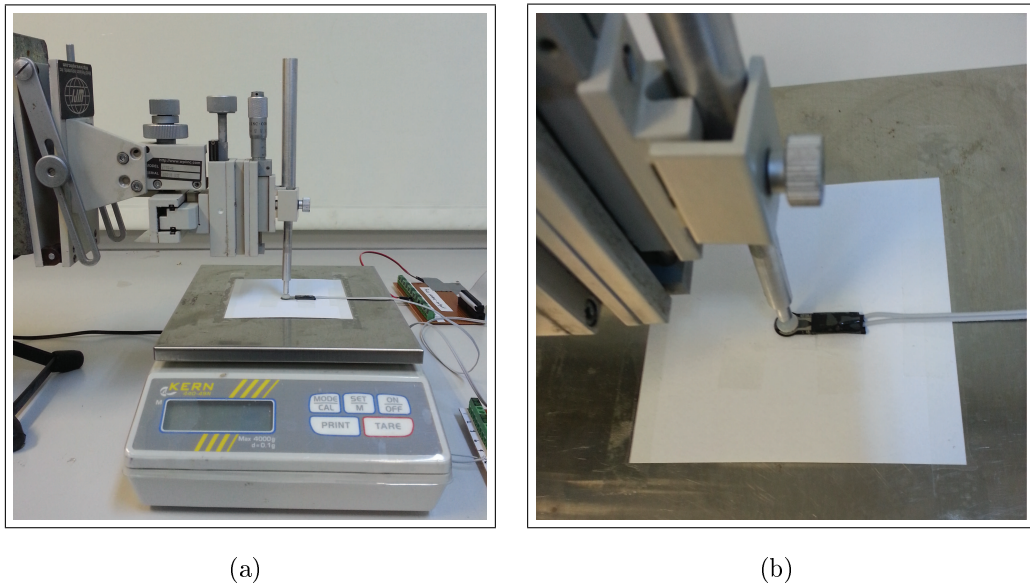


Figure 2.8 Force sensor calibration setup a) Side view b) Top view.

Since the behavior of bend sensors depend on the bending radius and flexion position on the piezoresistive carbon elements, their calibration was performed on the robotic hand. This ensured that the calibration was valid during the operation of the device. First, when the sensors were straight, the sensor outputs were set to zero by offset adjustment. Then, the gain was adjusted to span the bending range of the corresponding joint. The servo motor position of each finger was changed gradually and the sensor outputs were recorded by using a goniometer for both loading and unloading cycles.

2.2.3 Grasping experiment and data acquisition

We equipped all fingers of the robotic hand with sensors (Figure 2.9 and Figure 2.10). Bend sensors were placed on all metacarpophalangeal (MCP), proximal interphalangeal (PIP) and distal interphalangeal (DIP) joints on the dorsal side. One end of each bend sensor is fixed, while the other end can slide in a socket during movement. On the ventral side of the hand, we placed force sensors on all distal phalanges; additional sensors were placed on the proximal phalanges of index and middle fingers, and on the metacarpal heads of the long fingers. We could not use data from some sensors for classification due to technical limitations discussed in Section 2.4 (gray symbols in Figure 2.9).

Human hand can perform complex grasp patterns; however, most of them are not included in prosthetic hand designs. Some finger or hand postures are impossible to attain because of rigid mechanical limitations. Additionally, complexity of hand postures increases signal processing and cognitive load. Nevertheless, some critical grasp types are sufficient to securely grasp and manipulate objects during activities of daily living [109]. Since we used an underactuated prosthetic hand (fewer actuators than DOFs) with stiff joint mechanisms, precision grasps could not be implemented. Therefore, we had it perform the cylindrical grasp [110] during the experiment. Since our main aim was to apply data-driven classification from highly variable sensor data, the limitations of the robotic hand could be tolerated. As a matter of fact, this study

demonstrates how such limitations may be overcome with the data-driven approach for SF.

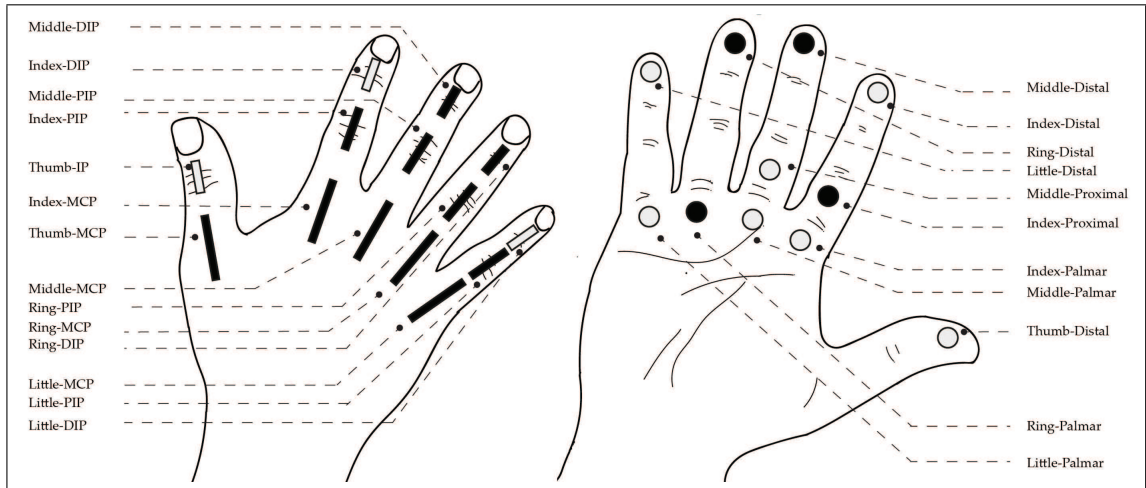


Figure 2.9 Sensor names and locations. 14 bend sensors (left) and 11 force sensors (right) were placed on the dorsal and ventral sides of the robotic hand, respectively. Data from only 11 bend sensors and 4 force sensors were used for classification analyses (black symbols). Data from the remaining sensors (gray symbols) could not be used due to technical limitations in this study.

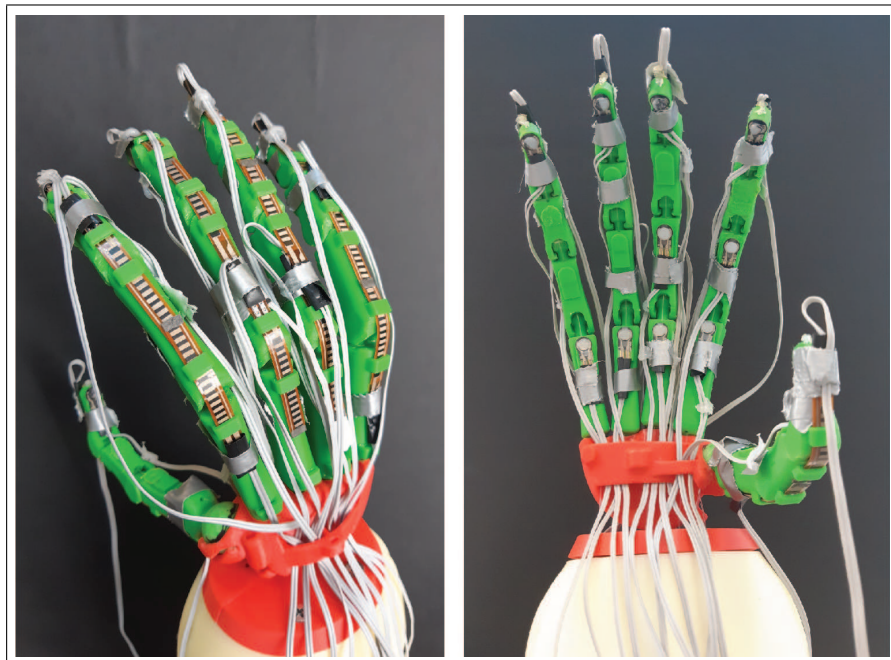


Figure 2.10 Simple underactuated robotic hand with off-the-shelf force and bend sensors.

Two same-sized cylindrical objects (diameter: 9 cm, length: 12 cm) differing

in stiffness (hard vs. soft object) were made for the experiment by 3D printing (Z-ABS, Zortrax) (Figure 2.11(a)). To produce the deformable soft object, a smaller diameter (4.5 cm) cylinder and a mold were printed. The outer surface of the smaller stiff cylinder was coated with silicon rubber (Ecoflex 00-10, Smooth On) such that the overall diameters of both hard and soft objects were identical. During the grasping experiment, each object was stabilized by a rod screwed along the cylindrical axis, and this axis was parallel to the ground (Figure 2.11(b)).

The target motor position of each finger was set to 180 degrees (upper limit of the motor), and the robotic hand was programmed to perform periodical flexion and extension in the form of cylindrical grasps (Figure 2.11(b)). During this movement, data from all sensors were collected from the outputs of the multi-channel interface circuits as shown in Figure 2.7 by using a data acquisition card (USB-6259, National Instruments) at a sampling frequency of 1 kHz. Each movement cycle (flexion + extension) lasted approximately 6 seconds. The overall data included 80 cycles (35 cycles each for hard and soft objects, 10 cycles without any object). The movement of the robotic hand was also captured on video by 2 cameras (frame rates: 25 and 30 Hz) for classification analyses.

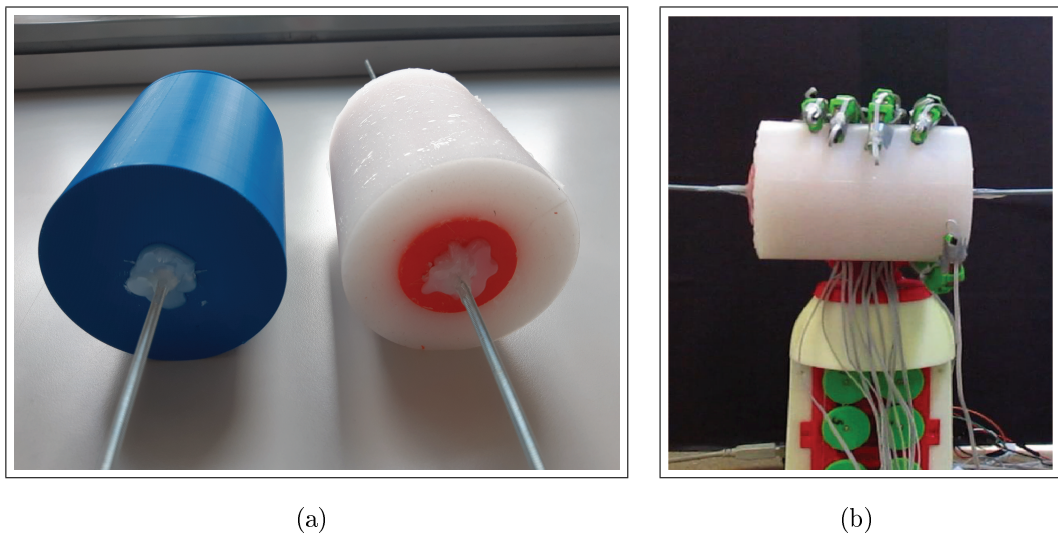


Figure 2.11 a) Cylindrical objects (hard vs soft) used in the experiment. b) The robotic hand performing cylindrical grasp on the soft deformable object.

2.2.4 Data processing and classification

The experimental sensor data was analyzed in MATLAB (Release 2017b, The MathWorks, Inc.) by following the procedure blocks given in Figure 2.12. It was initially low-pass filtered (second-order Butterworth, $f_c = 10$ Hz). The filtered data was used to estimate the joint angles and contact forces using the calibration equations presented in Section 2.3. Then, the first and second derivatives of the filtered data were calculated. The filtered estimates and their derivatives were segmented into non-overlapping windows (i.e. length of the window was adjusted to be equal to one video frame used for labeling: 40 or 33 data points depending on the camera) and time-averaged within each window. Thus, each final point was matched with a single video frame. These time-averaged values formed the feature matrices for each finger.

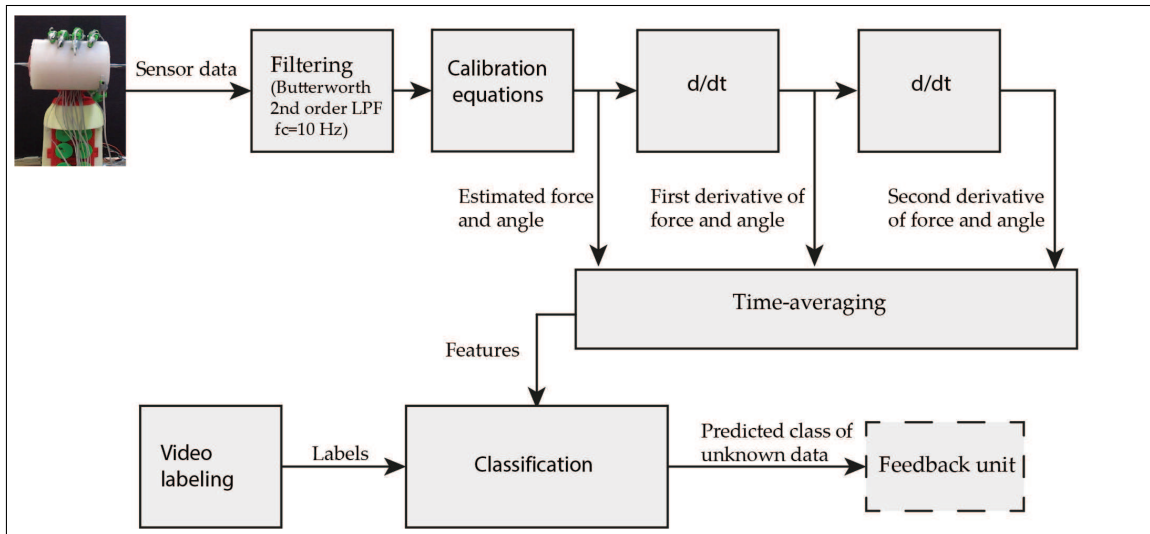


Figure 2.12 Data processing procedure blocks. Feedback unit will be explained in Chapter 3.

Three types of classifications were performed: object type classification with 3 classes, movement type classification with 5 classes and a combined type classification with 13 classes. In order to label the data, video frames were analyzed manually. As explained schematically in Figure 2.13, important event times (t_i) were recorded. The frames for the intervals between the events were labeled considering the object type and movement phase. The labels were as the following: 1) Stationary in air, 2) Flexion

in air, 3) Extension in air, 4) Contact to soft object, 5) Flexion in soft object, 6) Stationary in soft object, 7) Extension in soft object, 8) Release from soft object, 9) Contact to hard object, 10) Flexion in hard object, 11) Stationary in hard object, 12) Extension in hard object, 13) Release from hard object. These labels were directly used as classes for combined type classification. The class definitions for object type classification were derived by merging the labels in Figure 2.13 into three classes such as no object (1,2,3), soft object (4,5,6,7,8), and hard object (9,10,11,12,13). Similarly, the class definitions for movement type classification were defined as stationary (1,6,11), flexion (2,5,10), contact (4,9), release (8,13), and extension (3,7,12).

Events	Experiment conditions		
	No object	Soft object	Hard object
t₁: Motors ON command	-----	-----	-----
	1	1	1
t₂: Beginning of movement	-----	-----	-----
		2	2
t₃: Contact	2	-----	-----
		4	9
		5	
t₄: End of movement	-----	-----	10
	1	5	
t₅: Motors OFF command	-----	-----	-----
	1	6	11
t₆: Motors ON command	-----	-----	-----
	1	7	
t₇: Beginning of movement	-----	-----	12
		7	
t₈: Release	3	-----	-----
		8	13
		3	3
t₉: End of movement	-----	-----	-----
	1	1	1
t₁₀: Motors OFF command	-----	-----	-----

Figure 2.13 Class labeling procedure. Each number refers to one class in the combined type classification. Event times are shown with t_i and dashed lines where applicable for the given condition (no object, soft object, hard object). See text for the special cases and exceptions. Video frames for the intervals between the events were labeled (1 to 13) as defined in the text.

In Figure 2.13, event times are also indicated by dashed lines if they are valid for the given object condition. For example, since there is no contact in the no-object condition, all the frames between t_2 and t_4 were labeled as flexion in air (label 2), and a dashed line is not shown for t_3 . On the other hand, it was difficult to assess the exact contact/release times for the object conditions. Since machine learning requires multiple data points with those labels, t_3 and t_8 are shown with two dashed lines (as an interval instead of discrete events) for the soft- and hard-object conditions. Another complication occurred with the end/beginning of movement events (t_4 and t_7) within the hard object. This object is not deformable; therefore, these events are not valid and not shown by dashed lines in the hard-object condition (Figure 2.13). Nevertheless, the robotic hand structure still moves internally when the motors are on, so the relevant video frames were tagged with the labels 10 and 12.

The labeled data was normalized and randomly divided into training and test data sets with a ratio of 7:3 respectively. For each finger, the dimensions of the data used in classification are given in Table 2.1. We implemented three commonly used machine learning algorithms by built-in MATLAB functions: Multinomial Logistic Regression (MLR), k-Nearest Neighbour Classifier (kNN) and Support Vector Machines (SVM) [98]. For kNN and SVM, hyperparameters were also tuned to select the best model by applying 5-fold cross-validation. For this purpose, the number of neighbours and the distance metric of kNN classifier were varied. For SVM classification with radial basis kernel function, C (penalty for misclassification) and sigma (related to spread of kernel) parameters were tuned. After hyperparameter tuning, three classification algorithms were run for each finger and each classification type separately (45 classifications in total).

Table 2.1
Dimensions of classification data.

Finger	Sensors involved	Number of features	Training set	Test set
Thumb	MCP	3	10831	4642
Index finger	MCP, PIP, Proximal	9	10831	4642
Middle finger	MCP, PIP, DIP, Distal	12	10831	4642
Ring finger	MCP, PIP, DIP, Distal, Palmar	15	9019	3865
Little finger	MCP, PIP	6	9019	3865

2.3 Results

2.3.1 Sensor characterization

The sensors were calibrated by using the voltage outputs from the multi-channel interface circuits as described in Section 2.2.2. The calibration data of loading and unloading cycles (15 and 50 data points on average for each bend and force sensor, respectively) were fit by different equations for the two sensor types, and then the curve fits were averaged to obtain the overall calibration curve for each sensor (Figure 2.14 and Figure 2.15). Three-parameter power functions (Eq. 2.3) were fitted to the force sensor data:

$$y = ax^b + c \quad (2.3)$$

where x is force and y is circuit output.

Since the resistance of the bend sensor depends on both the bending radius and the flexion position, the average calibration curves of the bend sensors are very different from each other. Various simple functions were tested, and eventually two-parameter power functions (Eq. 2.4) were fitted to the bend sensor data:

$$y = ax^b \quad (2.4)$$

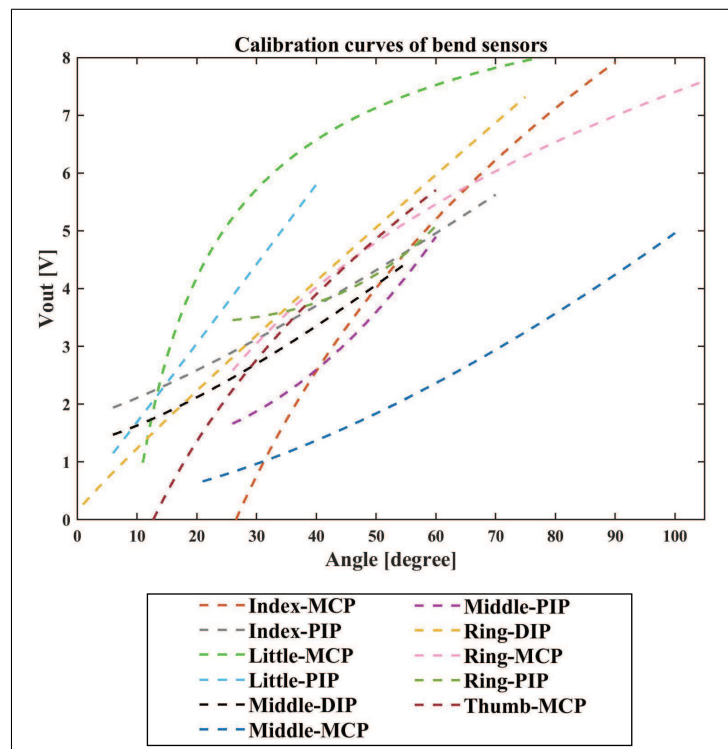
where x is bending angle and y is circuit output.

Parameter fits and the goodness of fit values (R^2) are given in Table 2.2. It can be seen that bend sensors yielded somewhat lower R^2 values, because sensor behavior was highly variable across the sample. On the other hand, there was a closer match between the individual force sensors. It is important to note that Eq. 2.3 and Eq. 2.4, and the fitted parameters are only valid within the calibration ranges given in Table 2.2. Because of the robotic hand conformation, zero degrees were not exactly attainable during the experiment below. On the other hand, force sensors had detection thresholds, and the minimum force reading obtained by inverting Eq. 2.3 was this threshold value.

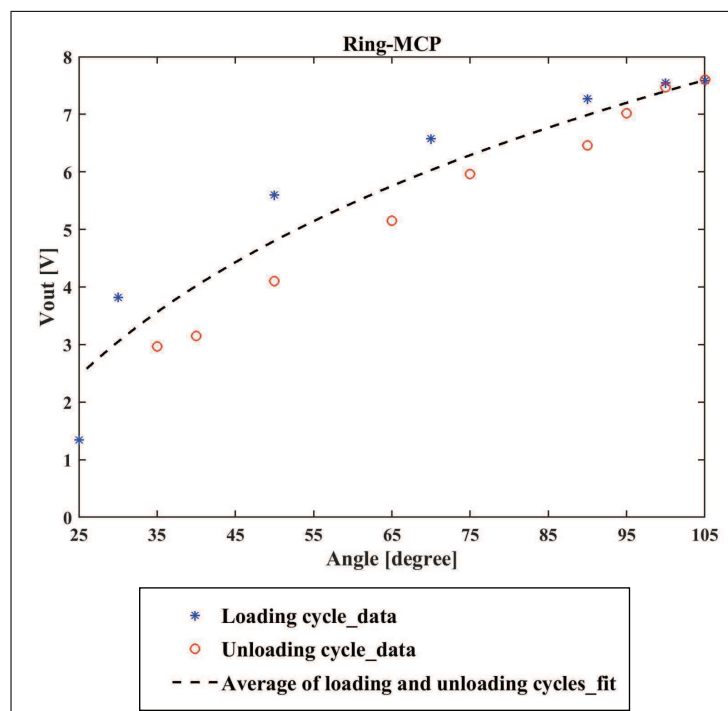
Table 2.2
Parameters of calibration equations.¹

Sensor type	Sensor name	a	b	c	R^2	Range
Bend sensors	Thumb-MCP	0.03	1.29	-	0.957	11-60
	Index-MCP	0.01	1.44	-	0.929	26-90
	Index-PIP	0.49	0.56	-	0.966	6-70
	Middle-MCP	0.01	1.40	-	0.995	21-100
	Middle-PIP	0.01	1.41	-	0.978	26-60
	Middle-DIP	0.33	0.63	-	0.954	6-55
	Ring-MCP	0.32	0.69	-	0.988	26-105
	Ring-PIP	0.66	0.48	-	0.902	26-60
	Ring-DIP	0.15	0.90	-	0.992	1-75
	Little-MCP	0.97	0.50	-	0.829	11-80
	Little-PIP	0.21	0.90	-	0.970	6-40
Force sensors	Index-proximal	-175.81	-0.83	8.74	0.983	31-500
	Middle-distal	-59.06	-0.54	9.62	0.994	31.4-500
	Ring-distal	-601.36	-1.11	8.08	1.000	45.5-500
	Ring-palmar	-55.34	-0.57	9.11	0.999	22.5-506.5

¹The units in the range values are degrees and gram-force for bend and force sensors respectively.

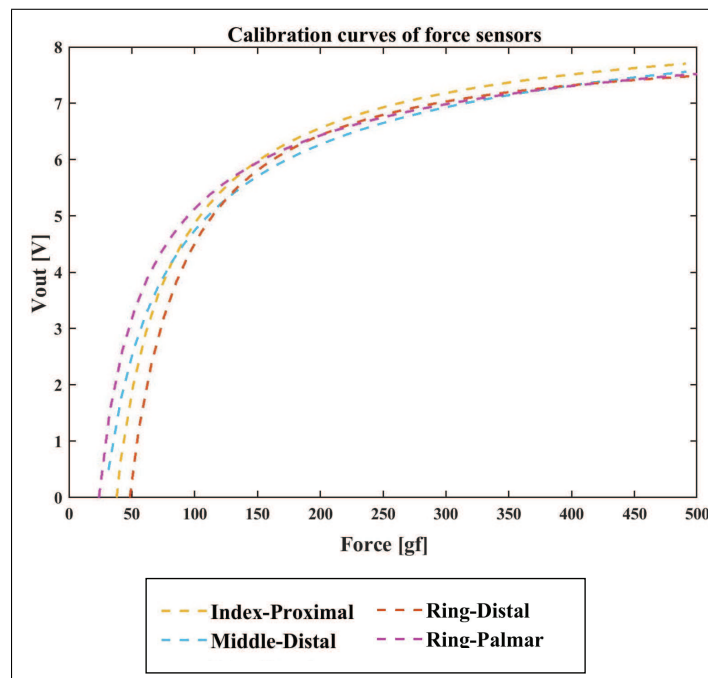


(a)

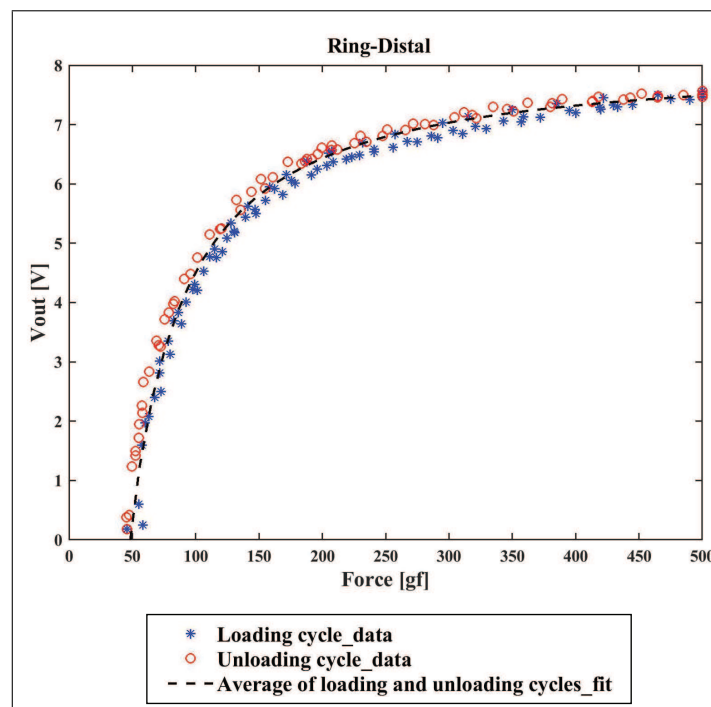


(b)

Figure 2.14 a) Average calibration curves of the bend sensors. b) Calibration data (1 loading/unloading cycle) and the average curve of an example bend sensor.



(a)



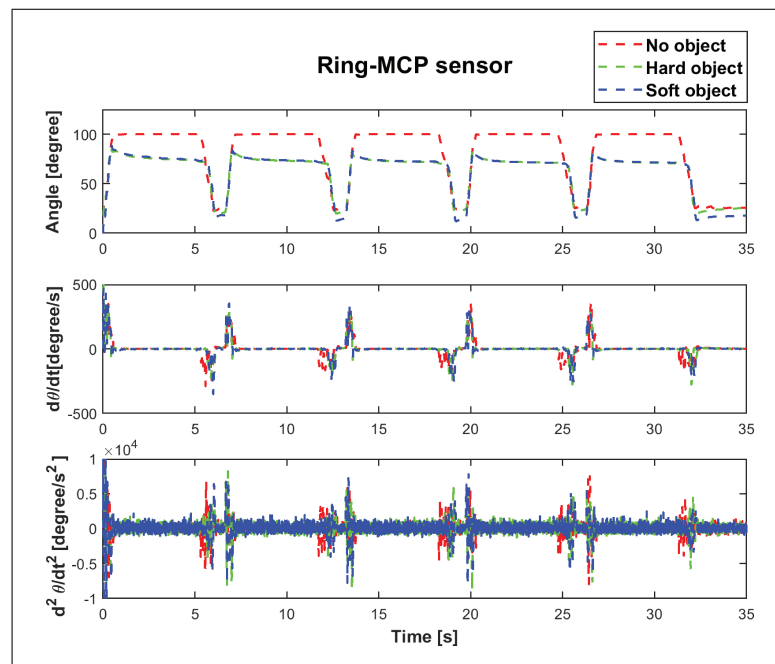
(b)

Figure 2.15 a) Average calibration curves of the force sensors in gram-force. b) Calibration data (3 loading/unloading cycles) and the average curve of an example force sensor in gram-force.

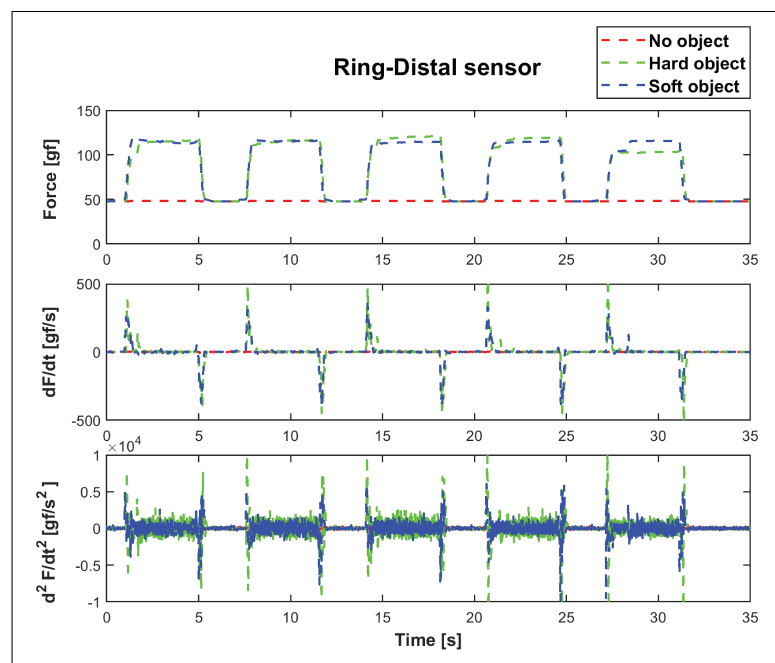
2.3.2 Cylindrical grasping data

Figure 2.16 shows experimental data from example bend and force sensors and their derivatives with respect to time during cylindrical grasping experiment. The angle and force estimates were obtained by filtering data and applying the calibration equations. Then, first and second derivatives were calculated as depicted in Figure 2.12. Based on object conditions (no object, soft object, hard object), the plots show appreciable differences. The bend sensor signals lower angles upon contact with objects as expected. Interestingly, this condition also results lower latency fluctuations in the time derivatives during extension, which implies that it takes more time for the robotic hand to decouple from the objects. The differences between the hard and soft objects are more discernable in the force sensor data. Although contact with both the hard and the soft object produced similar force readings, the time derivatives of the force were much higher for the hard object as opposed to the soft one.

The maximum forces recorded during the experiment are around 0.1 kgf, but these values do not indicate the grasp strength exactly due to inefficient coupling with the objects (see Section 2.4). It is also important to note that since the objects were secured with rods (Figure 2.11), there was no weight bearing on the force sensors. We observed that some bend sensor readings were out of calibration ranges during grasping due to changes in sensor behavior resulting from the underactuated mechanism of the hand (see Section 2.4). Therefore, we extrapolated the data on the calibration curve up to an acceptable limit (125 degrees). Any data points still out of range were considered undefined and not included in classification analyses. Since data were sampled at 1 kHz, there were sufficient amount of samples to obtain the time averages, i.e. features in Figure 2.12.



(a)



(b)

Figure 2.16 Examples of a) bend sensor and b) force sensor (in gram-force units) outputs and their derivatives with respect to time during cylindrical grasping.

As explained in Section 2.2.4, features were labeled according to Figure 2.13 for classification algorithms. For example, angle and force data from example sensors

are plotted in Figure 2.17 with color codes representing the labels. This data set was obtained during the grasping experiment with the soft object. Since labeling was performed manually by frame-by-frame video inspection, we can assume labeling errors were minimal.

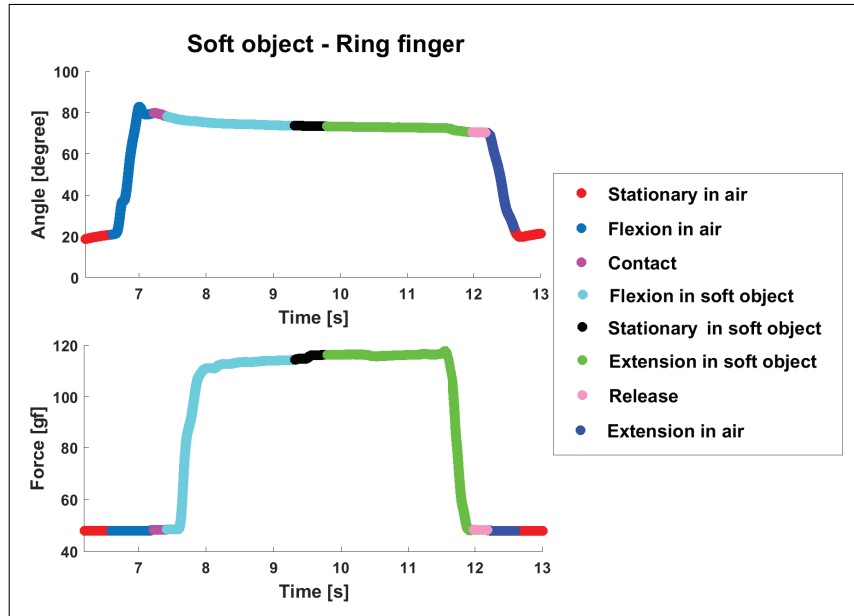


Figure 2.17 Labeled data from example bend and force sensors (in gram-force units) obtained during the grasping experiment with the soft object. Plots are color coded in sequential order according to the labels explained in Section 2.2.4 and Figure 2.13.

2.3.3 Classification results

Detailed classification results are presented in Table 2.3 and Table 2.4. For each classification type, 10 pairs of training/test data were generated randomly from the same dataset and the time and accuracy results were averaged. For all fingers and classification types, best results were obtained with kNN and SVM classifiers. Results with lowest accuracy were obtained with the MLR model. The prediction times are short for all of the methods and may be considered to be appropriate for real-time implementation. However, the SVM algorithm takes much longer time to train compared to the kNN algorithm. In terms of classification type, best results were achieved for object type classification. Although thumb and little finger do not have force sensors, the objects were classified accurately using kNN and SVM classifiers based on data from

bend sensors. When the classification accuracies are averaged across all the fingers, kNN classifier gave the highest results (0.983, 0.752, 0.751 for object type, movement type, and combined type classification respectively). Average accuracies from SVM were slightly lower. The accuracies averaged across fingers are given in Table 2.5

Table 2.3
Classification results for thumb and index finger.

Finger	Classif.	Method	Hyperparameters	Train. time (s)	Train. acc.	Classif. time (s)	Classif. acc.
Thumb	Obj. type	MLR	-	3.299	0.891	2.027E-07	0.892
		kNN	Dist=City. k=7	0.020	0.963	5.981E-06	0.949
		SVM	C=10 Sigma=0.022	4.790	0.960	5.080E-05	0.950
	Mov. type	MLR	-	12.323	0.457	3.021E-07	0.457
		kNN	Dist=Euc. k=14	0.024	0.688	7.497E-06	0.598
		SVM	C=2.154 Sigma=0.005	43.481	0.692	5.115E-04	0.590
	Comb. type	MLR	-	84.734	0.479	7.622E-07	0.477
		kNN	Dist=Mink. k=19	0.036	0.675	9.585E-06	0.600
		SVM	C=215.443 Sigma=0.022	187.924	0.654	3.997E-04	0.608
Index finger	Obj. type	MLR	-	16.623	0.852	3.159E-07	0.826
		kNN	Dist=Corr. k=1	0.018	1.000	1.638E-04	0.990
		SVM	C=1000 Sigma=0.464	10.671	0.995	1.528E-05	0.993
	Mov. type	MLR	-	25.629	0.568	3.391E-07	0.563
		kNN	Dist=City. k=7	0.028	0.892	4.986E-05	0.799
		SVM	C=215.443 Sigma=0.100	110.049	0.849	1.465E-04	0.778
	Comb. type	MLR	-	238.511	0.664	6.604E-07	0.654
		kNN	Dist=City. k=5	0.034	0.899	7.111E-05	0.792
		SVM	C=1000 Sigma=0.100	47.854	0.866	2.518E-04	0.781

Table 2.4
Classification results for middle, ring and little fingers.

Finger	Classif.	Method	Hyperparameters	Train. time (s)	Train. acc.	Classif. time (s)	Classif. acc.
Middle finger	Obj. type	MLR	-	15.202	0.981	1.206E-06	0.977
		kNN	Dist=City. k=55	0.020	0.992	1.676E-04	0.991
		SVM	C=46.416 Sigma=0.464	2.906	0.995	8.618E-06	0.992
	Mov. type	MLR	-	35.421	0.567	3.690E-07	0.569
		kNN	Dist=City. k=3	0.014	0.950	1.636E-04	0.777
		SVM	C=1000 Sigma=0.100	124.342	0.881	1.107E-04	0.788
	Comb. type	MLR	-	360.035	0.727	6.782E-07	0.722
		kNN	Dist=City. k=1	0.019	1.000	1.213E-04	0.769
		SVM	C=1000 Sigma=0.100	29.986	0.883	2.537E-04	0.788
Ring finger	Obj. type	MLR	-	14.153	0.986	2.912E-07	0.984
		kNN	Dist=City. k=5	0.009	0.995	1.650E-04	0.994
		SVM	C=1000 Sigma=2.154	2.623	0.996	3.894E-06	0.994
	Mov. type	MLR	-	54.586	0.723	3.545E-07	0.719
		kNN	Dist=City. k=1	0.012	1.000	1.595E-04	0.833
		SVM	C=1000 Sigma=0.100	58.525	0.963	1.403E-04	0.792
	Comb. type	MLR	-	377.268	0.778	8.989E-07	0.778
		kNN	Dist=City. k=5	0.017	0.944	1.459E-04	0.846
		SVM	C=215.443 Sigma=0.100	10.001	0.945	5.604E-04	0.796
Little finger	Obj. type	MLR	-	2.909	0.743	2.507E-07	0.740
		kNN	Dist=Euc. k=4	0.023	0.993	8.735E-06	0.989
		SVM	C=46.416 Sigma=0.100	1.552	0.997	7.259E-06	0.991
	Mov. type	MLR	-	14.884	0.499	3.792E-07	0.496
		kNN	Dist=Cityblock k=5	0.025	0.871	1.271E-05	0.754
		SVM	C=215.443 Sigma=0.022	71.192	0.869	2.965E-04	0.730
	Comb. type	MLR	-	118.983	0.571	8.417E-07	0.569
		kNN	Dist=City. k=3	0.026	0.897	1.164E-05	0.748
		SVM	C=1000 Sigma=0.100	32.710	0.812	1.331E-04	0.759

Table 2.5
Finger average of classification accuracy.

Type of classification	Classification methods	Accuracy
Object type	MLR	0.884
	kNN	0.983
	SVM	0.984
Movement type	MLR	0.561
	kNN	0.752
	SVM	0.736
Combined type	MLR	0.640
	kNN	0.751
	SVM	0.747

Best classification results were obtained from data of the ring finger by using kNN classifiers. In Figure 2.18(a), the confusion matrix of object type classification is given. It is seen that the misclassification rate is extremely low, because data from two functional force sensors were included for this finger. Table 2.6 lists the recall, precision, and F1 score values for each class. They are all very high for object-type classes. Classification for movement type yielded lower accuracy, and similarly lower recall, precision, and F1 score. The confusion matrix (Figure 2.18(b)) shows that some stationary labels were misclassified as flexion or extension. Similarly, some flexion labels were misclassified as stationary or extension, and some extension labels were misclassified as stationary or flexion. Since same angle values can be labeled as stationary, flexion, and extension, time derivatives were probably critical here to cause some confusion. On the other hand, contacts and releases were misclassified with flexion and extension respectively. This may be expected, because some flexion continues with contact, and some extension precedes release. Combined type classification yielded a slightly higher accuracy than the movement type classification, and its recall, precision, and F1 score values were of mixed performance based on a given class. In general, they were still high except the stationary in soft object and stationary in hard object classes, which were confused with flexion/extension in the corresponding object types

(Figure 2.18(c)). The labels for these two classes were difficult to assess as explained above (see Figure 2.13). The confusion matrices and detailed performance scores for all fingers are given in Appendix A.

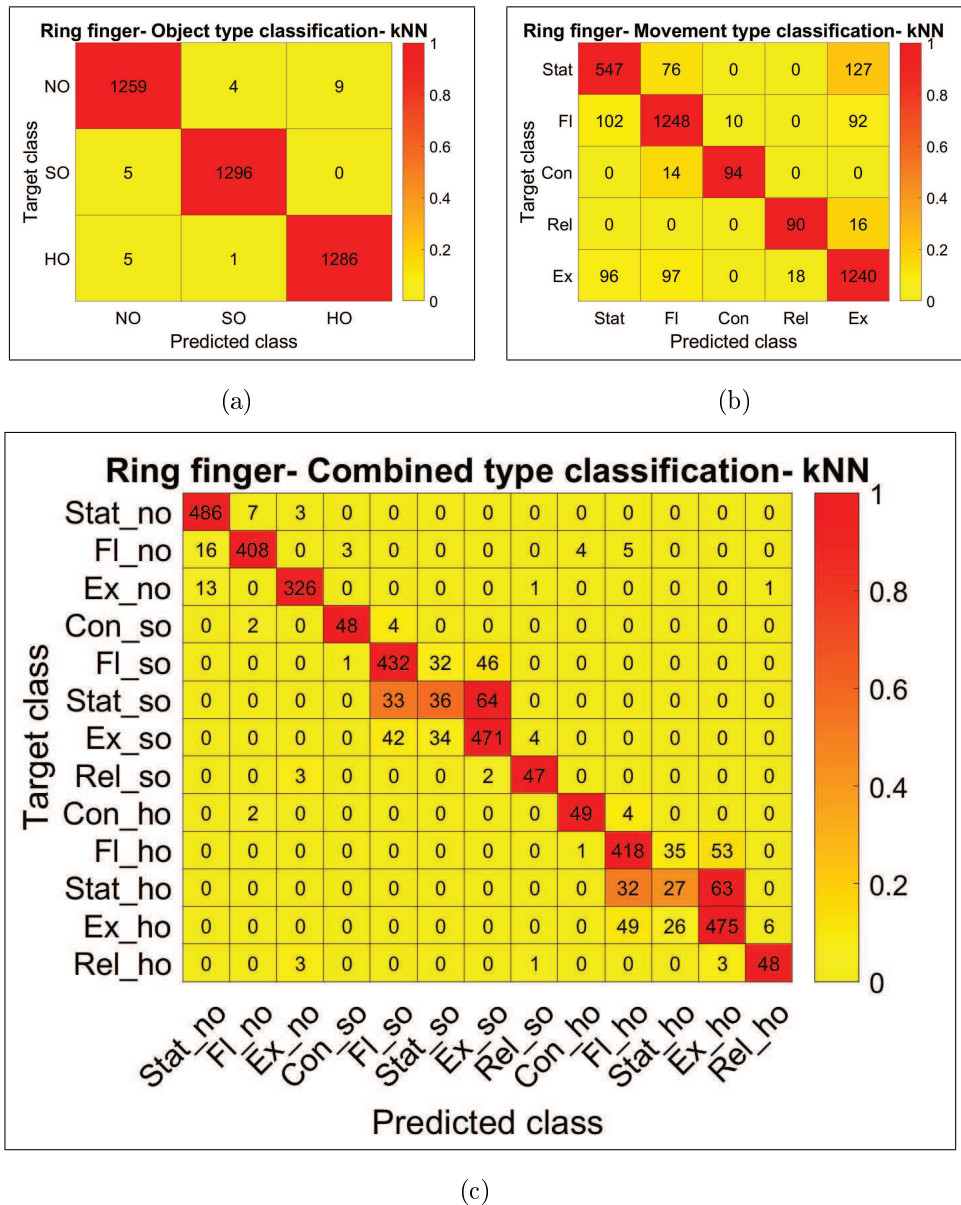


Figure 2.18 Confusion matrices of a) object type, b) movement type, and c) combined type kNN classification of sensor data from the ring finger. Counts are given as numbers in cells. Color code indicates a given count normalized by total instances of the target class.

Table 2.6
Classification results of kNN classifier for ring finger.

Type of classification	Class(Labels)	Recall	Precision	F1 Score
Object type	No (1,2,3)	0.989	0.992	0.991
	So (4,5,6,7,8)	0.996	0.996	0.996
	Ho (9,10,11,12,13)	0.996	0.993	0.994
Movement type	Stat (1,6,11)	0.730	0.735	0.732
	Fl (2,5,10)	0.860	0.870	0.865
	Con (4,9)	0.871	0.902	0.886
	Rel (8,13)	0.849	0.837	0.843
	Ex (3,7,12)	0.855	0.841	0.848
Combined type	Stat-no (1)	0.981	0.944	0.962
	Fl-no (2)	0.937	0.974	0.955
	Ex-no (3)	0.955	0.974	0.964
	Con-so (4)	0.891	0.930	0.910
	Fl-so (5)	0.846	0.846	0.846
	Stat-so (6)	0.273	0.353	0.308
	Ex-so (7)	0.855	0.809	0.831
	Rel-so (8)	0.904	0.892	0.898
	Con-ho (9)	0.893	0.914	0.903
	Fl-ho (10)	0.826	0.823	0.824
	Stat-ho (11)	0.218	0.306	0.255
	Ex-ho (12)	0.854	0.800	0.826
	Rel-ho (13)	0.886	0.870	0.878

2.4 Discussion

2.4.1 General conclusions

In the current study, we aimed to understand the flow of information from highly variable sensor data, which can be further used to provide SF from a simple prosthetic hand. Although advanced robotic designs usually have integrated sensors which are

specific to the device, and therefore, require considerable engineering investments to achieve accuracy and precision [13, 111, 112], biological sensors (i.e. mechanoreceptors) generate highly variable neural outputs [113–115]. The interplay of skin/muscle mechanics, mechanoreceptor anatomy/physiology, and central processing produces a very complex sensory system, quite unlike the engineering systems which have a deterministic design philosophy. However, with the help of several receptor types, redundancy, and population coding, the brain can extract the required information in any natural setting and can adapt remarkably by plasticity and learning. We adopted a similar biologically inspired approach with inexpensive, off-the-shelf force and bend sensors with highly variable mechanoelectric characteristics. Although individual sensor calibration was made meticulously, it is concluded that precise calibration of such sensors in practical applications may not be feasible because of unpredictable coupling with objects. Therefore, we used machine learning algorithms for data-driven classification. By using the robotic hand, we collected sensor data during cylindrical grasp movements. The hand performed periodic flexion and extension in three conditions: no object, soft object, and hard object. After hardware and software pre-processing, features obtained from filtered data and its first and second derivatives were used for offline classification of object type (no object, soft object and hard object) and movement phase (stationary, flexion, extension, contact, and release) by supervised machine learning algorithms (Multinomial Logistic Regression, k-Nearest Neighbor Classifier and Support Vector Machines). Offline classification performance was moderately high and it forms a valuable basis for our subsequent studies on real-time SF. The classes found via models set up through machine learning can be readily applied to determine the events in the DESC policy. DESC policy is very promising in that respect, and can prevent some bottlenecks in signal and cognitive processing.

Differently from the majority of object/grasp recognition studies in the literature, we included proprioceptive information in conjunction with force to classify object stiffness. Since we aim to use the system for prosthetics applications, we classified the object and movement type without any exploratory procedures as mostly used in the literature. Although the current study only used one grasp type, the results are promising. kNN algorithm achieved over 99% accuracy for object type with 9 ms training

time and 0.2 ms classification time.

2.4.2 Limitations

The simplicity of the robotic hand used in this study does not allow especially the precision grasp types. Since fingers do not have flexible joints and abduction/adduction DOF, object manipulation was very limited. The flexion/extension of the phalanges occur in conjunction with each other due to the underactuated design. This introduced some unpredictability regarding the exact values of the joint angles even in the same grasp type used in the experiment.

The piezoresistive sensors were inexpensive and yielded highly variable calibration curves across the tested sample. Furthermore, we observed that the behavior of some sensors changed due to repetitive use, probably due to worn out polymeric materials; these were not included in the study as depicted in Figure 2.9. Because of the hand mechanism, bending radius and flexion position also varied in the bend sensors. Force sensors yielded more consistent results, but their detection thresholds caused difficulty during operation. Coupling with the objects were not very reliable in particular, and this sometimes prevented stable readings from force sensors. Threshold also dependent on loading/unloading cycle and force direction (we tried to reduce that with the dome design in Figure 2.6(c)). In summary, the sensorized robotic hand used in this study provided a highly variable data set not amenable to analysis by a classical engineering approach (one that can be applied to strain gauges, for instance), but quite similar to biological mechanoreceptor outputs. This gave us the motivation to adopt a data-driven approach with good success.

Although we present results from a meticulous calibration procedure (by hardware and software), it may not be feasible to perform such a procedure in practical application of similar sensors because of the limitations discussed above. Instead, a cruder calibration may be adequate. Even though some voltage readings were mapped to out-of-range calibration values, and therefore discarded from further analyses, the

machine learning algorithms were able to cope with this issue because of the abundance of time samples (each at 1 ms). Given the highly variable sensor data, retraining the algorithms by adaptive calibration in well-defined daily tasks may be all that is needed. As a matter of fact, the kNN method, which gave the best results in this article, requires relatively large memory space, because the training data set needs to be stored. Therefore, for real-time applications, stored calibration/training sensor data sets may be periodically updated.

2.4.3 Future improvements

If the joint mechanics and the actuator mechanism of the presented robotic hand are improved, some of the limitations may be solved and a more natural grasping pattern may be formed. This is especially important for coupling with objects and manipulating them, in other words, regarding the motor aspect. However, the point we strove to make in this article is that, even though better sensor data would be available with an advanced hand and sensor design, machine learning algorithms would be still invaluable for processing data for SF. The current design may be specifically improved by adding sensors for tendon forces (similar to muscle receptors) to overcome the threshold issue of polymer-based piezoresistive force sensors. By designing flexible joints, the hand conformation would be improved, and the number of contact points would increase, and hence more sensor data would be available. Using an array of sensors would be helpful to measure forces from various directions.

So far, additional transition requirements and physical rules (e.g. contact cannot precede flexion or stationary phases) were not included in the classification. The classification models were only trained by static labels, so the results may be considered as a "worst-case" scenario. Even so, the accuracy results were high. During real-time implementation of the system, the transition requirements will be included to decrease the classification time of the acquired data. This method may also decrease the misclassification rate in movement-type classification. For this purpose, a decision tree may be used before the main classification method.

3. PSYCHOPHYSICAL CHARACTERIZATION AND VIBROTACTILE FEEDBACK

3.1 Background

3.1.1 Human somatosensory system

Human somatosensory system consists of three subsystems namely interoception, proprioception, and exteroception. Interoception is related to organ systems and functions to regulate internal state of the body. The other two subsystems helps motor control by providing information related to the body and environment. Proprioception refers to the mechanism on posture and body movements, containing specialized structures such as receptors in muscles, joints and skin. Exteroception comprises contact, pressure, vibration, motion, stroking, pain and thermal sensations [95]. Table 3.1 summarizes receptor types for each submodality of somatosensory system.

Table 3.1
Classification of somatosensory receptors (Reproduced from [95]).

Modality	Stimulus	Receptor class	Receptor cells
Touch	Skin deformation and motion	Mechanoreceptor	Skin
Proprioception	Muscle length, muscle force, and joint angle	Mechanoreceptor	Muscle spindles and joint capsules
Pain	Noxious stimuli (thermal, mechanical, and chemical stimuli)	Thermoreceptor, mechanoreceptor, and chemoreceptor	All tissues except central nervous system
Itch	Histamine	Chemoreceptor	Skin
Visceral (not painful)	Wide range (thermal, mechanical, and chemical stimuli)	Thermoreceptor, mechanoreceptor, and chemoreceptor	Gastrointestinal tract, urinary bladder, and lungs

In order to obtain information related to touch and proprioception, the physical energy is transformed to electrical energy by mechanoreceptors distributed throughout the body and transferred to the central nervous system through innervating fibers. The type and density of the mechanoreceptors are depend on the skin type. Human glabrous skin contains four types of mechanoreceptors which are Pacinian Corpuscles, Meissner's Corpuscles, Merkel disk receptors and Ruffini endings [116]. The hairy skin includes three of these mechanoreceptors except the Meissner corpuscles whose function is fulfilled by hair follicles (Figure 3.1). Field receptors, hair-guard receptors, hair-down receptors and C mechanoreceptors are the other types of mechanoreceptors found in hairy skin. The mechanoreceptors are also found in muscles and skeletal structures to transmit information on posture and body movements. These are muscle spindle primary and secondary, golgi tendon organ, joint capsule receptors and stretch-sensitive free endings [95].

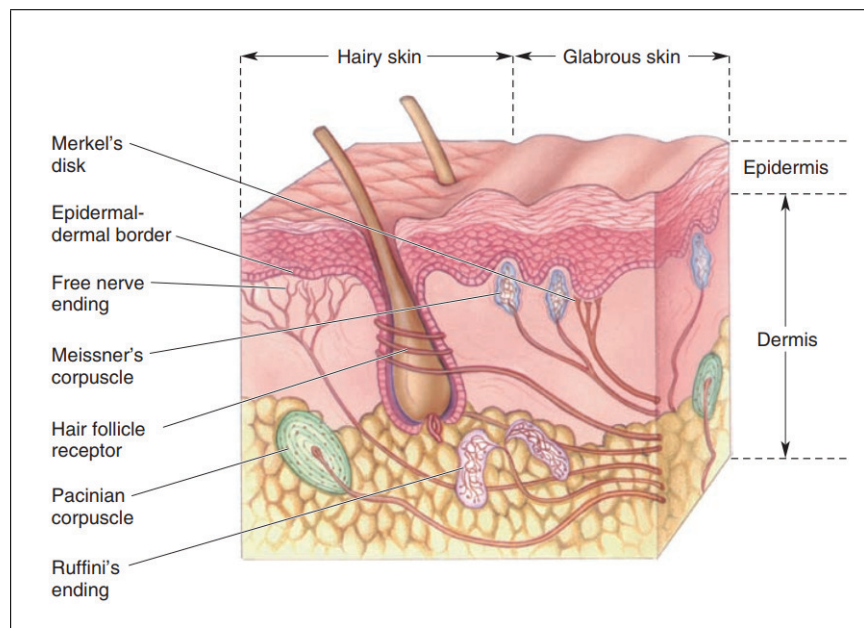


Figure 3.1 Skin anatomy and mechanoreceptors [117].

Each of the four (three in hairy skin) types of mechanoreceptors mediating the touch has different physiological properties and is sensitive to a different range of physical energy (Figure 3.2). Merkel cells and Ruffini endings are categorized as slowly adapting (SA) and innervated by slowly adapting type 1 (SA1) and slowly adapting

type 2 (SA2) fibers respectively. They keep firing during steady pressure. Meissner corpuscles and Pacinian corpuscles are called as rapidly adapting (RA) and innervated by rapidly adapting type 1 (RA1) and rapidly adapting type 2 (RA2) fibers respectively. They are sensitive to changes in mechanical stimuli and do not respond during steady pressure. The receptive fields and distribution densities are also differ for the four types of mechanoreceptors [95,116,118].

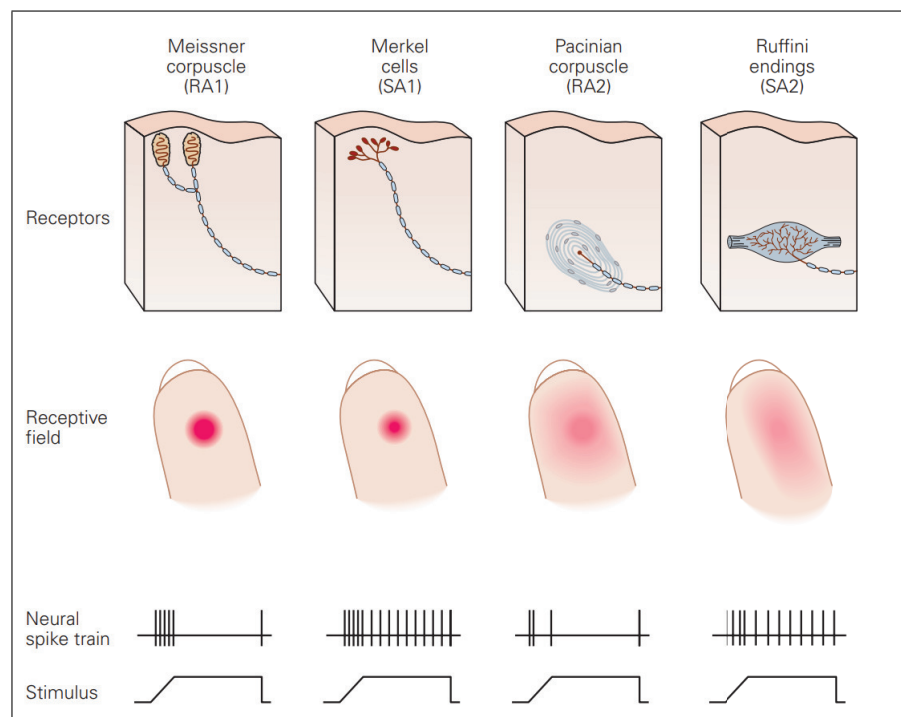


Figure 3.2 Physiological properties of mechanoreceptors [95].

The electrical energy generated by the mechanoreceptors are coded as spike trains by the nerves. The information from thousands of mechanoreceptors are integrated through somatosensory pathways starting from peripheral nerves and reaching to central nervous system (Figure 3.3) [117].

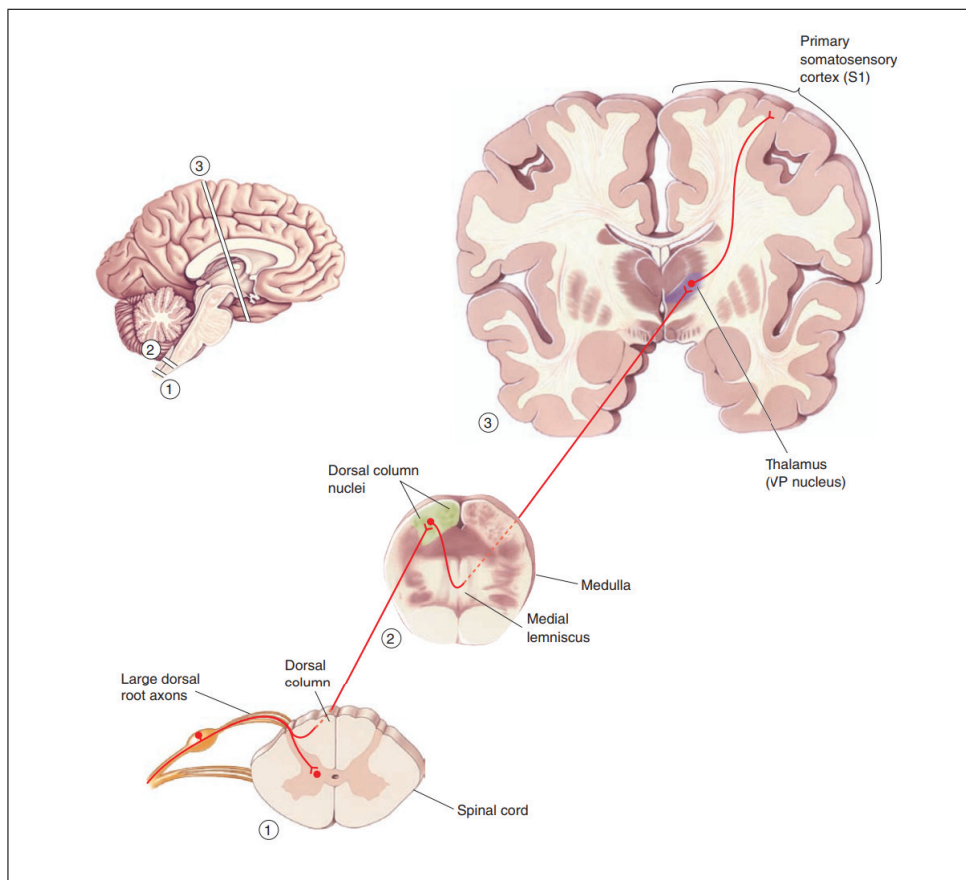


Figure 3.3 The dorsal column-medial lemniscal pathway [117].

3.1.2 Psychophysics & tactile perception

Psychophysics refers to the science of relating the properties of the physical energy to the responses of the central nervous system. Psychophysical studies began with the experimental studies of Ernst Weber, Gustav Feschner, Hermann Helmholtz and Wilhelm Wundt in the 19th century [95].

The detection threshold is defined as the lowest stimulus intensity which produces a sensation. In tactile psychophysics, the tactile detection thresholds are measured as the minimum detectable mechanical displacements. The discrimination threshold is defined as the minimum detectable change of stimulus intensity, also named as difference limen (DL) or just-noticeable difference (JND). Actually, this term is not only limited to intensity, can also be used for other stimulation parameters (frequency,

duration, number of pulses etc.). The relationship between the difference limen and the stimulus intensity is defined by Weber's law which states that the size of difference limen is a constant fraction of stimulus intensity [85].

Since biological systems are not fixed, the thresholds can not be defined using never/always approach. During repeated presentation of the same stimulus, the subject will detect it in some trials and will not detect it in the others. Thus, the measurement of threshold is a statistical procedure. A series of stimuli with varying intensities are presented to the subject randomly, and the probability of correct detection is calculated for each stimulus intensity. By fitting a sigmoid function to the data points, a psychometric function is obtained as in Figure 3.4 [85]. The threshold is generally defined as the stimulus intensity with 0.5 probability of correct detection. Despite that, in tactile psychophysics (also in this study), mostly stimulus intensity yielding 75% probability of correct detection is assumed as threshold depending on the task.

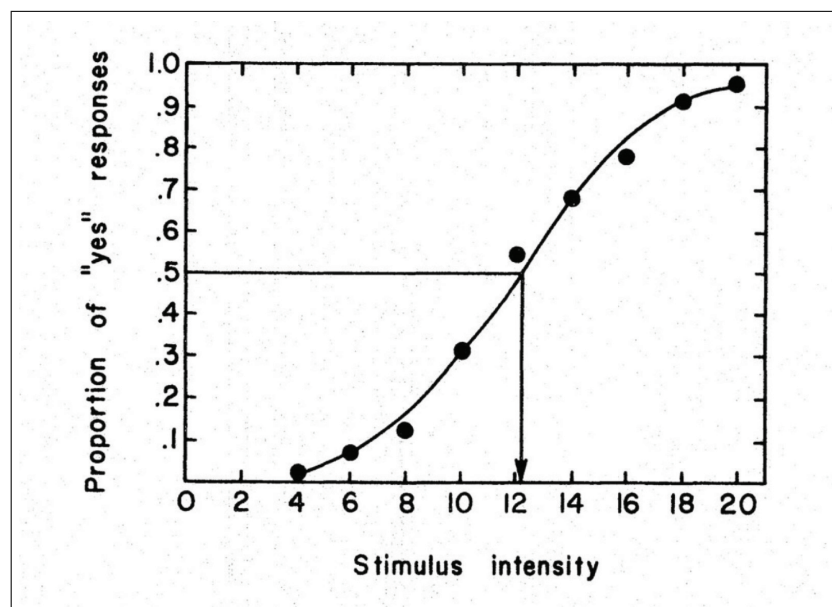


Figure 3.4 Psychometric function [85].

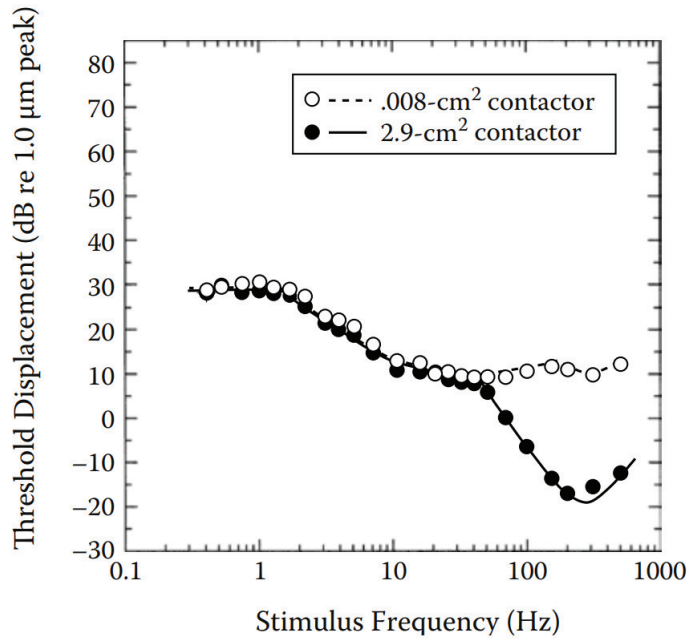
Well-established and standardized methods are used to measure human tactile thresholds which are method of constant stimuli, method of limits, method of adjust-

ment or staircase methods [85,95]. These can be applied either through yes/no task or forced choice tasks. In yes/no task, the stimulus is presented and the participant is asked whether she/he could detect the stimulus. In forced choice tasks, the participant is required to choose one of multiple options. In this study, we used method of constant stimuli and staircase method in a two-interval forced-choice task. According to the task, the stimulus is presented in one of two visually-cued time intervals and the participant is asked to choose the interval in which the stimulus was detected. For method of constant stimuli, the stimulus intensities are predefined and applied randomly. For staircase method, the stimulus intensity is started at a detectable level and changed following a tracking algorithm. We used modified three-down one-up rule in which the stimulus level is decreased one step after three not necessarily consecutive correct responses and increased one step after one incorrect response [119].

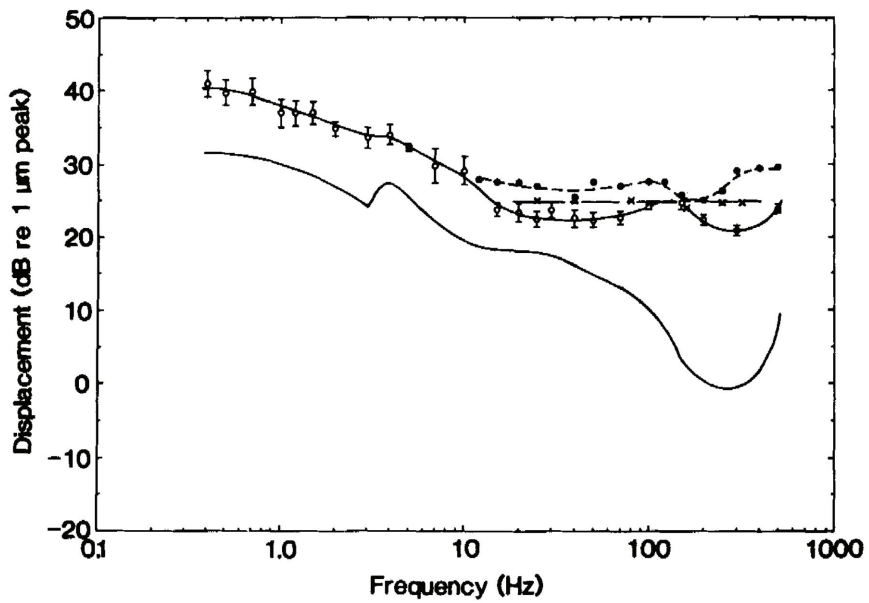
Threshold measurements provide information on the minimum physical energy required to produce a sensation, however they do not measure the sensation magnitude. In order to relate the parameters of physical energy with sensation level, psychophysical magnitude functions are produced by using scaling methods [85]. In this work, we used magnitude estimation method for subjective scaling of the sensation strength. In this method, participants are required to assign numbers to the sensation magnitude with an ordinal scaling. The responses are averaged and a magnitude estimate is obtained for each sensation level. The relationship between stimulus intensities and magnitude estimates are generally represented by a power law.

Psychophysics of vibrotactile stimulation has been studied in great detail previously and it was discovered that the thresholds and sensation strength are affected by a lot of factors [87–91] and depend on stimulation parameters [116,120–125]. First of all, the vibrotactile detection thresholds are frequency dependent for both glabrous (Figure 3.5(a)) and hairy skin (Figure 3.5(b)) and follows an U-shaped curve with the highest sensitivity at around 250 Hz [126–128]. However it is required to note that the frequency dependency is only for large contactor areas. For the small contactor sizes the vibrotactile thresholds remain same at higher frequencies as shown in Figure 3.5. The thresholds are also higher in the hairy skin compared to the glabrous

skin [89, 129–131].



(a)



(b)

Figure 3.5 Frequency sensitivity of a) glabrous skin [132] b) hairy skin. (open circles and solid line: 0.008 cm^2 contactor size, solid line only: 2.9 cm^2 contactor size. Remaining curves shows results from other studies) [130].

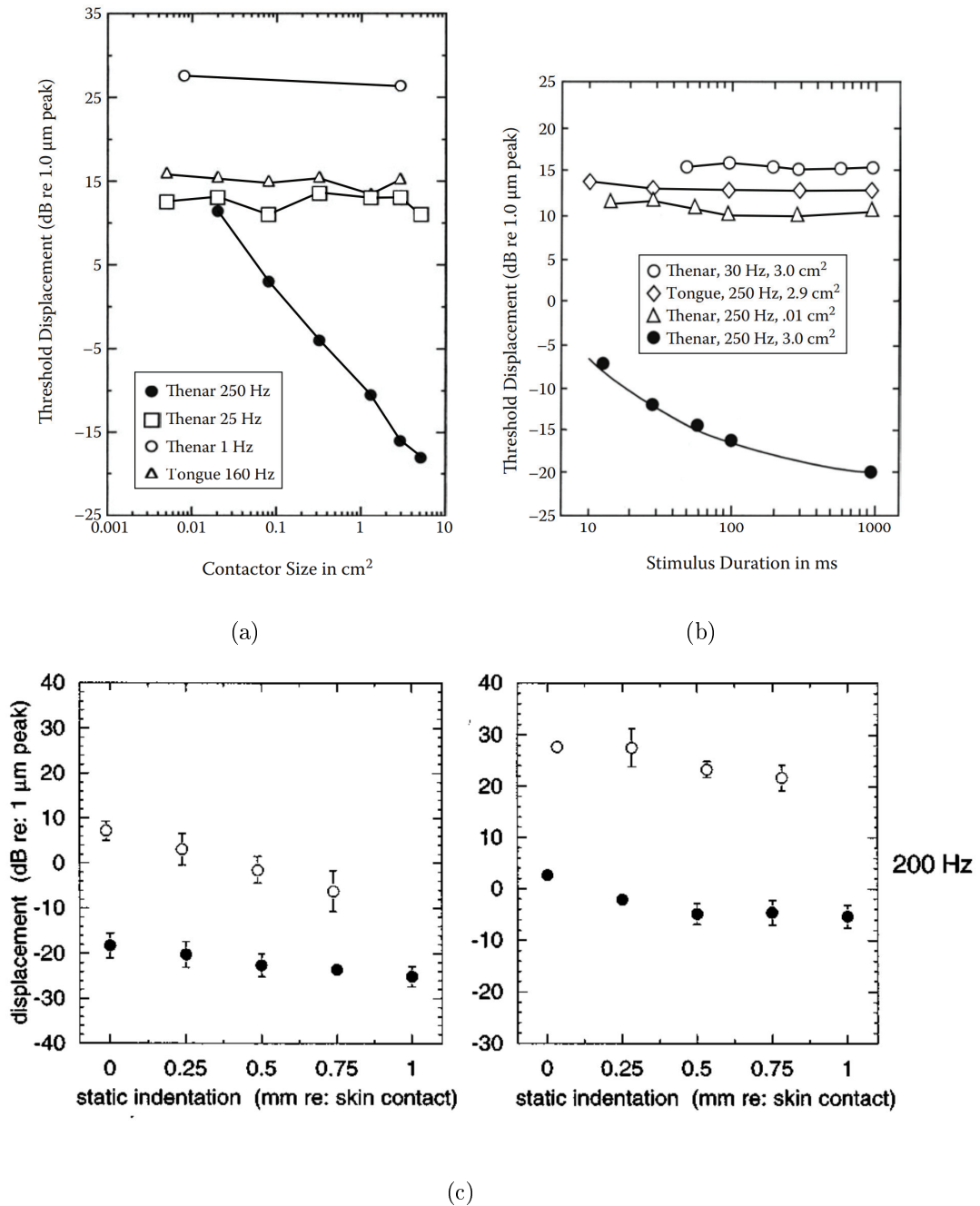


Figure 3.6 Effect of a)contactor size (glabrous skin) [132] b)stimulus duration (glabrous skin) [132] c)static indentation depth (left:glabrous skin, right:hairy skin) [133] on vibrotactile detection thresholds.

The vibrotactile thresholds are also affected by the size of contactor used for stimulation [120]. As it can be seen in Figure 3.6(a), the thresholds decrease with increased contactor size due to the spatial summation property of the tactile channels [126, 128, 134]. Figure 3.6(b) shows the effect of stimulus duration on vibrotactile

thresholds. As the stimulus duration increases, the threshold decreases because of the temporal summation property of the tactile channels [128, 135]. Static indentation depth of the contactor also has an effect on the thresholds. It can be seen in Figure 3.6(c) that the tactile thresholds decrease with increased static indentation both for glabrous and hairy skin.

For the applications with more than one stimulus simultaneously or successively, the tactile sensitivity is also affected by the temporal gap between two successive stimuli, masking effects and spatial distance between the stimulation sites [136–140].

3.2 Material and Methods

The work presented here has been published as:

İ. Karakuş, B. Güçlü, "Psychophysical principles of discrete event-driven vibrotactile feedback for prostheses", *Somatosensory and Motor Research*. Published online: 25 May 2020, DOI: 10.1080/08990220.2020.1769055.

3.2.1 Participants

Ten able-bodied adults (5 male, 5 female, age range: 24-33, mean: 26.9 years, all but one right-handed) participated in the study (S1-10). None of them had dermatological, neurological or psychiatric disorder that could affect experimental results. The experimental procedures were approved by the Institutional Review Board for Research with Human Subjects of Boğaziçi University and written consents were given by the participants. All participants performed the psychophysical characterization and same-different task. S4 did not attend the vibrotactile pattern recognition task. Discrete-event driven feedback experiments were conducted with seven participants (except S1, S4, S5).

3.2.2 Vibrotactile actuators and instrumentation

Electromagnetic recoil-based vibrotactile actuators (Haptuator Mark-IIC; Tactile Labs Inc., Montreal, Canada) with the characteristics given in (Figure 3.7) were used to apply vibrotactile stimuli. Two actuators were used on upper arms and custom made mounts were produced from a rubber foam to place the actuators perpendicularly to the skin (Figure 3.8(a)). Our preliminary experiments showed that it is difficult to maintain stimulus control at submicrometer level by using the actuator casing as a contactor; therefore, small plastic probes (diameter: 2 mm) were glued to the moving armature of the actuators for stimulation of the skin. The actuators were placed on lateral surfaces of the participant's upper arms by straps (Figure 3.8(b)).

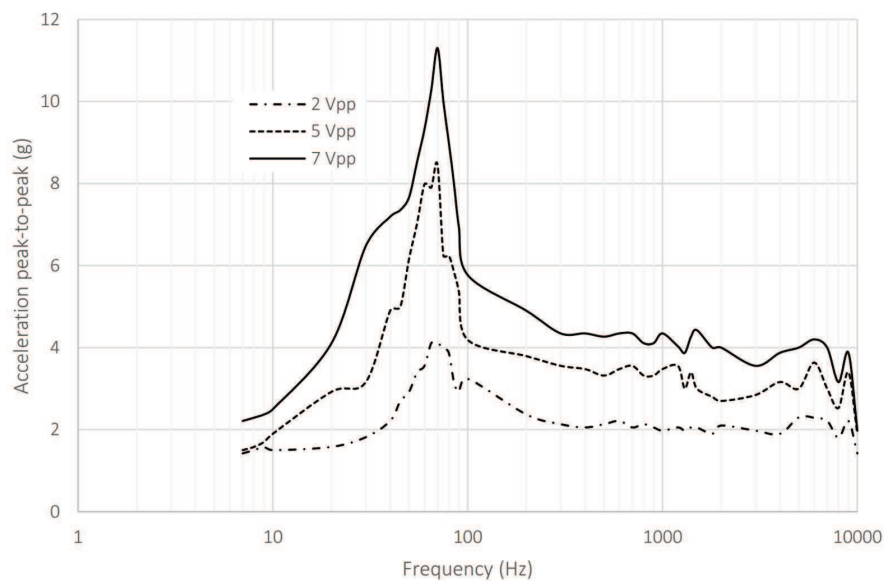
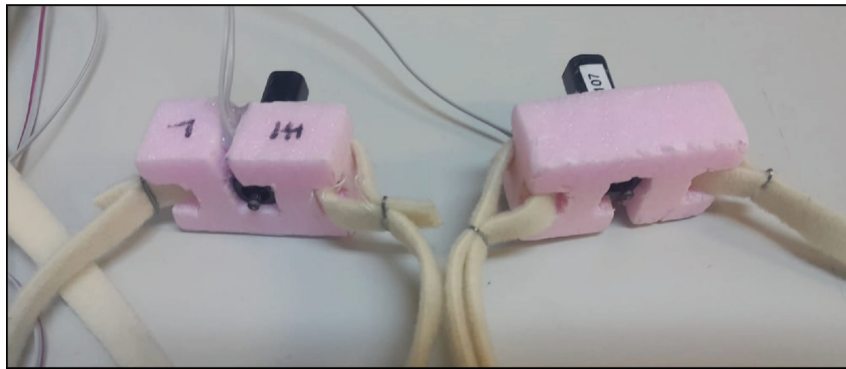
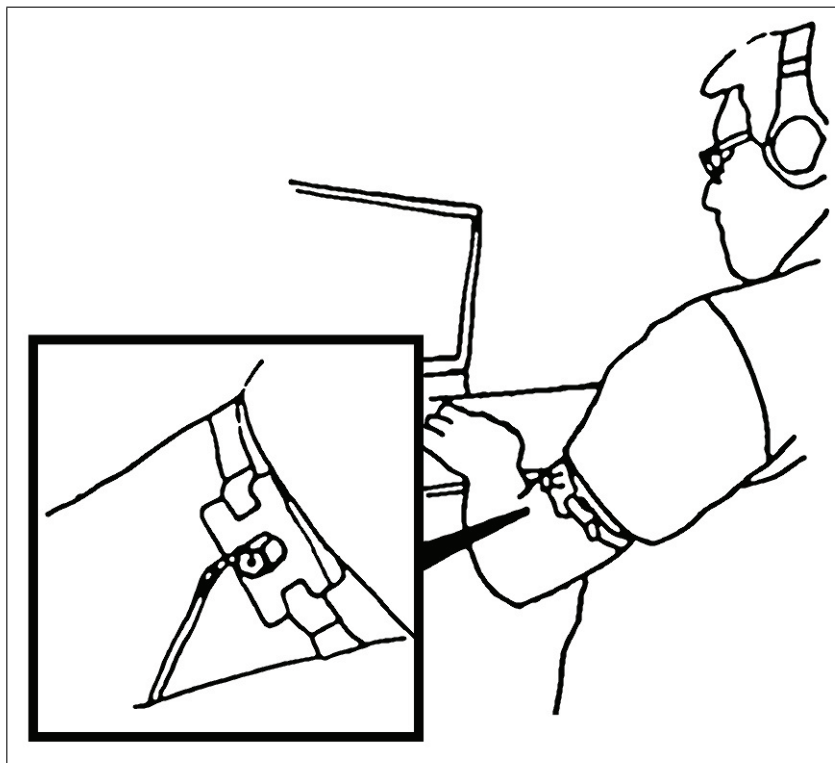


Figure 3.7 Characteristics of vibrotactile actuator.



(a)



(b)

Figure 3.8 a) Actuators on the mounting strap. b) Actuators on participant's arm.

A custom-made audio power amplifier was designed and used to drive the actuators. Actuators were calibrated using a photonic sensor (MTI-2100; MTI Instruments, Albany, NY, USA) at 80 Hz and 180 Hz prior to the experiments. The calibration curves are given in Figure 3.9.

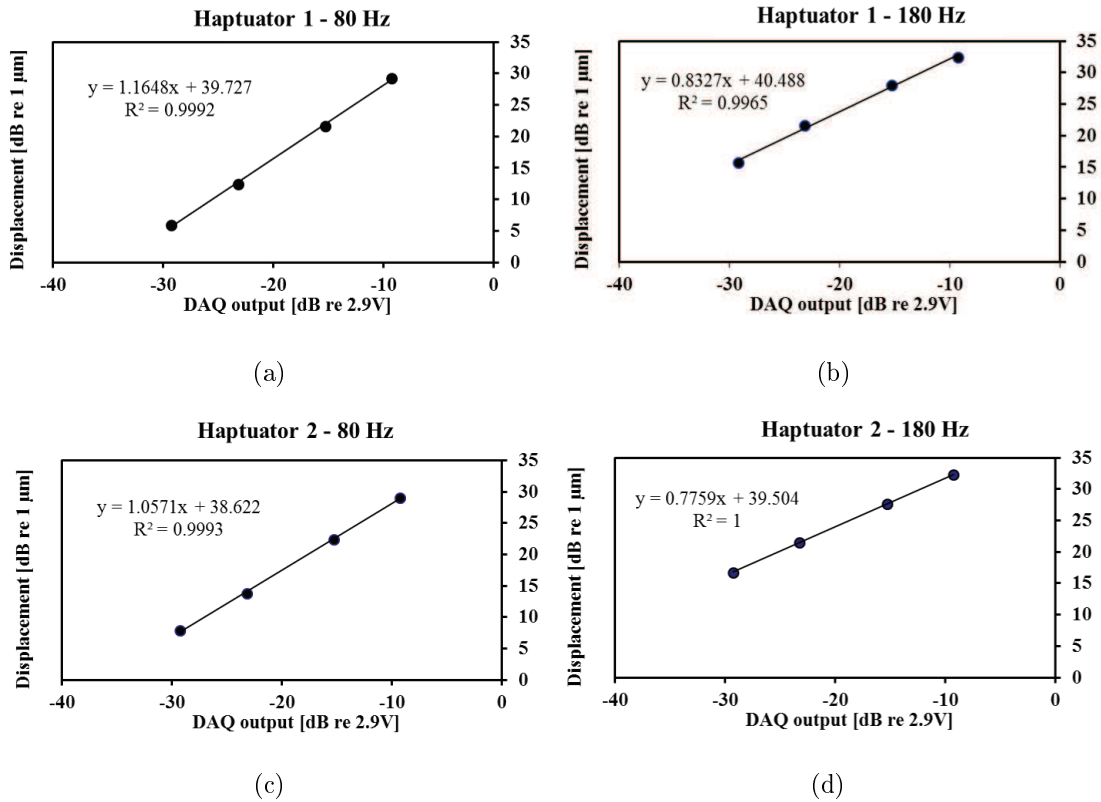


Figure 3.9 Actuator calibration curves. a) Haptuator-1 at 80 Hz b) Haptuator-1 at 180 Hz c) Haptuator-2 at 80 Hz d) Haptuator-2 at 180 Hz.

The experimental procedures were programmed in MATLAB (Release 2008, The MathWorks Inc.) and run on a desktop computer. The necessary images/icons were presented on the computer screen and the participant responses were obtained by the computer keyboard. The stimulus waveform was generated by a data acquisition card (NI USB-6259, National Instruments, Austin, Texas, USA). During the experiments, white noise was applied through headphones in order to mask the sound resulted from the actuators (named Haptuator-1 and -2 from now on).

3.2.3 Vibrotactile stimuli and the representation of discrete events

The vibrotactile stimuli were generated with a sampling frequency of 5 kHz at 16-bit resolution. The vibrotactile stimuli were sinusoidal displacements at 80 Hz and

180 Hz, generated as cosine-squared bursts with 50 ms rise and fall times. The stimulus duration was 0.5 s (measured between half power points) and the waveform was not changed during whole procedure. The stimulation frequencies (f_1 , f_2) were chosen as 80 Hz and 180 Hz considering the actuator specifications given in actuator device datasheet and the frequency discrimination thresholds in the human hairy skin [141]. Stimulation magnitudes (a_1 and a_2) were determined for each subject specifically through a set of psychophysical experiments

As it was explained in Chapter 2, we classified the sensor data for object-type (no object, soft object and hard object) and movement-type (stationary, flexion, extension, contact and release) previously [79]. For the work presented in this chapter, those classes were mapped to stimulus parameters (Table 3.2) regarding discrete hypothetical prosthesis events.

Table 3.2
Representation of discrete events.

	Event (code)	Magnitude	Frequency
Haptuator-1 (object-type/force related feedback)	Soft object/Low force (AL)	a_1	f_1
	Soft object/High force (CL)	a_2	f_1
	Hard object/Low force (BL)	a_1	f_2
	Hard object/High force (DL)	a_2	f_2
	No force (O)	-	-
Haptuator-2 (movement-type related feedback)	Flexion/No object (AR)	a_1	f_1
	Flexion/In object (CR)	a_2	f_1
	Extension/No object (BR)	a_1	f_2
	Extension/In object (DR)	a_2	f_2
	Stationary (O)	-	-

Haptuator-1 (for the left upper arm) was assigned to signal object-type and force-related discrete events. At the sinusoidal frequency of f_1 , the magnitude of a_1 represented manipulating a soft object with low force, whereas a_2 represented manipulating a soft object with high force. At the sinusoidal frequency of f_2 , similar represen-

tations of magnitude were used for manipulating a hard object. If Haptuator-1 was not actuated, this represented no contact force for a hypothetical prosthesis. On the other hand, Haptuator-2 (for the right upper arm) was assigned to signal movement-type discrete events. Sinusoidal frequency of f_1 and f_2 represented flexion and extension, respectively. Magnitudes of a_1 and a_2 represented movement in air (no object) and in object, respectively. If Haptuator-2 was not actuated, this signalled a stationary hypothetical prosthesis. It is important to note that Haptuator-1 and -2 were actuated sequentially in the final experiment. Although Haptuator-1 can imply object manipulation by itself, it was not actuated continuously, because the discrete events refer to transitions between states (see below). Therefore, manipulation with objects was also signalled with Haptuator-2 by using the parameter a_2 to reduce cognitive load. Contact and release events were represented implicitly by using the low-force events signalled by Haptuator-1.

3.2.4 Psychophysical characterization of participants

As it was stated previously, the psychophysical measures vary across participants (e.g. 10-15 dB in absolute and masked detection thresholds) [81,82] and sensation magnitudes are subjective [85,86]. Thus, it is important to calibrate a non-invasive vibrotactile feedback system for each user, and possibly before each use if the device is re-attached. In this study, we designed a psychophysical characterization procedure which was performed for each participant prior to the experiments. The overall characterization and experimental procedure is given in Figure 3.10.

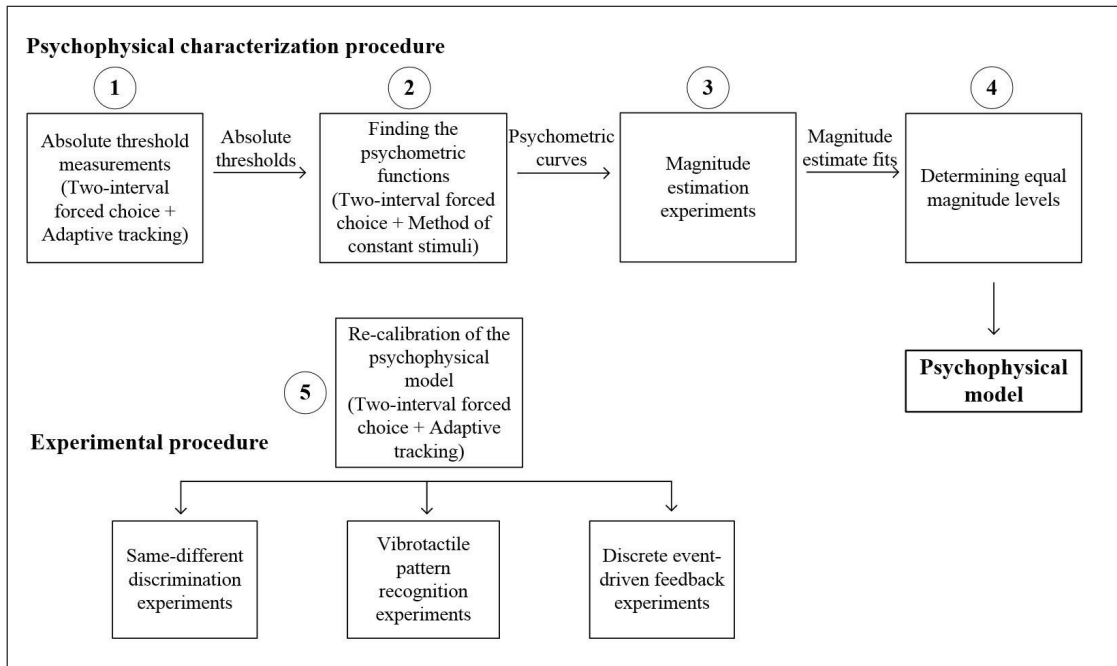


Figure 3.10 Psychophysical characterization and experimental procedures.

3.2.4.1 Absolute detection thresholds . Absolute detection thresholds were measured for each vibrotactile frequency ($f_1 = 80$ Hz and $f_2 = 180$ Hz) and each site/actuator (Haptuator-1 and Haptuator-2) in a two-interval forced-choice task by using the adaptive tracking method [91, 142]. Two time intervals (2 s) were cued to the participant by red and green squares shown on the computer screen. The stimulus was presented in either red-cued or green-cued interval and the participant was asked to select the interval in which the stimulus was detected. The participant responded in the yellow-cued interval by pressing the corresponding keys on the keyboard. If the response was correct, the yellow square blinked. The stimulus intensity in each trial was determined following an adaptive tracking algorithm with modified three-down one-up rule [119]. According to the rule, the stimulus intensity was decreased one step after three correct responses (not needed to be consecutive), and increased one step after one incorrect response. The experiment was started with a clearly sensible stimulus intensity and step size was 5 dB at the beginning. It was changed to 1 dB after the first incorrect response (reversal). The algorithm stopped automatically if the stimulus level was in the range of ± 1 dB for the last 20 trials. The threshold was recorded by

choosing the middle value in this range. This resulted a 75% detection threshold [119]. The threshold measurement was repeated two times and the results were averaged. The timing diagram of the two interval forced choice task is given in Figure 3.11.

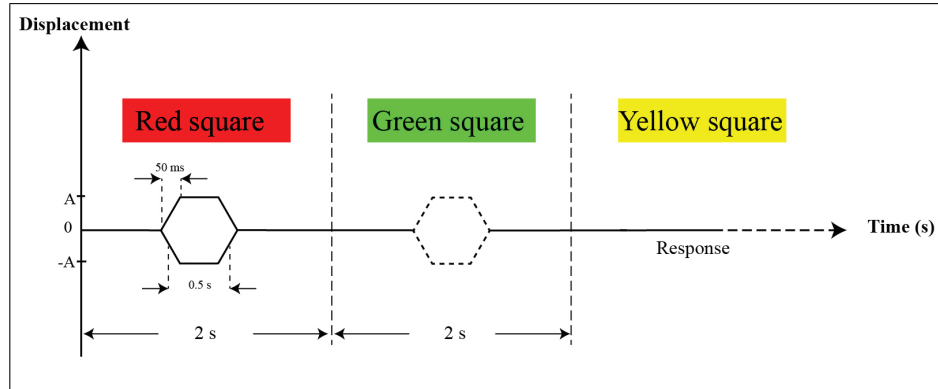


Figure 3.11 Stimulus timing diagram of two-interval forced-choice task.

3.2.4.2 Psychometric functions. Psychometric functions [85] were obtained to understand the level at which the vibrotactile stimuli become detectable with probability ~ 1 . Using the absolute thresholds measured in the previous experiment, a stimulus intensity range was determined. Five stimulus levels were selected (one at detection threshold from adaptive tracking, one below threshold and three above threshold) and presented with method of constant stimuli in a two interval forced choice task. The timing diagram was the same as explained in the previous step (Figure 3.11). However the stimulus intensity in each trial was chosen randomly as one of the five selected levels. 40 repetitions were applied randomly for each stimulus level.

The probability of correct detection was calculated for each stimulus level and a sigmoid function was fitted to experimental data (Eq. 3.1). From the obtained psychometric function, the saturation level was calculated (the stimulus amplitude yielding detection probability of 0.99).

$$p(c) = \left(0.5 + \frac{0.5}{1 + e^{-(A-\alpha)/\beta}} \right) \quad (3.1)$$

In Eq. 3.1, p is the probability of detection and A is the stimulus amplitude. α

is the amplitude at which $p = 0.75$, i.e. the threshold derived from the psychometric function. The slope at this amplitude is $1/(4\beta)$.

3.2.4.3 Subjective magnitude estimates. It was discovered from the results of the previous psychophysical studies [85] that, the perceived stimulus magnitude is subjective. The growth of sensation as a function of stimulus amplitude can reproducibly be measured in a given participant, and is typically described as a power law [86]. Different stimulus frequencies and stimulation sites may result in different power laws [80]. In order to obtain power laws for each participant, magnitude estimation experiments were performed as a part of psychophysical characterization procedure.

Four stimulus amplitudes which were above saturation level were selected. Each level was applied randomly 25 times with the timing given in Figure 3.12 and the participant was asked to assign a positive number to the sensation magnitude. The range of positive numbers was not limited, and use of decimals and fractions were allowed. The responses were averaged for each stimulus level and divided by the grand average of responses to all trials. Thus, a normalized magnitude estimate was obtained for each stimulus intensity. To fit a power function, a straight line was fitted to the logarithm (base 10) of normalized magnitude estimates as a function of sensation level (SL: dB above the threshold from psychometric function). The experiment was conducted for each vibrotactile frequency and stimulation site separately.

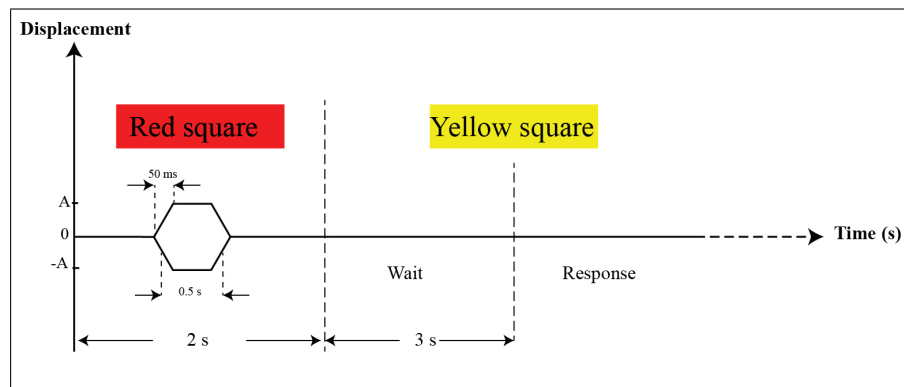


Figure 3.12 Stimulus timing diagram of magnitude estimation task.

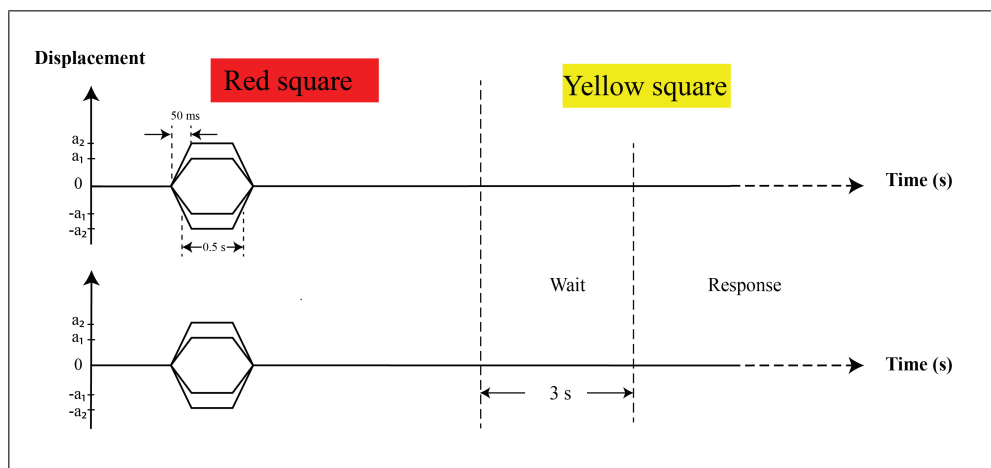
3.2.4.4 Equal magnitude levels. A magnitude equalization procedure was applied to achieve vibrotactile feedback effect independent of participant's psychophysical and biomechanical (due to actuator-skin coupling) properties. It was aimed to create approximately the same sensation magnitude at a given stimulus amplitude regardless of vibrotactile frequency and stimulation site.

We selected two magnitude levels on the y-axes of four power functions (f_1 and f_2 of Haptuator-1 and -2) obtained from each participant. Those levels were separated as much as possible, considering the psychophysical and actuator limits. The corresponding eight sensation levels were converted to stimulus amplitudes, relative to the thresholds from psychometric functions. These amplitudes were applied as a_1 and a_2 at each stimulus condition. In other words, a_1 referred to a different amplitude for each frequency-site pair, but it always produced approximately the same sensation magnitude. Similarly, a_2 referred to different amplitudes, but approximately the same sensation magnitude at each condition; and was larger than that of a_1 .

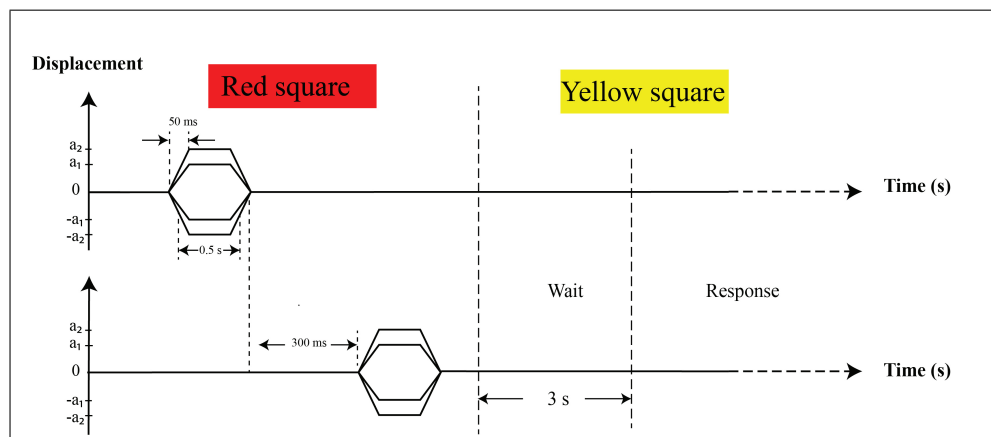
3.2.4.5 Re-calibration of the psychophysical model: . Ideally, the stimulus amplitudes should be re-adjusted after re-attachment of the device due to the changes in tactile sensitivity and contact conditions. It is not practical because of the considerable time and effort spent for psychophysical characterization procedure. Since the model (the SL values yielding equal magnitude levels at different stimulus conditions) is set relative to the absolute detection thresholds and assumed to be constant, re-calibration step can be done just by a quick absolute threshold measurement. The stimulus amplitudes can be re-calculated using the model SLs, referencing to the measured threshold. This procedure was applied at the beginning of the following experiments for each participant.

3.2.5 Same-different discrimination experiments

Subsequent to psychophysical characterization, same-different experiments were conducted to test if the stimuli used were discriminable in magnitude and frequency dimensions. Prior to the experiments, a localization test was run to validate that all signals were perceivable. All stimulus types were presented randomly to either right or left arm and the participant was asked to tell the site of stimulation. The same different experiments were performed for simultaneous (Figure 3.13(a)) and successive stimulation (Figure 3.13(b), interstimulus interval: 300 ms) of the arms.



(a)



(b)

Figure 3.13 Stimulus timing diagram of the same different discrimination task. a) Simultaneous stimulation b) Successive stimulation.

For magnitude discrimination task, the frequencies of the two stimuli at each trial were the same, while the magnitudes were different (a_1 and a_2). Oppositely, in frequency discrimination task the stimulation magnitudes were the same in each trial, but the frequencies were different (f_1 and f_2). The participant decided if the two stimuli were the same or different regarding the target parameter. Same-stimuli trials and catch trials (i.e. single-site stimulation trials) were also included. Participants responded by pressing keys (S: same, D: different, X: single-site). Each simultaneous or successive stimulation experiment included 200 trials (80 same and 80 different trials with 20 repetitions of each pair, 40 catch trials with 5 repetitions of each stimulus type).

3.2.6 Vibrotactile pattern recognition experiments

The vibrotactile feedback procedure explained previously (Table 3.2) is applied as short-lasting stimulus at the beginning of each discrete event. Thus, the recognition of different stimulus patterns is needed in the final part of the study. In order to set a psychophysical baseline for the recognition rate of stimulus patterns, a set of experiments were conducted without including information on discrete events. First, the participants were trained to match each vibrotactile stimulus type with a visual representation (a sine wave with corresponding magnitude and frequency cue). The images were displayed on the computer screen simultaneously with the stimuli. We generated the test patterns considering the possible consecutive discrete-events (Table 3.2) and grouped into four:

- (i) One-pattern stimulation: only one site was stimulated
- (ii) Two-pattern, same-site stimulation: the same arm was stimulated successively
- (iii) Two-pattern, right-first stimulation: both sites were stimulated successively with the right arm first
- (iv) Two-pattern, left-first stimulation: both sites were stimulated successively with the left arm first

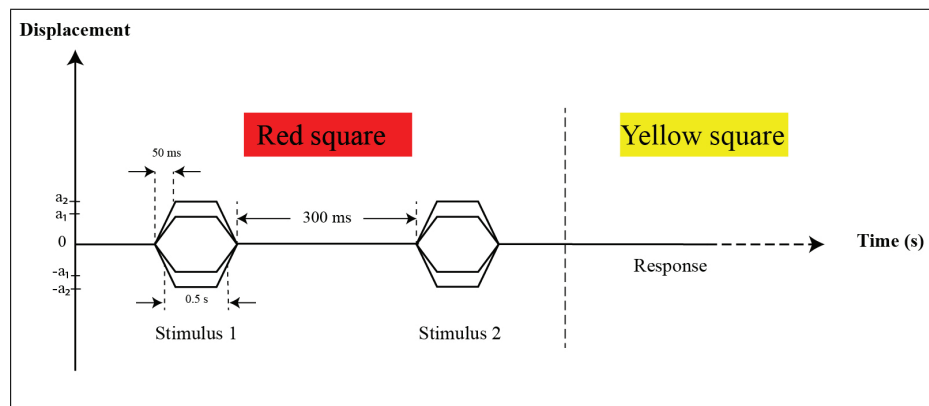


Figure 3.14 Stimulus timing diagram of vibrotactile pattern recognition task.

The successive stimuli were presented with an interstimulus interval of 300 ms (Figure 3.14) and the participant was required to select the vibrotactile pattern from a list of images. Images of some patterns were given in Figure 3.15. The actuators were represented with different colors (Haptuator-1: red, Haptuator-2: blue). The magnitude (a_1 or a_2) and frequency (f_1 or f_2) of the stimulus were shown through a sine-wave representation.

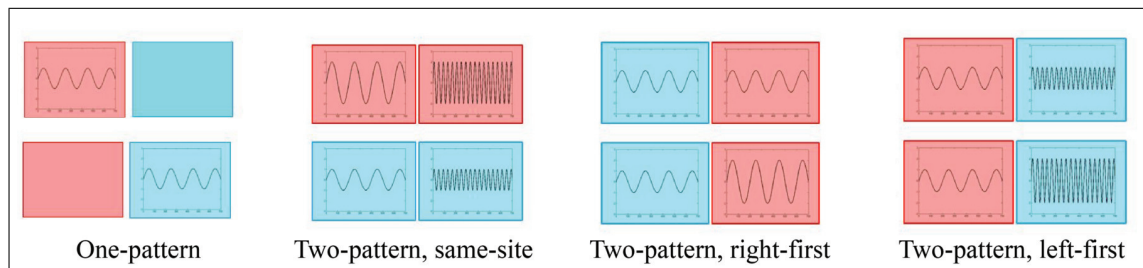


Figure 3.15 Images representing eight of vibrotactile patterns for different stimulation types.

Catch trials were also included to prevent some patterns being easily recognizable (e.g. being the only pattern with low amplitude and low frequency in the list). The catch trials were only presented in the image list and not used as stimuli during the experiment. The experiments included 400 trials (80, 100, 120, 100 trials for Group i, Group ii, Group iii and Group iv respectively, 10 repetitions for each pattern) and was completed in one session (2.5 hours with breaks) for each participant.

3.2.7 Discrete event-driven feedback experiments

Discrete event-driven feedback experiments were conducted to test if the patterns were recognizable when the discrete events in Table 3.2 were also included rather than only representative images of vibrotactile patterns.

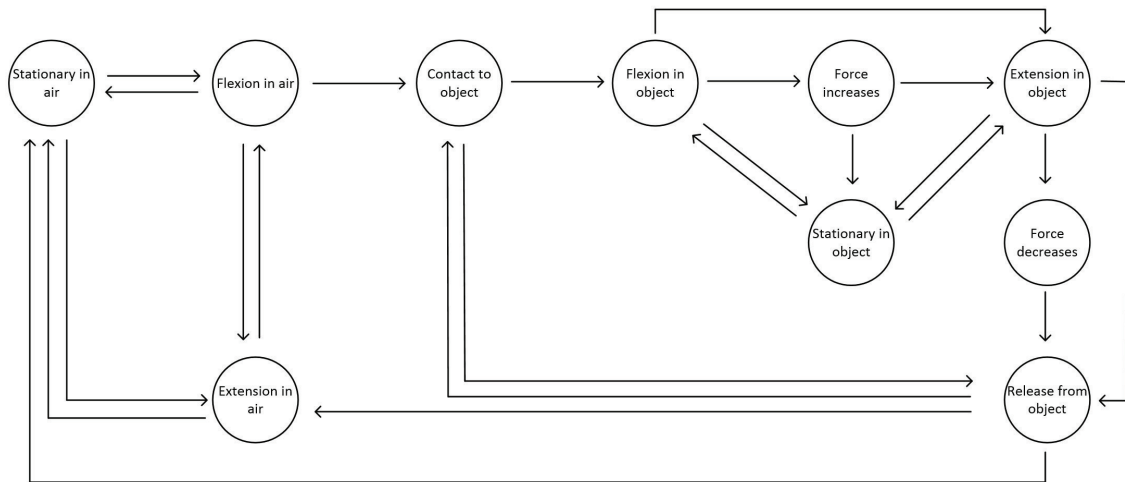


Figure 3.16 Full movement cycle of the robotic hand showing the almost all possible transitions between events.

In Figure 3.16, almost all possible transitions (discrete events) between states in a cylindrical grasping movement are shown. In the experiments, the transition to a state was represented by a picture on the computer screen (Figure 3.17). The participants were informed about the pictures before the experiment and trained to match the vibrotactile stimuli with those pictures. For the testing, 14 sequences consisting two or three consecutive discrete events were selected. The vibrotactile patterns were presented with 300 ms interstimulus intervals (Figure 3.18) and the participant was required to select the sequence from a list of pictures. The experiment included 140 trials (10 repetitions for each sequence) and lasted 2.5 hours with breaks.

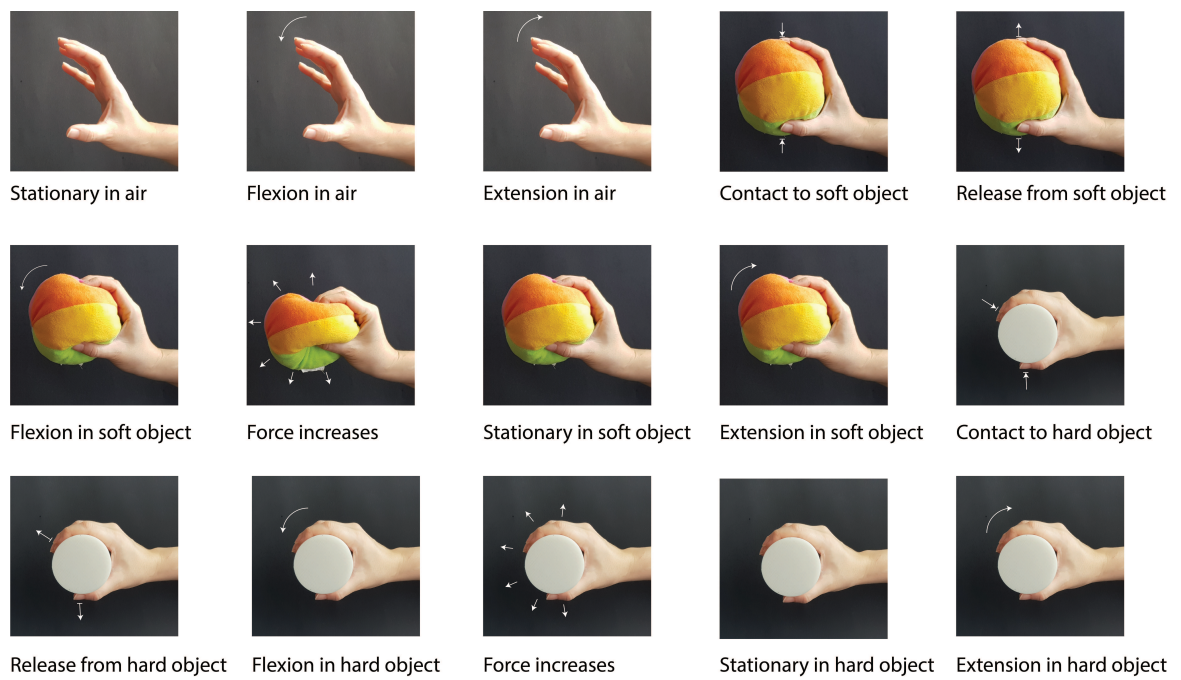


Figure 3.17 Pictures representing discrete events.

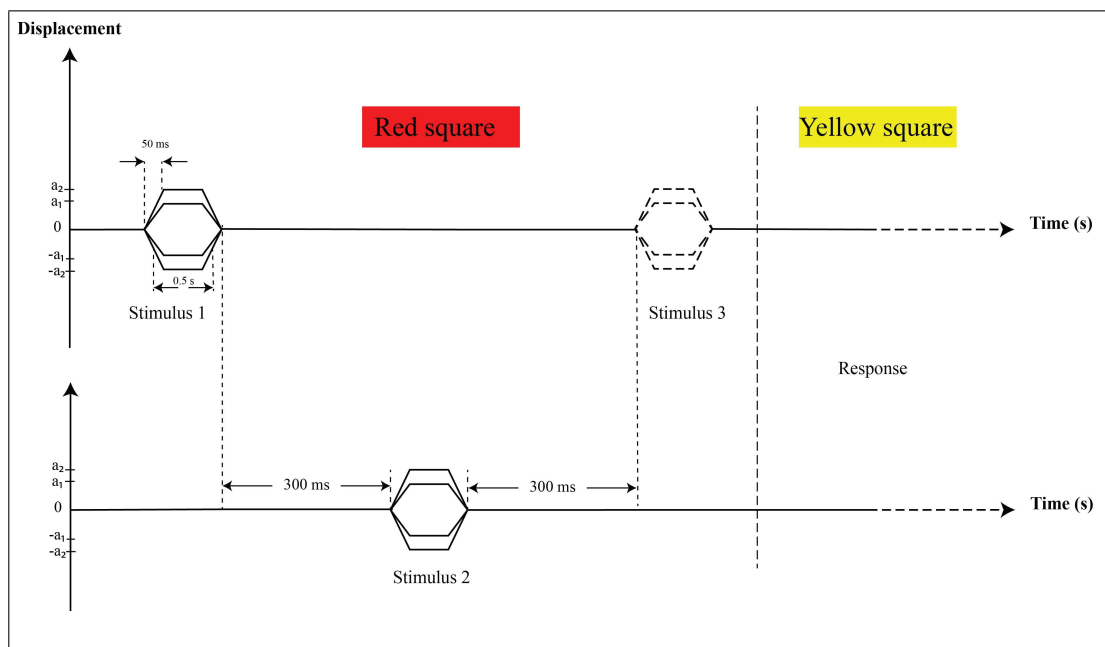


Figure 3.18 Stimulus timing diagram of discrete event-driven feedback experiment.

3.2.8 Statistical analyses

Experimental data were analyzed in MATLAB and SPSS (Ver. 25, IBM, Armonk, NY, USA). Absolute detection thresholds in dB were converted to micrometer units. The differences in means of thresholds were analyzed with repeated measures ANOVA using stimulus frequency (80 Hz vs. 180 Hz), stimulus site (left vs. right arm), and measurement session (four adaptive tracking measurements and one method of constant stimuli measurement) as within-subject factors. Additionally, multifactorial effects on α and β parameters of the psychometric functions were studied using repeated measures ANOVA with stimulus frequency and site as within-subject factors. The slopes and intercepts of power functions for the magnitude estimates were analyzed similarly based on the same factors. The accuracies in the same-different discrimination experiments were also tested in a multifactorial model based on repeated measures ANOVA. Here, the comparison parameter (magnitude vs. frequency), presentation method (simultaneous vs. successive), and trial type (same vs. different) were set as within-subject factors. Separate one-way ANOVAs were performed for the class-averaged recall, precision, and F1 scores of the classification results in the pattern recognition experiments. These performance scores were calculated as the following for a class C:

$$Recall = \frac{\text{true class } C \text{ responses}}{\text{all responses given to actual } C} \quad (3.2)$$

$$Precision = \frac{\text{true class } C \text{ responses}}{\text{all responses given as } C} \quad (3.3)$$

$$F1 \text{ score} = 2 \times \frac{Precision \times Recall}{Precision + Recall} \quad (3.4)$$

The factor in these experiments was the type of stimulation (one pattern, two-pattern same-site, two-pattern right-first, two-pattern left-first). Additionally, proportions of correct responses in the confusion matrices were compared to chance level by the z-test with Bonferroni correction. For the confusion matrices, the homogeneity of the proportion of predicted classes was assessed by the chi-squared test. Although

not necessarily pointing to the correct class, rejection of the null hypothesis in this test implies that the predicted class proportions change for each target class. This is equivalent to some dependence between target and predicted classes. Results from the discrete-event driven feedback experiments were analyzed with methods similar to those used for the pattern recognition experiments. Classification performance metrics from those two types of experiments were also compared by using Wilcoxon signed rank test. Additionally, the relationship between differences of magnitude estimates (i.e. those corresponding to a_1 and a_2) and performance metrics was studied across the participants by using Pearson correlation.

3.3 Results

3.3.1 Psychophysical characterization

Psychophysical characterization and experimental procedures required measurement of absolute detection thresholds with two methods at different days. Figure 3.19 shows the thresholds of all participants for each vibrotactile frequency and stimulation site. The first and second bars represent the thresholds from adaptive tracking and psychometric function respectively. The remaining three bars are thresholds measured for the re-calibration procedure by using adaptive tracking. The y-axes are plotted in dB referenced to $1 \mu\text{m}$.

For statistical analyses, the absolute thresholds in dB were converted to micrometers and averaged across seven participants who performed all experiments (Table 3.3). The differences in means of thresholds were tested with repeated measures ANOVA. None of the factors (frequency, site and measurement type) had a significant effect on thresholds. No interactions were also found between within-subject factors. The lack of effect of site and measurement type shows that the psychophysical characterization and re-calibration approaches are reliable. The similarity of thresholds for different frequencies is also consistent with the literature for the small contactor sizes [129].

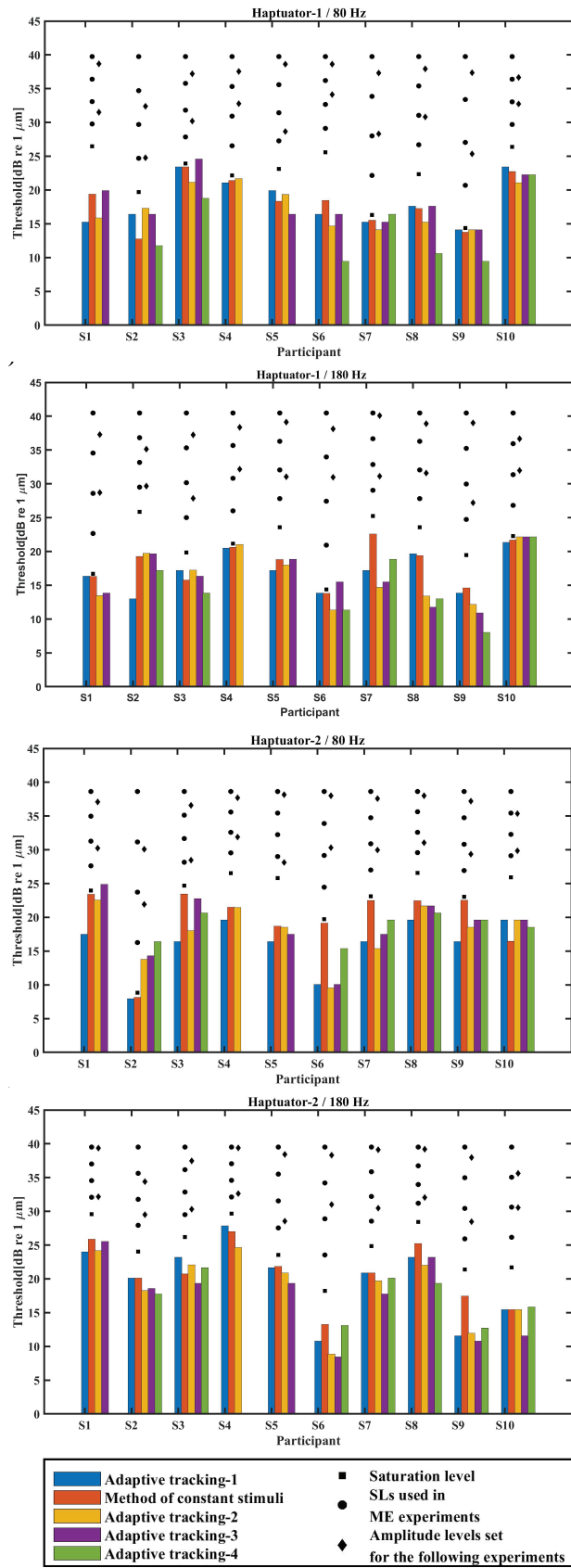


Figure 3.19 Absolute threshold measurements and important stimulus levels of psychophysical characterization.

Table 3.3

Average absolute detection thresholds of the participants who attended to all procedures.

		Haptuator-1		Haptuator-2	
		80 Hz	180 Hz	80 Hz	180 Hz
Adaptive tracking-1	Mean	8.766	7.150	6.379	9.045
	Std. Error	1.592	1.019	1.040	1.777
Method of constant stimuli	Mean	8.490	8.645	10.450	9.764
	Std. Error	1.585	1.261	1.713	1.708
Adaptive tracking-2	Mean	7.351	6.806	7.413	7.980
	Std. Error	1.080	1.277	1.163	1.499
Adaptive tracking-3	Mean	8.804	6.906	8.697	7.121
	Std. Error	1.673	1.246	1.407	1.583
Adaptive tracking-4	Mean	5.924	6.344	8.798	7.755
	Std. Error	1.429	1.344	0.730	1.105

The parameters of psychometric curves are given in Table 3.4 for all participants. R^2 values indicate that the fits were very good for all conditions and participants. The parameter α corresponds to the 0.75 probability of correct detection (threshold) and β is related to the slope of the curve. For Haptuator-1, the mean alpha values are $8.9 \pm 1.1 \mu\text{m}$ and $9.0 \pm 1.1 \mu\text{m}$ for 80 Hz and 180 Hz, respectively. They are $10.6 \pm 1.4 \mu\text{m}$ and $12.2 \pm 1.9 \mu\text{m}$ for Haptuator-2 at 80 Hz and 180 Hz, respectively. From the mean beta values, the slopes ($1/(4\beta)$) are calculated as $0.21 \mu\text{m}^{-1}$ and $0.18 \mu\text{m}^{-1}$ at 80 Hz and 180 Hz respectively for Haptuator-1. For Haptuator-2, they are $0.21 \mu\text{m}^{-1}$ and $0.13 \mu\text{m}^{-1}$ at 80 Hz and 180 Hz respectively. The differences in means of α and β parameters were tested by using repeated measures ANOVA. The effects of neither frequency nor site on the parameters was significant. There was also no interaction between stimulation site and frequency.

Table 3.4
Parameters of psychometric functions for all participants.

Participant	Haptuator 1 - 80 Hz			Haptuator 1 - 180 Hz		
	α	β	R^2	α	β	R^2
S1	9.405	2.850	0.955	6.510	0.125	0.978
S2	4.387	1.294	0.994	9.015	2.989	0.948
S3	14.825	0.232	0.975	6.086	1.033	0.958
S4	12.012	0.389	0.982	13.827	3.092	0.984
S5	8.300	1.470	1.000	8.769	1.847	0.997
S6	8.464	2.557	0.995	4.901	0.104	0.947
S7	5.968	0.122	0.954	13.609	1.192	0.988
S8	7.314	1.349	0.997	9.299	1.733	0.960
S9	4.874	0.090	0.938	5.446	1.267	0.997
S10	13.756	1.727	1.000	12.224	0.255	0.998
Mean	8.930	1.208		8.969	1.364	
Std. Error	1.139	0.315		1.050	0.341	
Participant	Haptuator 2 - 80 Hz			Haptuator 2 - 180 Hz		
	α	β	R^2	α	β	R^2
S1	14.754	0.263	0.981	19.500	2.569	0.918
S2	2.545	0.050	0.974	10.123	1.752	0.996
S3	15.203	0.296	0.987	10.718	2.706	0.994
S4	11.928	2.368	0.994	22.303	2.216	0.996
S5	8.615	2.745	0.996	12.505	0.990	0.997
S6	6.294	0.117	0.981	4.718	1.150	0.988
S7	13.455	0.184	0.954	11.084	2.004	0.997
S8	13.275	2.088	0.929	18.034	2.086	0.998
S9	13.456	0.234	0.990	6.996	1.225	0.979
S10	6.679	3.292	0.999	5.905	1.978	1.000
Mean	10.620	1.164		12.189	1.868	
Std. Error	1.360	0.409		1.885	0.186	

Example psychometric functions for one participant (S1) are given in Figure 3.20. Filled circles are data points from the experiments, and solid lines represent the fitted sigmoid functions. The thresholds (0.75 probability of detection) are marked with

empty circles. The stimulus amplitudes with 0.99 probability of detection (saturation) were calculated from the psychometric functions (represented by empty squares) to select higher levels in the subsequent experiments. The psychometric functions of all participants can be seen in Appendix B.

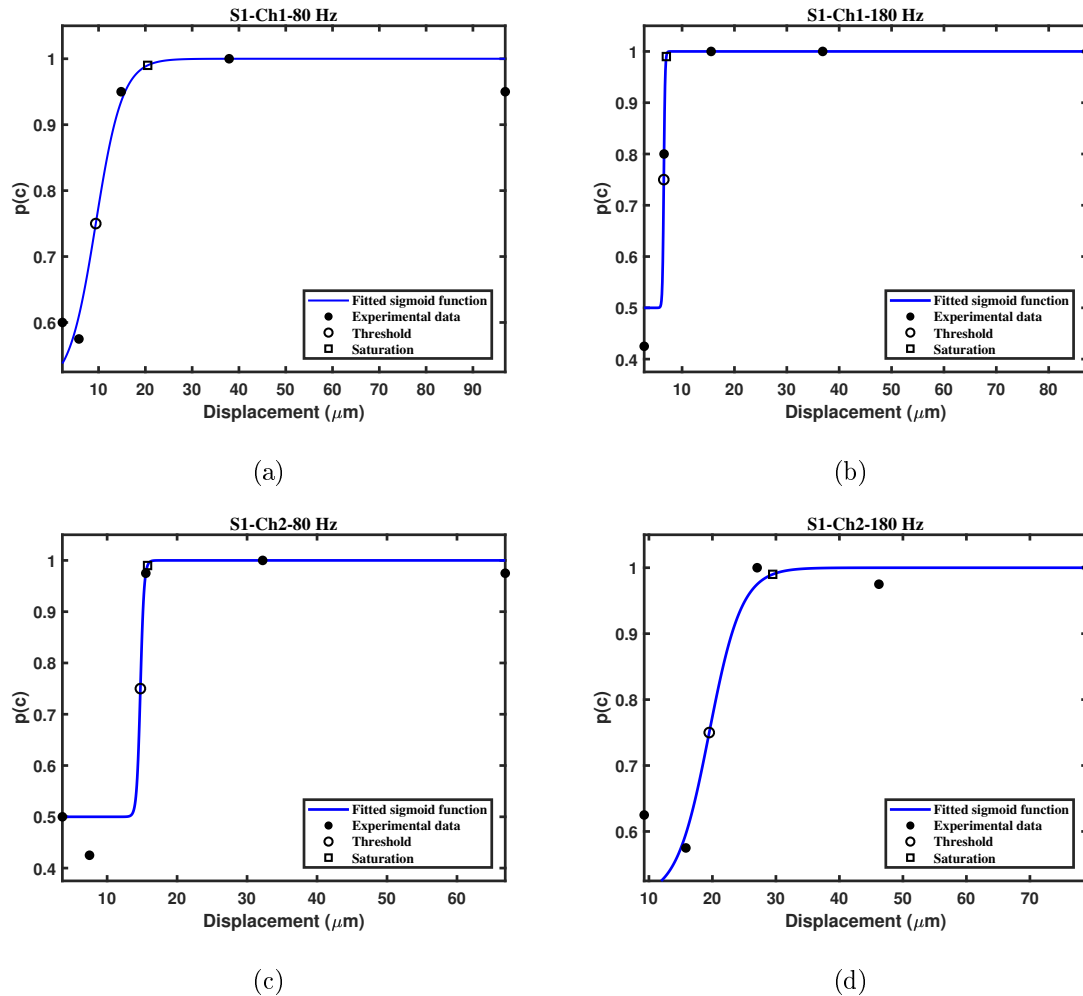


Figure 3.20 Psychometric functions for S1. a) Haptuator 1 - 80Hz b) Haptuator 1 - 180Hz c) Haptuator 2 - 80Hz d) Haptuator 2 - 180Hz.

Four stimulus levels were selected (filled circles in Figure 3.19) above saturation to be used in magnitude estimation experiment. For deriving the power functions for magnitude estimation, the stimulus levels (A) were referred to the threshold (A_{th}) of each participant, i.e. as sensation level (SL in dB: $20 \log_{10}(A/A_{th})$). Power functions at logarithmic x- and y-axes result in straight lines. Table 3.5 shows the linear fits to base-10 logarithm of normalized magnitude estimates as a function of SL with high R^2

values. Considering power functions of the form $M = k(A/A_{th})^\gamma$ in which M is the normalized magnitude estimate, γ is the exponent, and k is a coefficient, the slopes and intercepts listed in Table 3.5 refer to $\gamma/20$ and $\log_{10}(k)$, respectively. As such, the mean exponents for the growth of magnitude are 1.88 ± 0.28 and 1.24 ± 0.18 for Haptuator-1 at 80 Hz and 180 Hz, respectively. For Haptuator-2, they are 1.54 ± 0.16 and 1.18 ± 0.14 respectively at 80 Hz and 180 Hz. On the other hand, negative intercepts imply $k < 1$.

The differences in slope and intercept of the fits were analyzed using repeated measures ANOVA. There was a significant effect of frequency on slope of the fits ($F(1,9)=23.584$, $p=0.001$). The exponent is lower for the higher frequency and the growth of subjective magnitude is slower. The effect of stimulation site on the intercept of the fits was significant ($F(1,9)=6.077$, $p=0.036$), with slightly less negative intercepts resulted from Haptuator-2. No interactions were found between factors for both parameters. Magnitude estimation fits for one participant (S1) are given in Figure 3.21. Empty squares represent magnitude estimation data and the solid lines are fitted lines. Filled circles show the saturation levels calculated from psychometric functions. The fits for all participants are given in Appendix B.

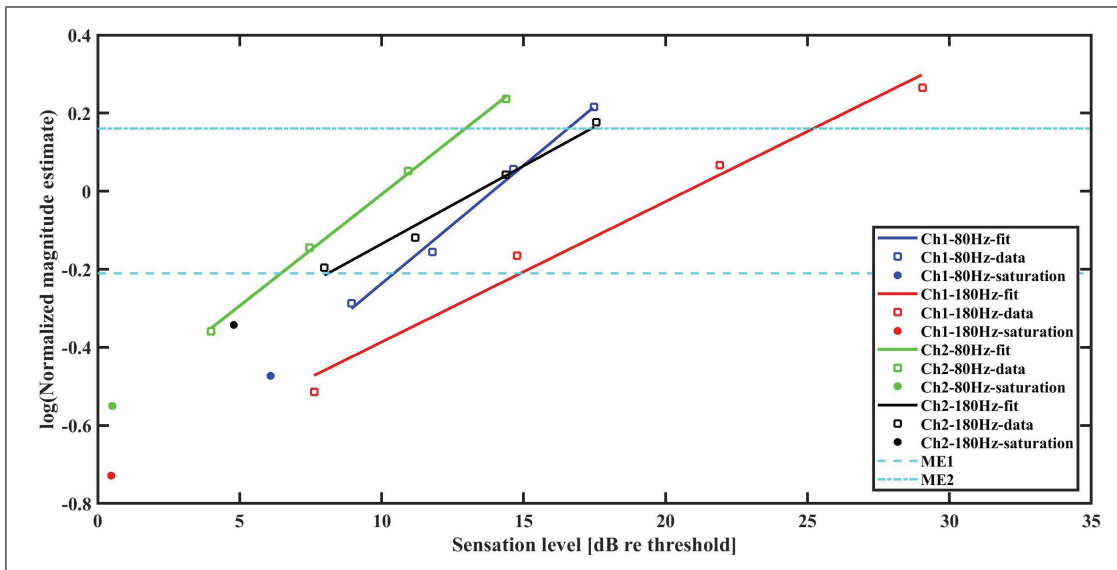


Figure 3.21 Magnitude estimation fits for S1.

Table 3.5
Parameters of magnitude estimation fits for all participants.

Participant	Haptuator 1-80 Hz			Haptuator 1-180 Hz		
	Slope	Intercept	R^2	Slope	Intercept	R^2
S1	0.061	-0.842	0.993	0.036	-0.746	0.982
S2	0.073	-1.356	0.995	0.073	-1.514	0.987
S3	0.142	-1.526	0.983	0.076	-1.796	0.988
S4	0.130	-1.567	0.952	0.071	-1.284	0.991
S5	0.117	-1.739	0.994	0.103	-2.213	0.993
S6	0.078	-1.141	0.961	0.035	-0.823	0.983
S7	0.047	-0.691	0.996	0.033	-0.522	0.983
S8	0.074	-1.107	0.987	0.051	-1.000	0.997
S9	0.049	-0.782	0.989	0.035	-0.833	0.991
S10	0.174	-2.092	0.986	0.105	-1.896	0.991
Mean	0.094	-1.284		0.062	-1.263	
Std. Error	0.014	0.144		0.009	0.180	
Participant	Haptuator 2-80 Hz			Haptuator 2-180 Hz		
	Slope	Intercept	R^2	Slope	Intercept	R^2
S1	0.057	-0.579	0.999	0.040	-0.535	0.982
S2	0.062	-1.411	0.977	0.076	-1.524	0.997
S3	0.111	-1.228	0.993	0.092	-1.843	0.993
S4	0.097	-1.250	0.989	0.061	-0.740	0.974
S5	0.105	-1.641	0.995	0.078	-1.373	0.990
S6	0.041	-0.535	0.949	0.032	-0.825	0.916
S7	0.050	-0.534	0.991	0.032	-0.576	0.993
S8	0.069	-0.809	0.988	0.049	-0.679	0.968
S9	0.067	-0.733	0.986	0.041	-0.879	1.000
S10	0.113	-2.030	0.933	0.091	-2.363	0.982
Mean	0.077	-1.075		0.059	-1.134	
Std. Error	0.008	0.164		0.007	0.195	

For the magnitude equalization, two magnitude estimate levels (LME1, LME2; cyan horizontal lines in Figure 3.21) were selected which were crossing all lines. Since the magnitude estimation range was different for the participants, the resulting magni-

tude estimate gap (equals to LME2-LME1) varied across participants. The corresponding eight sensation levels (referenced to absolute detection thresholds) were calculated for each participant as given in Table 3.6, establishing a psychophysical model.

Table 3.6

Models obtained from psychophysical characterization procedure (LME: Logarithm of magnitude estimate, SL: Sensation level, ME Gap: difference of magnitude estimates).

Participant	LME1	LME2	ME Gap	Haptuator 1-80 Hz		Haptuator 1-180 Hz	
				SL1	SL2	SL1	SL2
S1	-0.21	0.16	0.37	10.442	16.559	14.904	25.190
S2	-0.60	0.12	0.72	10.328	16.884	12.486	19.043
S3	-0.70	0.10	0.80	5.834	11.836	14.507	25.758
S4	-0.30	0.23	0.53	9.757	13.840	13.848	21.309
S5	-0.60	0.30	0.90	8.878	17.427	14.679	24.380
S6	-0.10	0.20	0.30	13.436	17.307	20.628	29.189
S7	-0.18	0.18	0.36	10.966	18.698	10.256	21.066
S8	-0.25	0.20	0.45	11.636	17.742	14.634	23.419
S9	-0.30	0.20	0.50	9.945	20.254	15.118	29.315
S10	-0.60	-0.01	0.59	8.568	11.957	12.358	17.983
Participant	ME1	ME2	ME Gap	Haptuator 2-80 Hz		Haptuator 2-180 Hz	
				SL1	SL2	SL1	SL2
S1	-0.21	0.16	0.37	6.463	12.941	8.125	17.384
S2	-0.60	0.12	0.72	13.055	20.784	12.131	18.431
S3	-0.70	0.10	0.80	4.757	12.412	12.386	21.595
S4	-0.30	0.23	0.53	9.826	15.309	7.239	15.953
S5	-0.60	0.30	0.90	8.938	18.433	8.599	21.384
S6	-0.10	0.20	0.30	10.560	17.835	22.852	32.314
S7	-0.18	0.18	0.36	7.092	14.297	12.330	23.531
S8	-0.25	0.20	0.45	8.147	14.705	8.769	17.974
S9	-0.30	0.20	0.50	6.431	13.863	14.204	26.461
S10	-0.60	-0.01	0.59	12.656	17.877	19.474	25.992

The model parameters (SLs) were assumed to stay constant throughout experimental procedures. The SLs corresponding to LME1 and LME2 were used to calculate

low (a_1) and high (a_2) amplitudes of vibrotactile stimuli respectively, referenced to the absolute detection threshold from the re-calibration measurement at the beginning of each session. The displacements corresponding to those amplitude levels at the initial psychophysical characterization are shown with filled diamonds in Figure 3.19.

3.3.2 Magnitude and frequency discrimination

We calculated the accuracies of same-only trials, different-only trials and all trials from participant responses for same-different discrimination task (Figure 3.22). The average accuracies of simultaneous stimulation were $63.7 \pm 5.3\%$ and $56.4 \pm 2.7\%$ for magnitude and frequency discrimination respectively. For successive stimulation, the accuracy was $66.6 \pm 2.6\%$ for magnitude discrimination and $57.3 \pm 2.3\%$ for frequency discrimination. Although the magnitudes were calibrated for each participant specifically and the frequency difference was higher than the discrimination threshold, the participant performance is moderate. The average accuracies for same-only and different only trials are also given in Table 3.7.

Table 3.7

Average accuracies for all conditions of same-different discrimination experiments.

		Simultaneous stimulation			Successive stimulation		
		"S" Accuracy	"D" Accuracy	"S-D" Accuracy	"S" Accuracy	"D" Accuracy	"S-D" Accuracy
Magnitude discrimination	Mean	0.610	0.668	0.637	0.598	0.735	0.666
	Std. Error	0.059	0.073	0.053	0.039	0.046	0.026
Frequency discrimination	Mean	0.581	0.544	0.564	0.623	0.523	0.573
	Std. Error	0.047	0.036	0.027	0.036	0.034	0.023

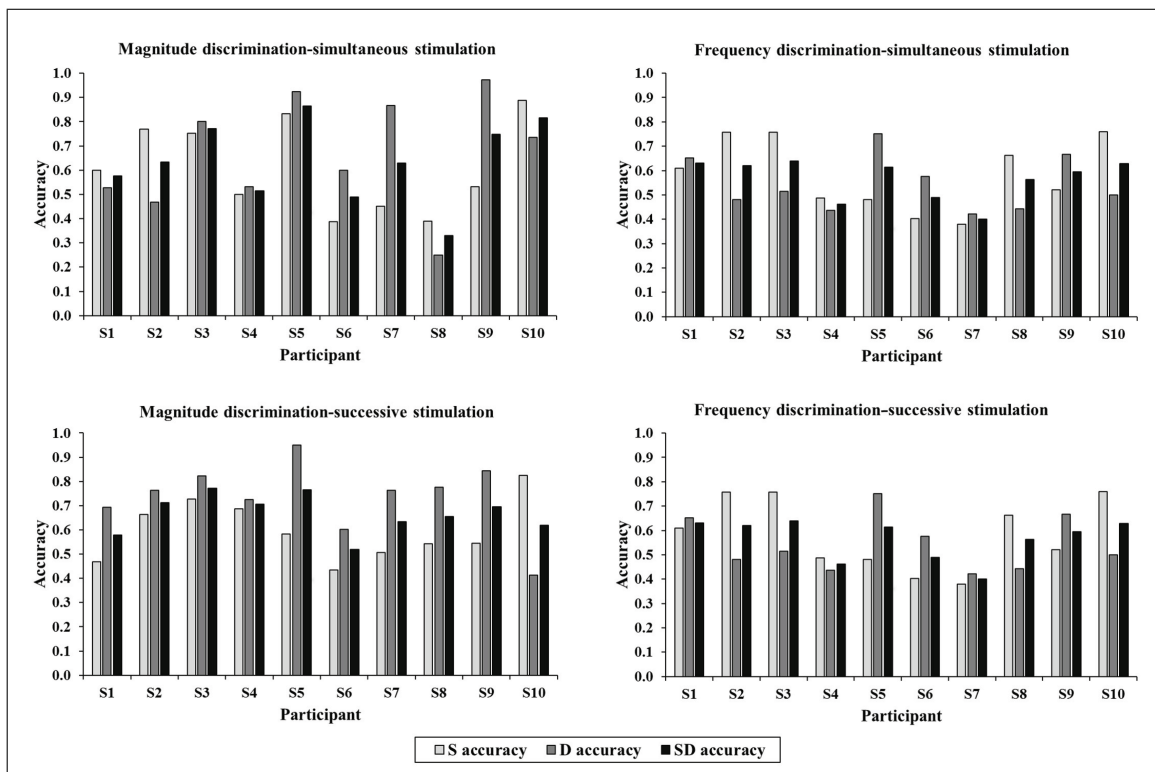


Figure 3.22 Results of same-different discrimination experiments.

The differences in means of accuracies were tested by using repeated measures ANOVA. Within subject factors were chosen as comparison parameter (magnitude or frequency), presentation method (simultaneous or successive) and trial type (same or different). Magnitude discrimination accuracies were significantly higher than frequency discrimination accuracies ($F(1,9)=8.198$, $p=0.019$). An interaction of comparison parameter and presentation method was also found ($F(1,9)=18.221$, $p=0.002$) implying that the difference between magnitude and frequency discrimination was higher with successive stimulation. The responses from all trials were pooled and the effects of comparison parameter and stimulation method on the mean accuracies were analyzed by using repeated measures ANOVA. There was a significant effect of parameter on mean accuracies ($F(1,9)=8.567$, $p=0.017$).

We also studied the correlation between magnitude estimate gap and each of the discrimination accuracies in Table 3.7. There was a significant positive correlation between magnitude estimate gap and magnitude discrimination accuracies of pooled

trials for both simultaneous ($r=0.658$, $p=0.039$) and successive ($r=0.862$, $p=0.001$) stimulation. This indicates that as the magnitude estimate gap increases, magnitude discrimination accuracy increases. A significant correlation was also found between magnitude estimate gap and the magnitude discrimination accuracy of simultaneous stimulation experiment ($r=0.797$, $p=0.006$). It means that the participants with wider magnitude estimate gaps could perceive the same-magnitude stimuli more accurately than the others.

3.3.3 Vibrotactile pattern recognition

The data from all participants were pooled and the confusion matrices were obtained as given in Figure 3.23 for the vibrotactile pattern recognition experiments. In the confusion matrices, the stimuli with different magnitude and frequency combinations are represented by letters (see figure caption for explanation). The stimulation sites are also represented by R (right) and L (left). Rows and columns correspond to actual pattern and participant response respectively.

In one-pattern stimulation, patterns mostly with one common parameter were confused with each other. In two-pattern stimulation, it is hard to make a generalization on confused patterns. The class-averaged performance metrics (recalls, precisions and F1 scores) have the same trend (Table 3.8). The F1 score is 0.71 for one-pattern stimulation while they are 0.67, 0.46 and 0.47 for same-site, right-first and left-first stimulation respectively. The individual performance of participants for all tasks are given in Figure 3.24.

The correct responses given to each pattern were compared with the chance level by using z-test. For all stimulation types and all patterns, the proportions of correct responses were statistically significantly above the chance level (all p 's < 0.001). Results of the independence test showed that there was significant dependence (all p 's < 0.001) between actual patterns and participants' responses.

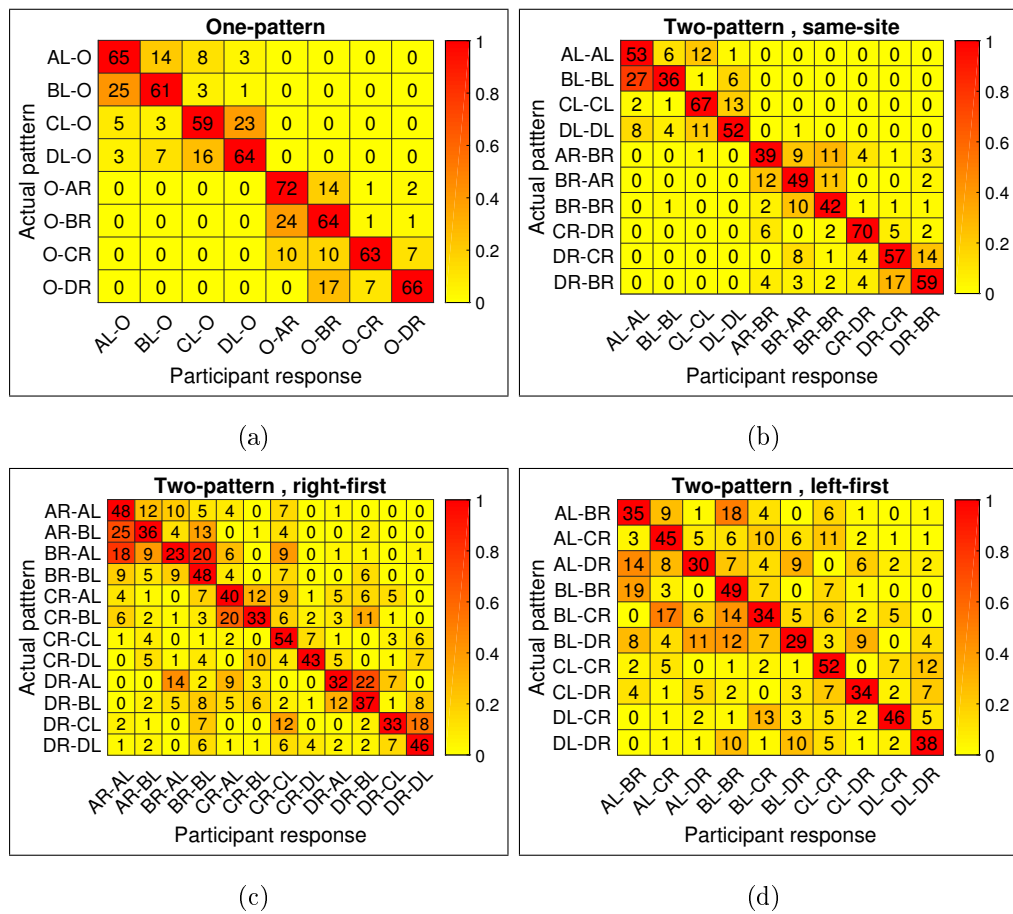


Figure 3.23 Confusion matrices for vibrotactile pattern recognition experiments. a) one-cell stimulation b) two-cells stimulation-same arms b) two-cells stimulation, different arms, right arm first d) two-cells stimulation, different arms, left arm first (A: low frequency-low amplitude, B: high frequency-low amplitude, C: low frequency-high amplitude, D: high frequency-high amplitude, L and R represents left and right arms).

The performance scores for all stimulation types and all participants are given in Figure 3.24. The differences in participant performance scores for different stimulation types (Table 3.8) were tested using one-way ANOVA. There was a significant effect of stimulation type (site and order of stimulation) on recall ($F(3,24)=21.726$, $p=0.002$), precision ($F(3,24)=20.465$, $p=0.002$), and F1 score ($F(3,24)=22.103$, $p=0.002$). We also performed correlation analyses and found no significant correlation between magnitude estimate gap and averaged performance scores. This shows that the effect of differences between participants becomes less important while performing a complex task.

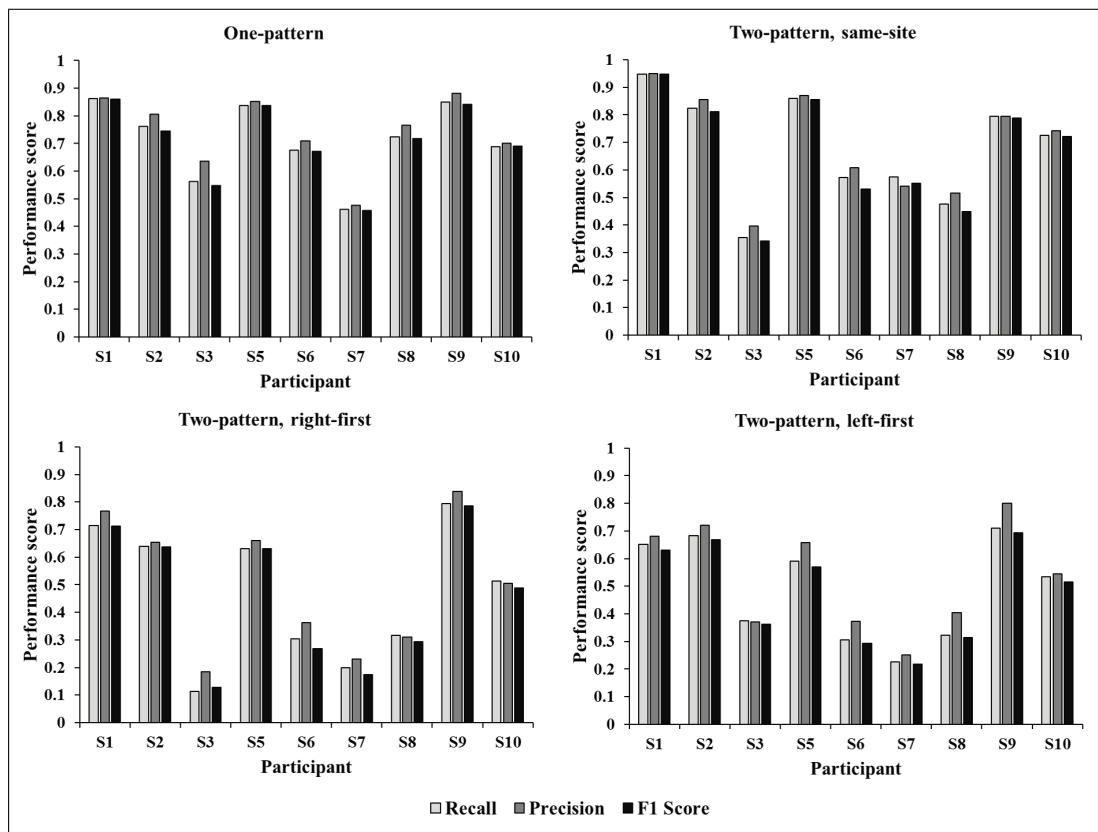


Figure 3.24 Performance scores of all participants for all stimulation types in vibrotactile pattern recognition experiments.

Table 3.8
Average results of vibrotactile pattern recognition experiments.

		One-pattern	Two-pattern, same-site	Two-pattern, right-first	Two-pattern, left-first
Recall	Mean	0.714	0.682	0.470	0.489
	Std. Error	0.045	0.066	0.081	0.061
Precision	Mean	0.744	0.697	0.501	0.534
	Std. Error	0.043	0.063	0.080	0.064
F1 Score	Mean	0.708	0.666	0.457	0.474
	Std. Error	0.046	0.069	0.082	0.060

3.3.4 Discrete event-driven feedback

The data from all participants were pooled and the confusion matrix was obtained as given in Figure 3.25. The number codes represent sequences which were generated by mapping the vibrotactile patterns to the discrete events given in Table 3.2. The rows and columns correspond to actual sequences and participant responses respectively.

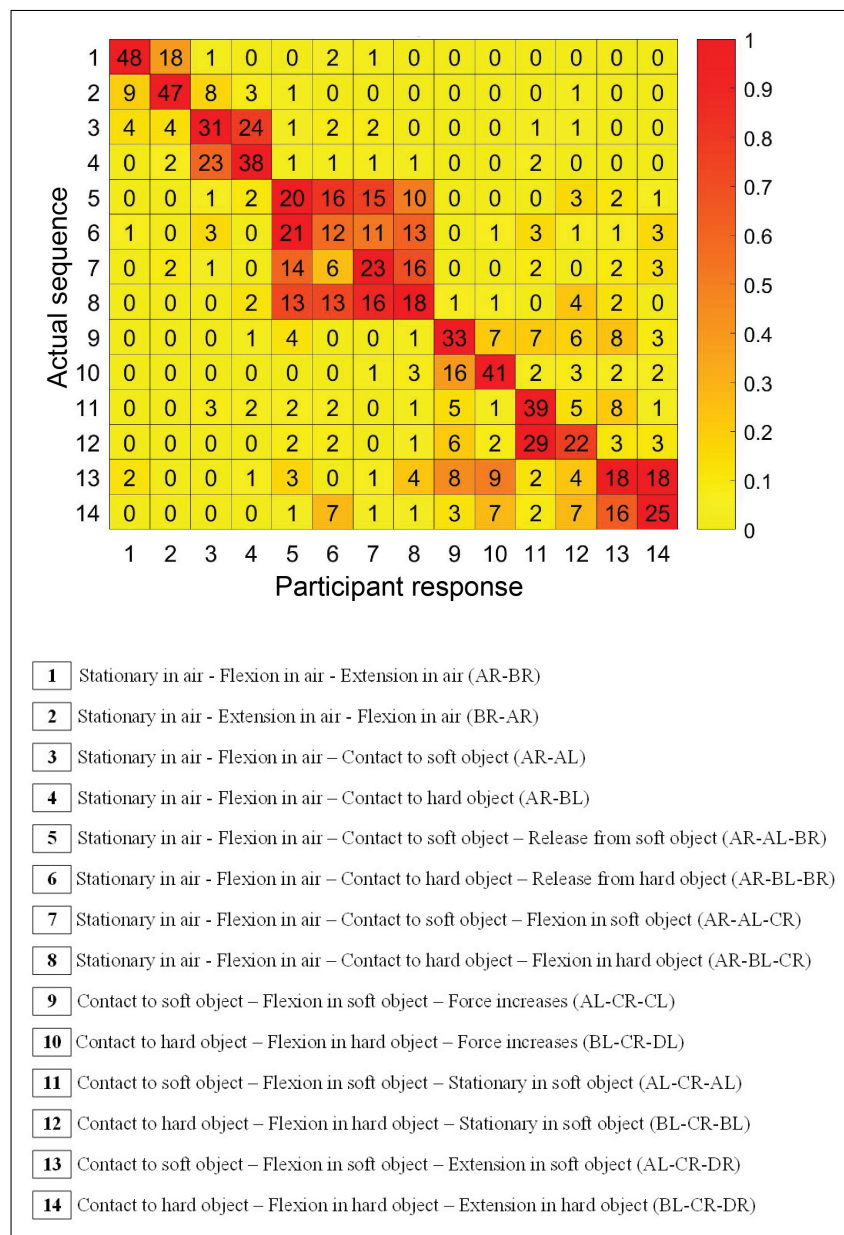


Figure 3.25 Confusion matrix for discrete event-driven feedback experiments (A: low frequency-low amplitude, B: high frequency-low amplitude, C: low frequency-high amplitude, D: high frequency-high amplitude, L and R represents left and right arms).

It can be seen from the confusion matrices that mostly patterns in the neighboring cells of the actual sequence were confused. These cells have patterns in common, as seen from the sequence list in Figure 3.25. The correct responses to all sequences were significantly above the chance level (all p 's < 0.002). Additionally, results of independence analysis showed that there was significant dependence between actual sequence and participant responses ($p < 0.001$). The individual confusion matrices and sequence-based performance scores are given in Appendix C.

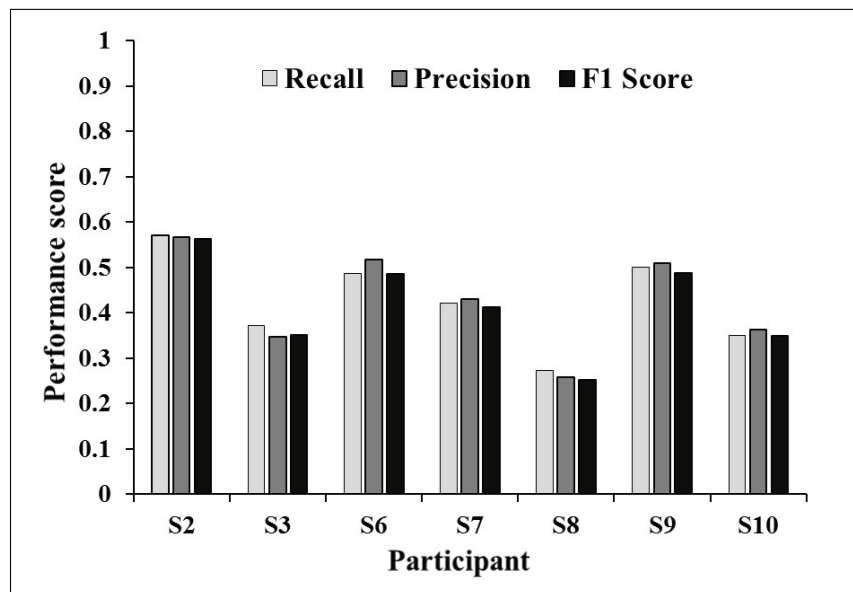


Figure 3.26 Performance scores of discrete event-driven feedback experiments.

The performance scores in discrete event-driven feedback experiments are given in Figure 3.26 for all participants. These were compared with the performance scores in vibrotactile pattern recognition experiments. For this, the scores from all stimulation types in pattern recognition experiment were averaged (recall: 0.54 ± 0.07 , precision: 0.57 ± 0.07 , F1 score: 0.53 ± 0.07). For the discrete event-driven experiment, the class-averages of performance scores (Figure 3.26) were calculated and then averaged across participants (recall: 0.42 ± 0.04 , precision: 0.43 ± 0.04 , F1 score: 0.41 ± 0.04). The average scores are also given in Figure 3.27. The differences in means were tested using the Wilcoxon signed-rank test and no significant difference was found between two methods. We also studied the correlation between magnitude estimate gap and performance scores and could not find any significant correlation.

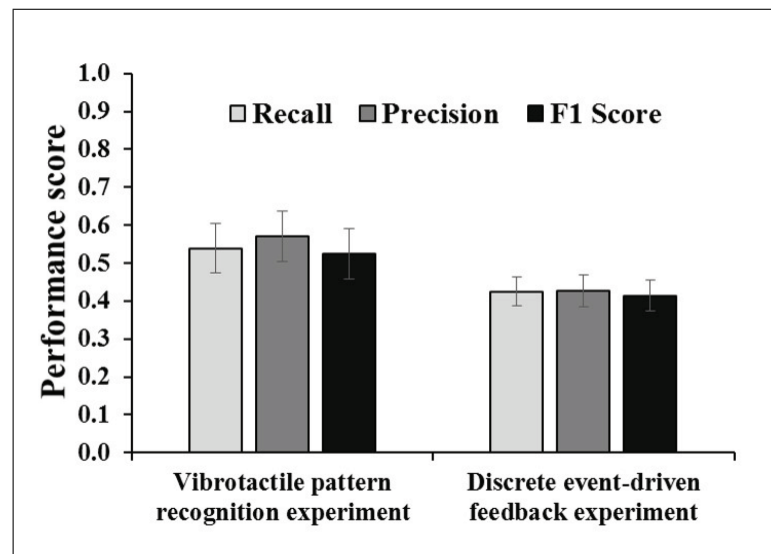


Figure 3.27 Averaged performance scores for vibrotactile pattern recognition and discrete event-driven feedback experiments.

3.4 Discussion

3.4.1 General conclusions

In this study, psychophysical principles of DESC-based vibrotactile feedback was studied in able-bodied participants. Discrete-events observed during the movement of a robotic hand were mapped to the vibrotactile patterns. Since psychophysical measures are subjective and affected by a lot of factors, a step-by-step psychophysical characterization was performed before the experiments. Thus, an individual model was established for each participants, and stimulation amplitudes in the experiments were determined according to this model. Additionally, the psychophysical characterization procedure provided balanced magnitude sensation for different frequencies and stimulation sites.

Same-different discrimination experiments were conducted for magnitude and frequency. Magnitude discrimination was better than frequency discrimination the performance scores were correlated with the model differences. Next, vibrotactile pattern

recognition experiments were done and moderate recall/precision rates were obtained. Finally, the discrete event-driven feedback experiments were performed by using the novel mapping procedure which includes both object-type and movement-type related information. The identification rates were similar to the pattern recognition experiments. When the identification of a full sequence is considered, the recall rate is around 0.5. However, if selecting 2 discrete events in a 3-event sequence is calculated, the accuracy becomes 68%. Similarly, selecting at least 1 correct event from 2- and 3-event sequences resulted an accuracy of 85%. These results show that DESC- based feedback is well founded based on psychophysical criteria.

3.4.2 Previous studies with DESC policy

In the sensory feedback literature, DESC policy was mostly used for vibrotactile feedback [35, 37, 48, 54]. In these studies, the transitions between critical events were presented to the user by a vibrotactile stimulus with short duration. The vibration intensity, frequency and duration were kept constant for different events and adjusted manually to a perceivable level. In our study, the amount of information transmitted to the user was increased by using two vibrotactile actuators and using two settings for both frequency and magnitude of the vibration. Thus, both object-type/force and movement-type signals were presented to the participant. By psychophysical characterization, the sensation magnitudes were balanced for different conditions and the amplitudes were selected for each participant specifically. Our study also differs by the type and placement of the vibrotactile actuators compared to other studies in the literature. We preferred to use Haptuator device which has good linearity over a wide frequency range. We placed the actuators on different arms to increase the discriminability of the feedback signals.

3.4.3 Technical limitations

The sensory feedback system used in this study was considered mostly for upper limb amputees. As a first prototype, we mounted the actuators on foam rubber perpendicularly and attached to the upper arm by straps. When the motor applied vertical displacement, the skin may also have reacted in reverse direction and could have damped some of the displacements. This can be partially compensated by mounting the actuator on a more rigid structure, such as a prosthesis socket.

Another observation during the experiments was the variation of thresholds across sessions. This was due to mainly two factors: expected psychophysical variation as reported in the literature and variation due to re-attaching of the actuators. We placed the actuators approximately on the same site by measuring the arm circumference and proximodistal distance at the beginning of each session. However, small location and static indentation shifts could not be prevented entirely. In order to decrease the effects of these small shifts, we applied a re-calibration procedure by calculating the amplitudes with respect to the thresholds measured at the beginning of the sessions.

In this study, Haptuator devices were preferred as the vibrotactile actuators since they are small, light and can reproduce sinusoidal waveforms with varying amplitude and frequency. However, these actuators were not produced for prosthetic applications. Due to the recoil effect, they generate vibrations on the casing, which is how they are mostly used for. The vibrations on the casing cause complex stimuli due to boundary conditions when directly attached to the skin.

Since focused stimulus at submicrometer level was needed for our study, we mounted them with their long axes perpendicular to the skin, by glueing small plastic probes to their armatures. In some cases, we had to repeat this procedure due the breakage of the probes during use. A more reproducible solution would be achieved if a contactor probe is designed by the manufacturer.

3.4.4 Psychophysical issues

The absolute threshold results in the current study were compatible with the previously reported values in the literature for hairy skin [129], despite all technical limitations discussed above. Vibrotactile detection and discrimination thresholds are frequency dependent. In Verrillo (1966), the detection thresholds were shown to decrease from 80 Hz to 180 Hz, but only for relatively larger contactor areas [129]. The contactor area in our study was approximately 0.03 cm^2 ; at such small sizes, the spatial summation effect of the Pacinian channel is negligible and the sensitivity does not follow a U-shaped trend as a function of frequency [81, 134]. As such, we did not find a significant difference between results at 80 Hz and 180 Hz.

We considered the possible effect of the magnitude estimate gap on the participant performance after psychophysical characterization. A correlation was found for magnitude discrimination, implying better discrimination accuracy for larger gaps. However, there was no significant correlation for vibrotactile pattern recognition and discrete event-driven feedback experiments. This states that the psychophysical model differences did not affect the performance in more complex tasks which is a promising result for the applicability of the presented methods for prosthesis use.

In brief, the lack of correlation shows that regardless of the psychophysical model variation across users, the performance baseline would be expected to be as reported in the current study. The improvement from this baseline would be more dependent on the cognitive estimation of the sequence of events during actual use, and not determined by psychophysical factors. One can argue that during a long sequence of events, understanding the vibrotactile feedback may also increase the cognitive load and decrease performance. On the contrary, this is the reason why DESC policy is indeed useful, and why we used only a few events for identification. The user is not required, and does not probably need in practical use, to follow a long list of events per se. Control decisions can be made after the feedback to only a few events. Additionally, we observed that the performance did not deteriorate from the pattern recognition task to the DESC-based task, which shows implicitly that going from 2 to 3 patterns was

well handled, with the caveat that pattern recognition task did not have any prosthetic meaning.

3.4.5 Future directions and practical use

The results of the current study show that both object/force and movement information can be provided sequentially with moderate identification rates. The next step would be the use of presented approach and methods in a real prosthesis. We based this study on the offline classification of sensor data from a robotic hand [79]. The subsequent studies will be on real-time classification and generation of vibrotactile patterns, which are currently within progress in our laboratory. There have been studies in the literature which investigated the usability of various feedback systems with real prosthetic hands [25, 26, 49, 50]. Although the stimulation modality (invasive vs non-invasive) and its method (continuous vs discrete) differ in those, some comparisons can be made prior to the real-time implementation of our method in a real prosthesis.

In Markovic et al. (2018), a novel vibrotactile stimulation system was tested using a Michelangelo hand prosthesis (Otto Bock Healthcare GmbH, Vienna, AT.) [49]. Similar to our study, the system transmitted multiple variables such as contact (by activating all factors), prosthesis state (by spatial modulation) and level of grasping force (by spatial and amplitude modulation) through multiple actuators. For the complex daily-use tasks, the user performance showed an improvement with feedback. On the other hand, in D’Anna et al. (2019), position information was applied simultaneously with tactile feedback through intraneural stimulation for two amputees using the IH2 Azzurra hand (Prensilia, Italy) [26]. The results of functional tests (object size and compliance identification) showed that both the tactile and position information can be processed simultaneously. Similar results were obtained by Schiefer et al. (2018) with peripheral nerve stimulation for tactile and proprioceptive feedback information, regarding object size and compliance [25]. Our results are in line with these studies such that multimodal information can be conveyed to the somatosensory system by artificial feedback in (neuro-)prostheses, but possibly better in the discrete mode. In

Pena et al.'s study [50], it was indeed found that continuous modulation of the burst width proportional to the grasp force or hand aperture in one actuator yielded results worse than the sequential actuation of five coin-type factors as the stimulus level increased. Based on these reported results in the literature, we presume that the system and methods presented here is promising to be used with a real prosthesis. After an initial psychophysical characterization, the system should be easily re-calibrated by measuring the absolute detection thresholds using an simple embedded system. It is also expected that, the repetitive use of the system during daily life in conjunction with visual, and possibly auditory, cues will heighten the cognitive awareness with learning and increase the embodiment of the prosthesis [143]. We also think that, stimulation of both arms will not be a cognitive burden for the user. In daily use, the user is not always required to detect the events as a sequence. Some object-type information may be obtained implicitly through the actuator signaling movement-type information.

Lastly, the methods and results of the current work may have implications for other tactile feedback applications not related with prostheses including rehabilitation [144, 145], assistive technologies [146], teleoperation [147, 148], gaming and virtual reality [149–151]. We think that the efficiency of those systems may be increased with user-specific psychophysical characterization and discrete event-driven feedback as described here.

4. CONCLUSION

4.1 Overall summary

In this study, a DESC-based vibrotactile sensory feedback system was presented including some novel methods in terms of signal processing and feedback method. First, high number of force and bend sensors were placed on a robotic hand. In contrast to deterministic approaches, machine learning methods were used to classify sensor data. This approach is very similar to biological systems with variable neural outputs and central processing capable of extracting information from a big amount of data. By this method, object type/force and movement type/position information could be extracted from highly variable sensor outputs. The classification results were promising to be used in the future studies on real time sensory feedback.

Next, a non-invasive feedback system was designed using two recoil based vibrotactile actuators. The actuators were placed on the upper arms of able-bodied participants. The stimulation procedure was based on the DESC policy and class labels from the previous study. The information flow was increased by transmitting both force and position information. A novel step-by-step psychophysical characterization procedure was presented for user-specific calibration of the system. Using the vibrotactile stimuli with two participant specific stimulation magnitudes and two frequencies, discrimination and recognition experiments were conducted. Finally, the stimuli were mapped to the discrete transition events from a hypothetical prosthesis (related to class labels) and discrete event-driven feedback experiments were performed. Although the participant performance scores were moderate, it represents a baseline for the expectations from such systems. Therefore, it can be concluded that the proposed system and methods can be incorporated into prosthetic devices to provide sensory feedback.

4.2 Limitations

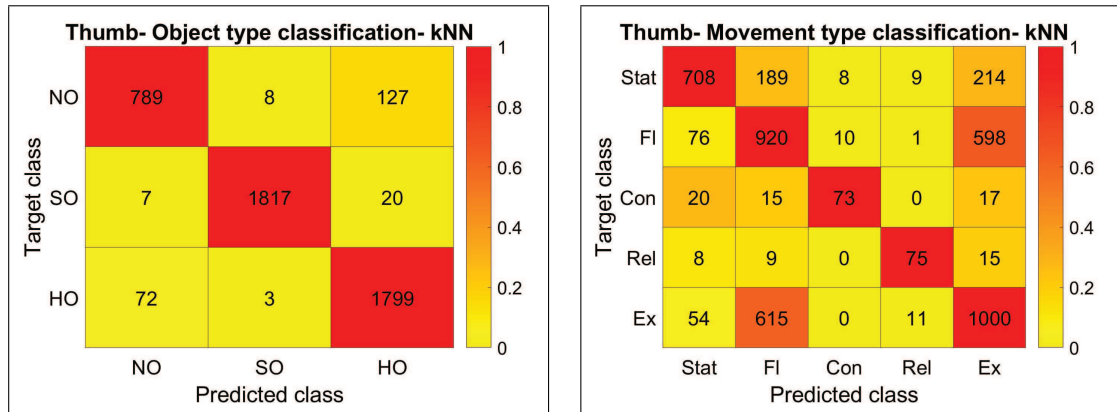
The robotic hand used in this study is not a prosthesis and was not controlled by a user, instead it was pre-programmed for specific grasp types. However, due to mechanical limitations of the hand and the varying behavior of the sensors, it was not possible to implement all grasp types. Thus, we focused on the cylindrical grasping which provided more stable sensor output compared to the others. By using a real prosthesis with embedded force and position sensors may provide better classification results.

In terms of vibrotactile feedback system, the main limitation was the placement of actuators on the arm. They were mounted on foam rubber perpendicularly and attached on the arm using strap. Thus, some actuator-skin decoupling problems occurred, resulting in variations of psychophysical measures. An easy re-calibration procedure was implemented to compensate these variations. The placement of actuators on a prosthesis socket may solve this problem and the static indentation may be adjusted through mechanisms inserted into socket. Thus, stimulus recognition and discrimination performance may be increased which are known to be effected from these factors.

4.3 Future work

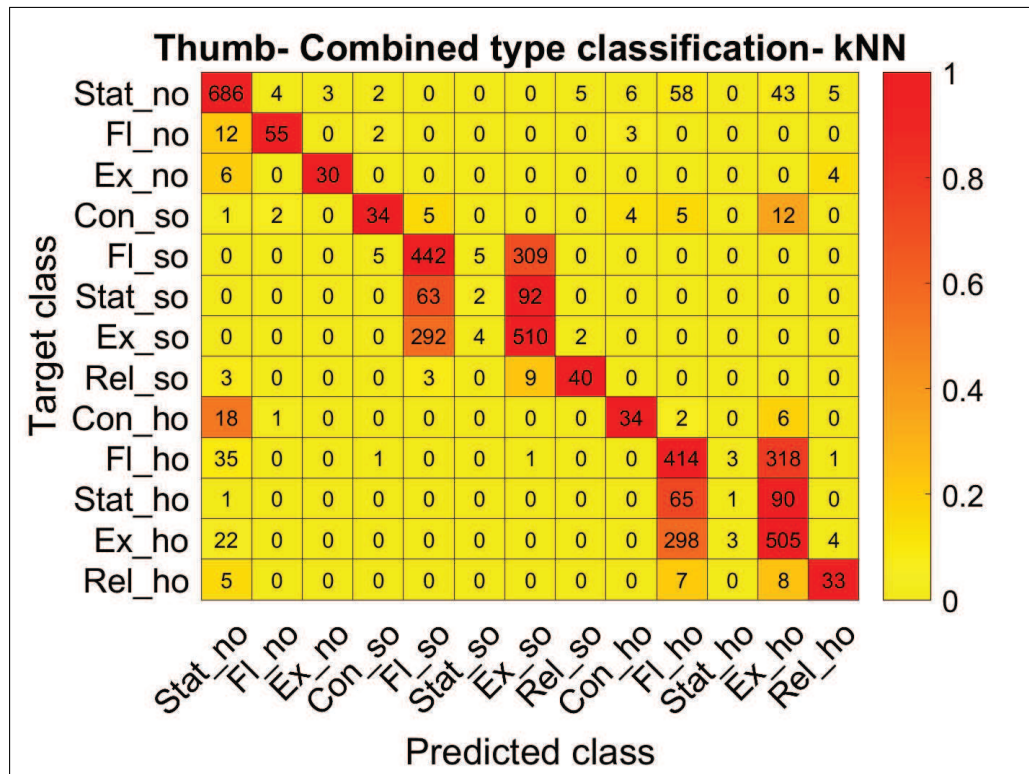
In this study, we did not use a prosthetic hand with real-time control of a human user. The future studies will be on implementing the same methods using a real prosthetic hand with embedded sensors. Additionally, the classification of sensor data and generation of vibrotactile stimuli will be performed real-time. We believe that the proposed methods will be helpful for object manipulation during daily use of a prosthesis, due to cognitive awareness and learning effects with repetitive use.

APPENDIX A. CLASSIFICATION RESULTS



(a)

(b)

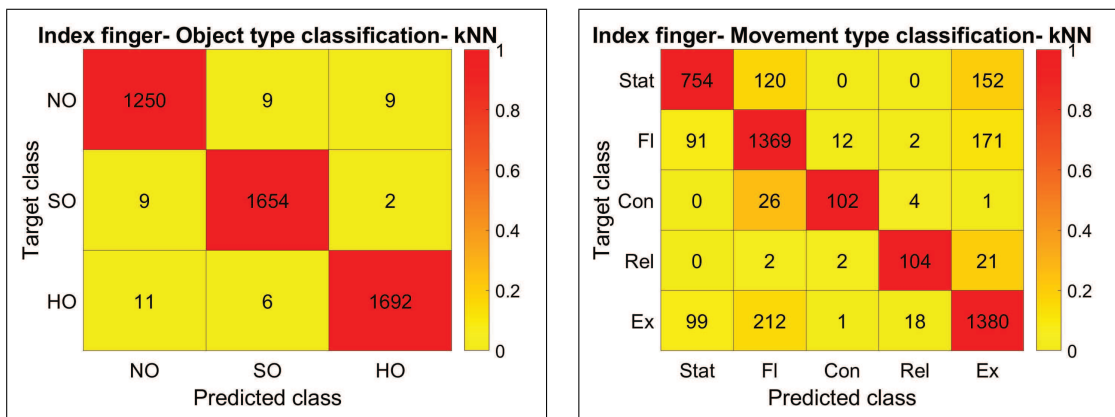


(c)

Figure A.1 Confusion matrices of a) object type, b) movement type, and c) combined type kNN classification of sensor data from the thumb. Counts are given as numbers in cells. Color code indicates a given count normalized by total instances of the target class.

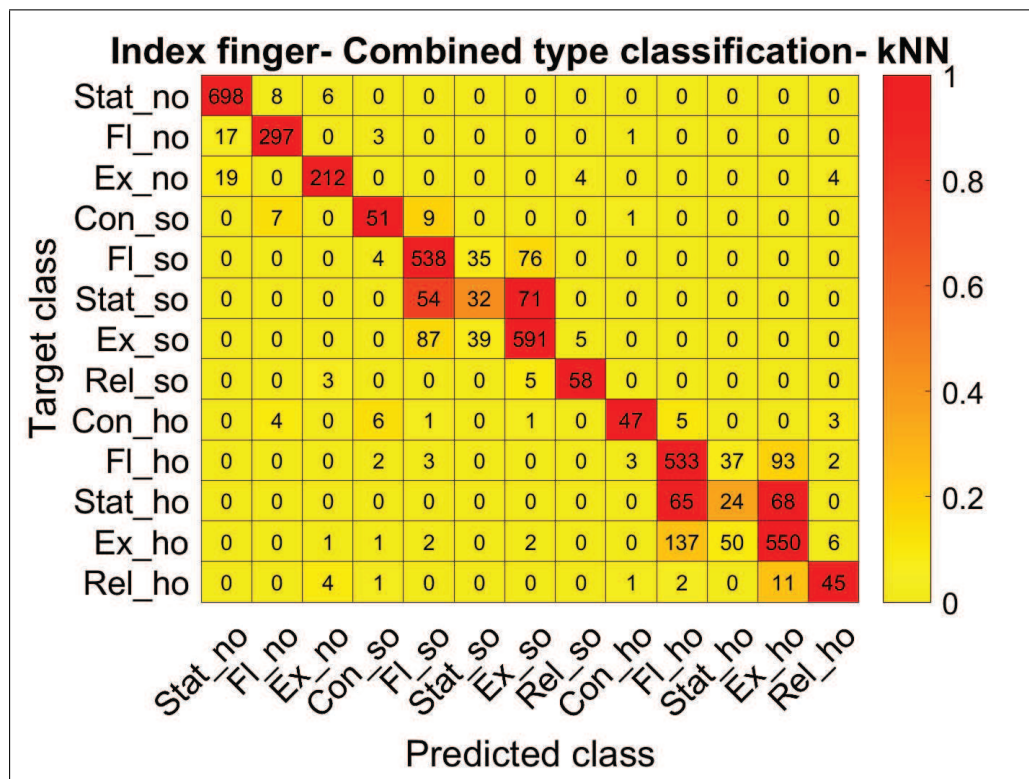
Table A.1
Classification results of kNN classifier for thumb.

Type of classification	Class(Labels)	Recall	Precision	F1 Score
Object type	No (1,2,3)	0.854	0.909	0.881
	So (4,5,6,7,8)	0.985	0.994	0.990
	Ho (9,10,11,12,13)	0.960	0.924	0.942
Movement type	Stat (1,6,11)	0.628	0.818	0.710
	Fl (2,5,10)	0.573	0.526	0.549
	Con (4,9)	0.584	0.802	0.676
	Rel (8,13)	0.701	0.781	0.739
	Ex (3,7,12)	0.595	0.542	0.568
Combined type	Stat-no (1)	0.845	0.869	0.857
	Fl-no (2)	0.764	0.887	0.821
	Ex-no (3)	0.750	0.909	0.822
	Con-so (4)	0.540	0.773	0.636
	Fl-so (5)	0.581	0.549	0.564
	Stat-so (6)	0.013	0.182	0.024
	Ex-so (7)	0.631	0.554	0.590
	Rel-so (8)	0.727	0.851	0.784
	Con-ho (9)	0.557	0.723	0.630
	Fl-ho (10)	0.536	0.488	0.510
	Stat-ho (11)	0.006	0.143	0.012
	Ex-ho (12)	0.607	0.514	0.557
	Rel-ho (13)	0.623	0.702	0.660



(a)

(b)

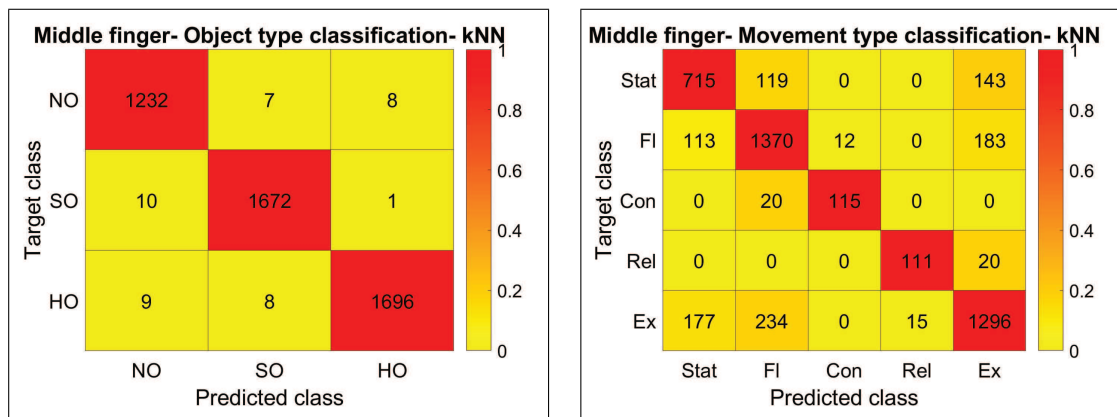


(c)

Figure A.2 Confusion matrices of a) object type, b) movement type, and c) combined type kNN classification of sensor data from the index finger. Counts are given as numbers in cells. Color code indicates a given count normalized by total instances of the target class.

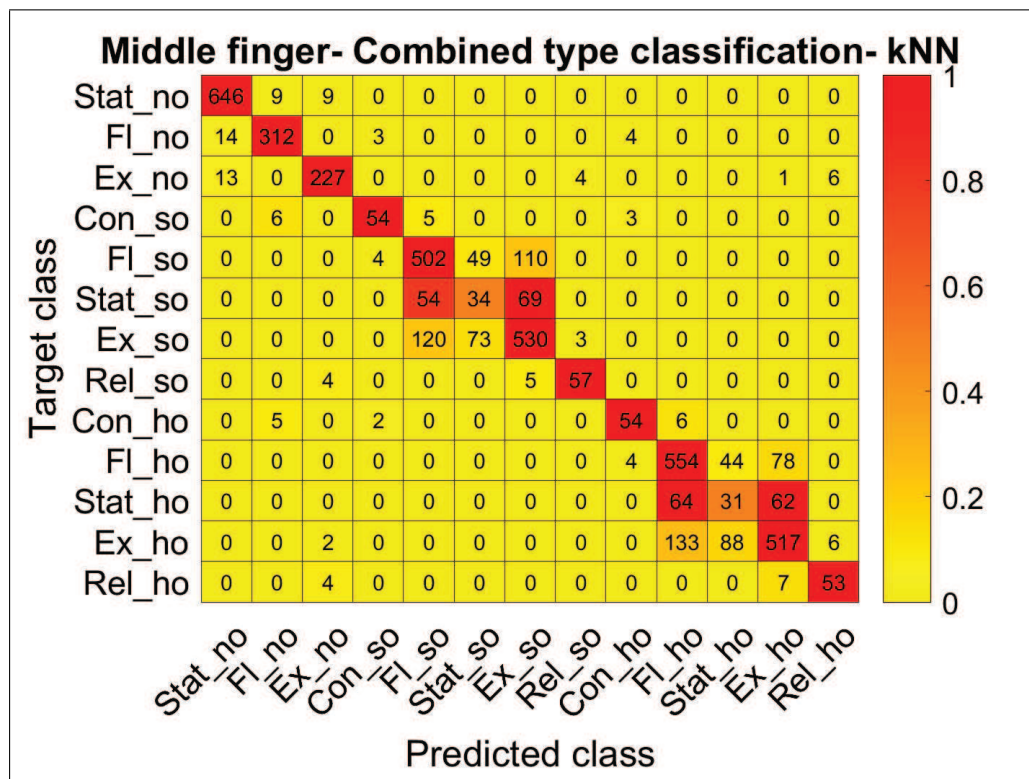
Table A.2
Classification results of kNN classifier for index finger.

Type of classification	Class(Labels)	Recall	Precision	F1 Score
Object type	No (1,2,3)	0.986	0.984	0.985
	So (4,5,6,7,8)	0.993	0.991	0.992
	Ho (9,10,11,12,13)	0.990	0.994	0.992
Movement type	Stat (1,6,11)	0.735	0.799	0.765
	Fl (2,5,10)	0.832	0.792	0.811
	Con (4,9)	0.767	0.872	0.816
	Rel (8,13)	0.806	0.813	0.809
	Ex (3,7,12)	0.807	0.800	0.803
Combined type	Stat-no (1)	0.980	0.951	0.965
	Fl-no (2)	0.934	0.940	0.937
	Ex-no (3)	0.887	0.938	0.912
	Con-so (4)	0.750	0.750	0.750
	Fl-so (5)	0.824	0.775	0.799
	Stat-so (6)	0.204	0.302	0.243
	Ex-so (7)	0.819	0.792	0.805
	Rel-so (8)	0.879	0.866	0.872
	Con-ho (9)	0.701	0.887	0.783
	Fl-ho (10)	0.792	0.718	0.753
	Stat-ho (11)	0.153	0.216	0.179
	Ex-ho (12)	0.734	0.762	0.748
	Rel-ho (13)	0.703	0.750	0.726



(a)

(b)

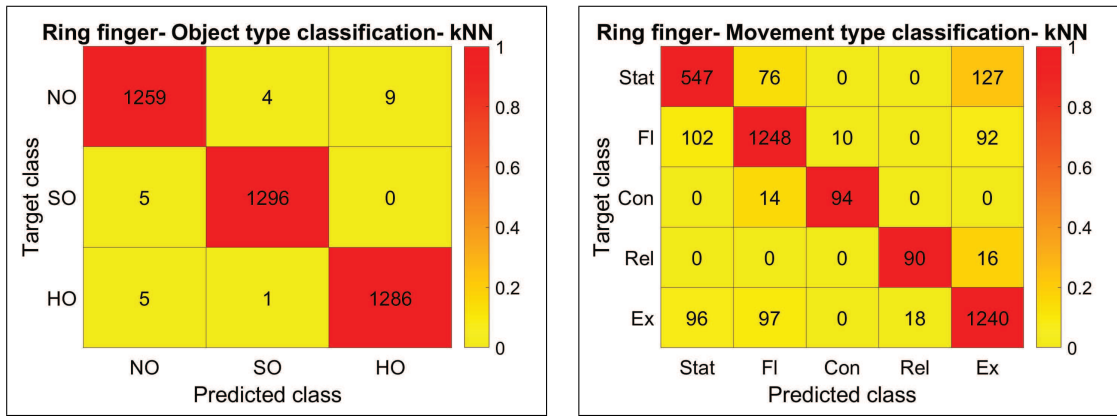


(c)

Figure A.3 Confusion matrices of a) object type, b) movement type, and c) combined type kNN classification of sensor data from the middle finger. Counts are given as numbers in cells. Color code indicates a given count normalized by total instances of the target class.

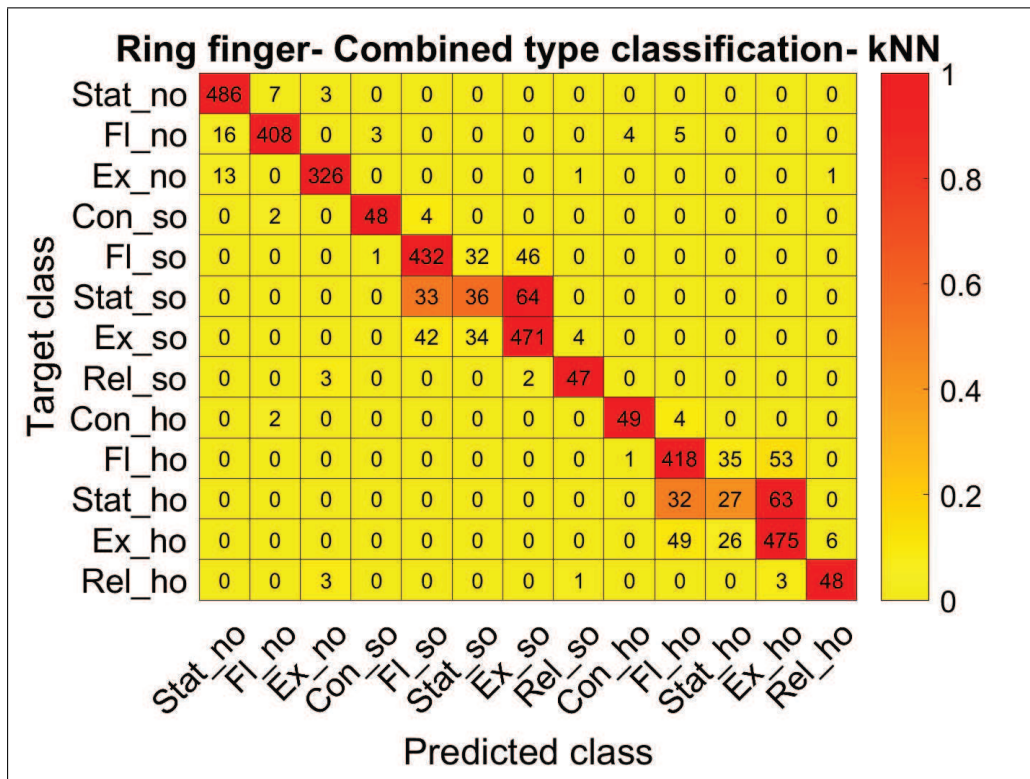
Table A.3
Classification results of kNN classifier for middle finger.

Type of classification	Class(Labels)	Recall	Precision	F1 Score
Object type	No (1,2,3)	0.988	0.985	0.986
	So (4,5,6,7,8)	0.993	0.991	0.992
	Ho (9,10,11,12,13)	0.990	0.995	0.992
Movement type	Stat (1,6,11)	0.732	0.711	0.721
	Fl (2,5,10)	0.816	0.786	0.801
	Con (4,9)	0.852	0.906	0.878
	Rel (8,13)	0.847	0.881	0.864
	Ex (3,7,12)	0.753	0.789	0.771
Combined type	Stat-no (1)	0.973	0.960	0.966
	Fl-no (2)	0.937	0.940	0.938
	Ex-no (3)	0.904	0.923	0.913
	Con-so (4)	0.794	0.857	0.824
	Fl-so (5)	0.755	0.737	0.746
	Stat-so (6)	0.217	0.218	0.217
	Ex-so (7)	0.730	0.742	0.736
	Rel-so (8)	0.864	0.891	0.877
	Con-ho (9)	0.806	0.831	0.818
	Fl-ho (10)	0.815	0.732	0.771
	Stat-ho (11)	0.197	0.190	0.194
	Ex-ho (12)	0.693	0.777	0.733
	Rel-ho (13)	0.828	0.815	0.822



(a)

(b)

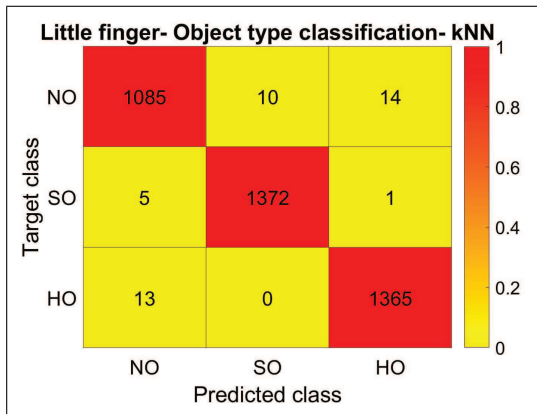


(c)

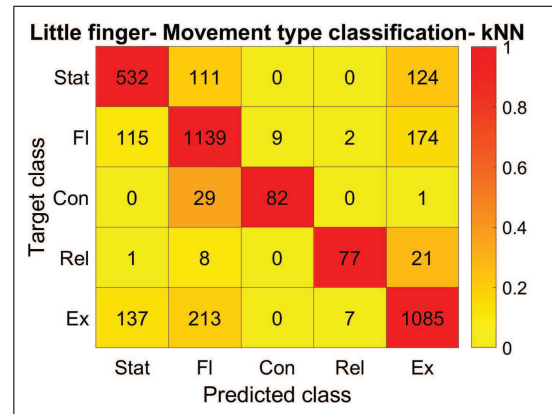
Figure A.4 Confusion matrices of a) object type, b) movement type, and c) combined type kNN classification of sensor data from the ring finger. Counts are given as numbers in cells. Color code indicates a given count normalized by total instances of the target class.

Table A.4
Classification results of kNN Classifier for ring finger.

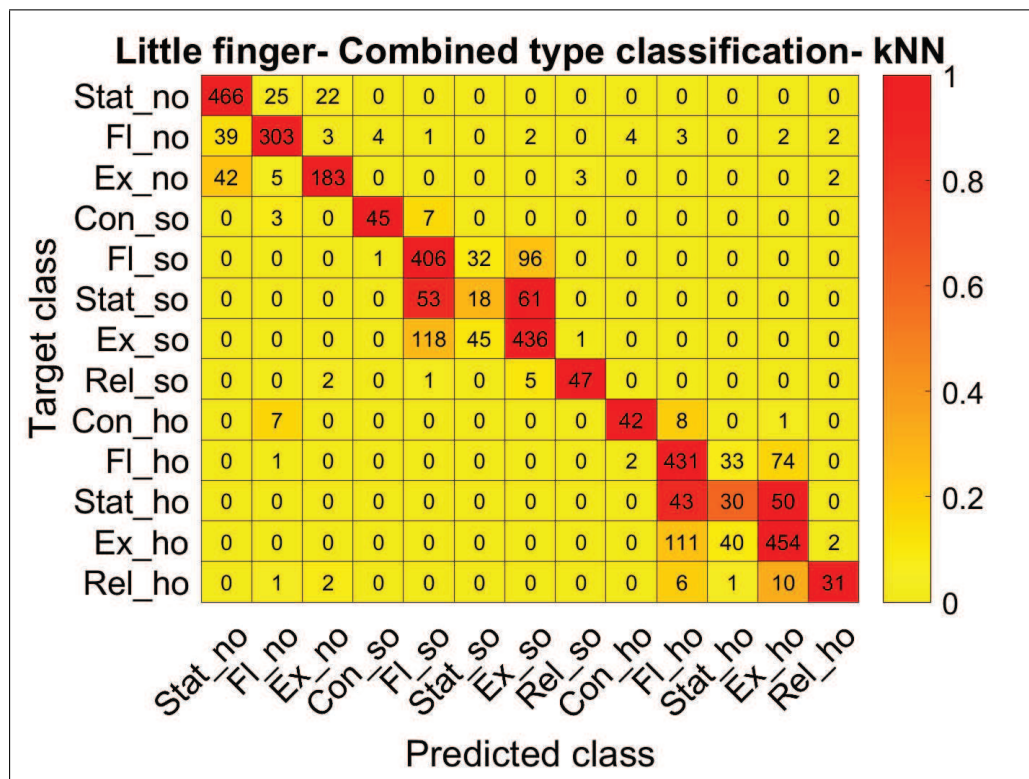
Type of classification	Class(Labels)	Recall	Precision	F1 Score
Object type	No (1,2,3)	0.989	0.992	0.991
	So (4,5,6,7,8)	0.996	0.996	0.996
	Ho (9,10,11,12,13)	0.996	0.993	0.994
Movement type	Stat (1,6,11)	0.730	0.735	0.732
	Fl (2,5,10)	0.860	0.870	0.865
	Con (4,9)	0.871	0.902	0.886
	Rel (8,13)	0.849	0.837	0.843
	Ex (3,7,12)	0.855	0.841	0.848
Combined type	Stat-no (1)	0.981	0.944	0.962
	Fl-no (2)	0.937	0.974	0.955
	Ex-no (3)	0.955	0.974	0.964
	Con-so (4)	0.891	0.930	0.910
	Fl-so (5)	0.846	0.846	0.846
	Stat-so (6)	0.273	0.353	0.308
	Ex-so (7)	0.855	0.809	0.831
	Rel-so (8)	0.904	0.892	0.898
	Con-ho (9)	0.893	0.914	0.903
	Fl-ho (10)	0.826	0.823	0.824
	Stat-ho (11)	0.218	0.306	0.255
	Ex-ho (12)	0.854	0.800	0.826
	Rel-ho (13)	0.886	0.870	0.878



(a)



(b)



(c)

Figure A.5 Confusion matrices of a) object type, b) movement type, and c) combined type kNN classification of sensor data from the little finger. Counts are given as numbers in cells. Color code indicates a given count normalized by total instances of the target class.

Table A.5
Classification results of kNN classifier for little finger.

Type of classification	Class(Labels)	Recall	Precision	F1 Score
Object type	No (1,2,3)	0.978	0.984	0.981
	So (4,5,6,7,8)	0.996	0.993	0.994
	Ho (9,10,11,12,13)	0.991	0.989	0.990
Movement type	Stat (1,6,11)	0.694	0.678	0.686
	Fl (2,5,10)	0.792	0.759	0.775
	Con (4,9)	0.732	0.901	0.808
	Rel (8,13)	0.720	0.895	0.798
	Ex (3,7,12)	0.752	0.772	0.762
Combined type	Stat-no (1)	0.908	0.852	0.879
	Fl-no (2)	0.835	0.878	0.856
	Ex-no (3)	0.779	0.863	0.819
	Con-so (4)	0.818	0.900	0.857
	Fl-so (5)	0.759	0.693	0.724
	Stat-so (6)	0.136	0.189	0.159
	Ex-so (7)	0.727	0.727	0.727
	Rel-so (8)	0.855	0.922	0.887
	Con-ho (9)	0.724	0.875	0.792
	Fl-ho (10)	0.797	0.716	0.754
	Stat-ho (11)	0.244	0.288	0.264
	Ex-ho (12)	0.748	0.768	0.758
	Rel-ho (13)	0.608	0.838	0.705

APPENDIX B. PSYCHOPHYSICAL CHARACTERIZATION OF PARTICIPANTS

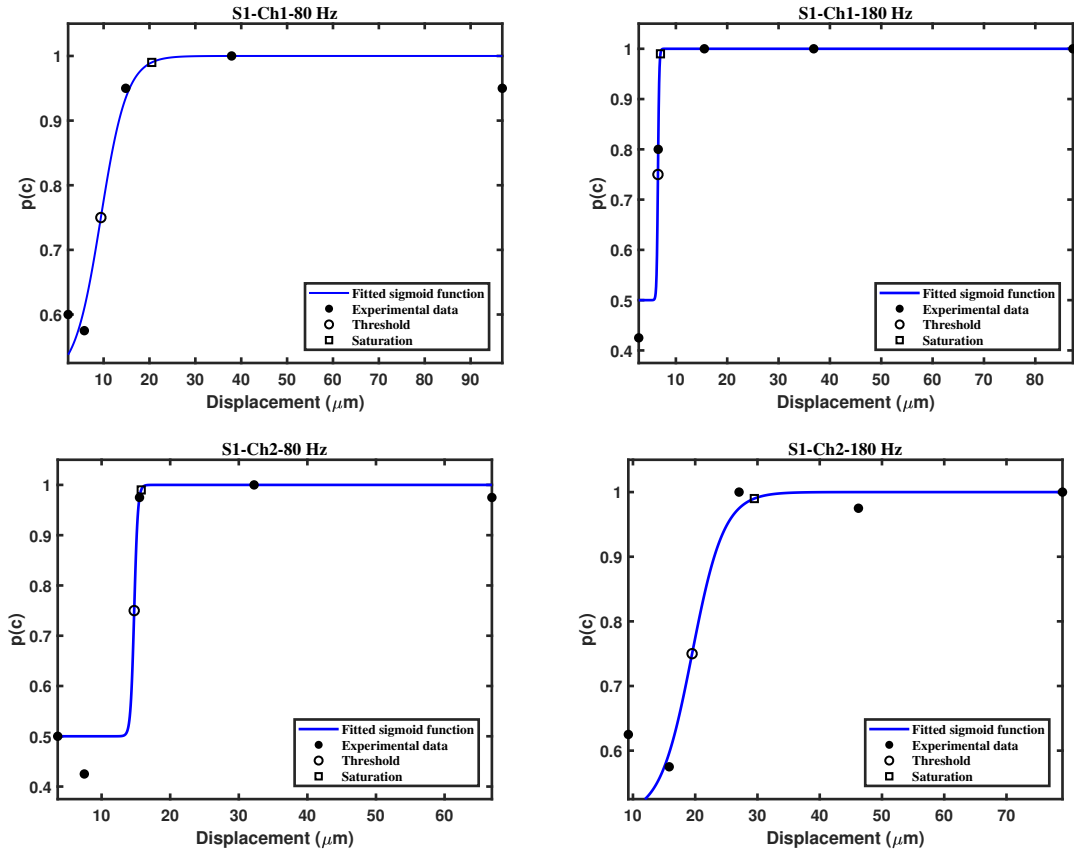


Figure B.1 Psychometric curves for S1.

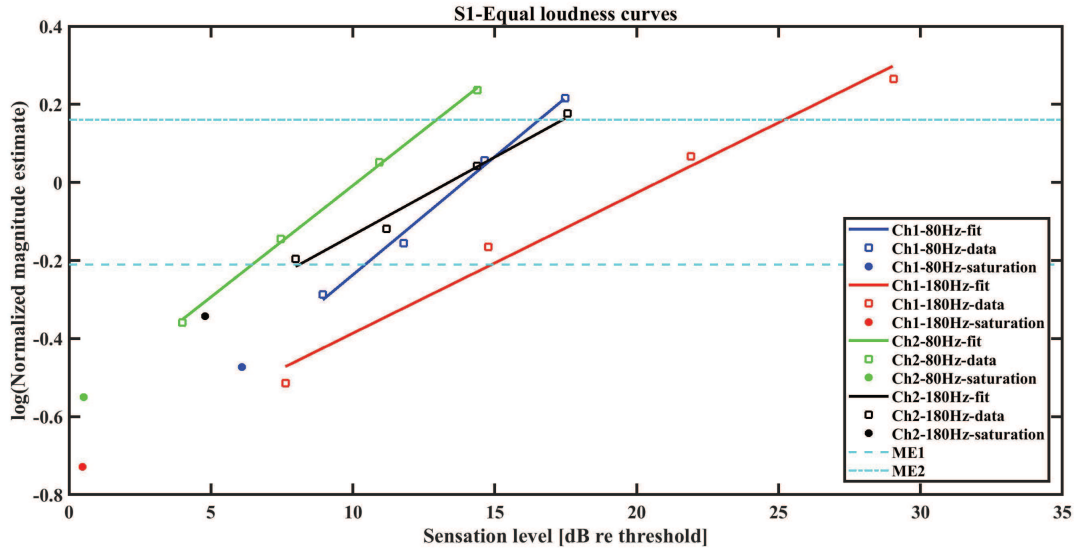


Figure B.2 Equal loudness curves for S1.

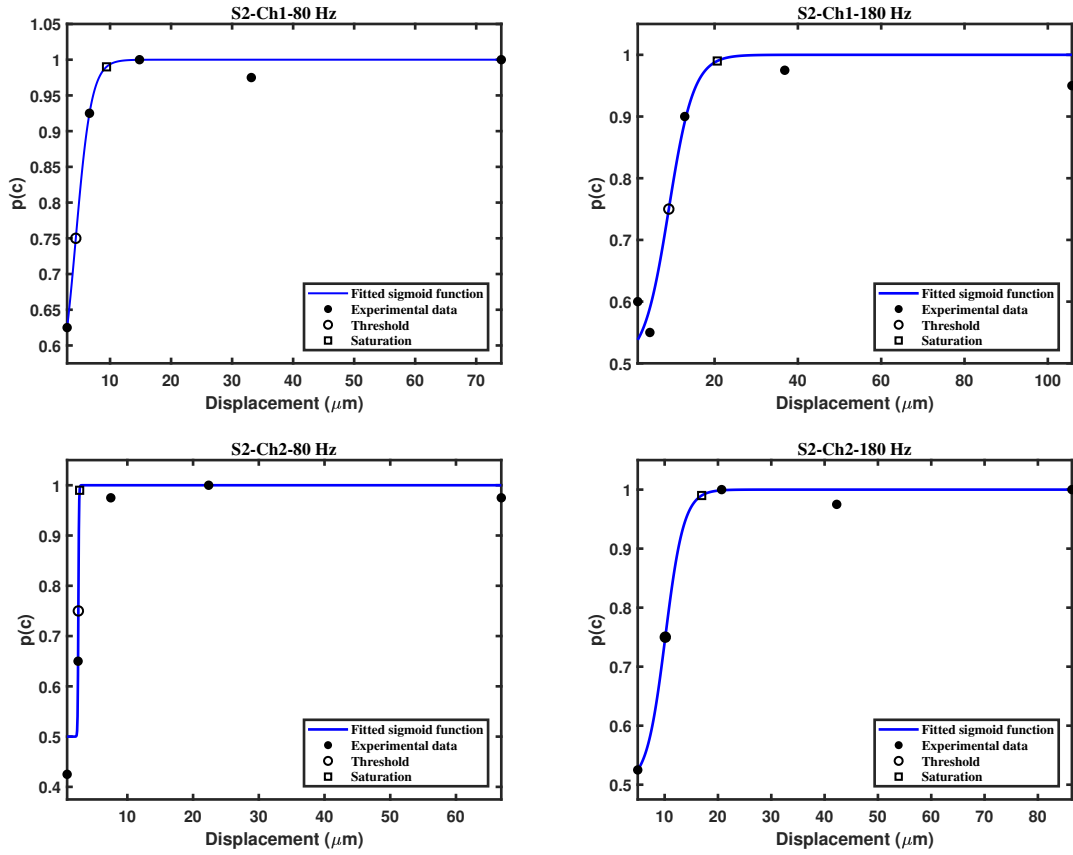


Figure B.3 Psychometric curves for S2.

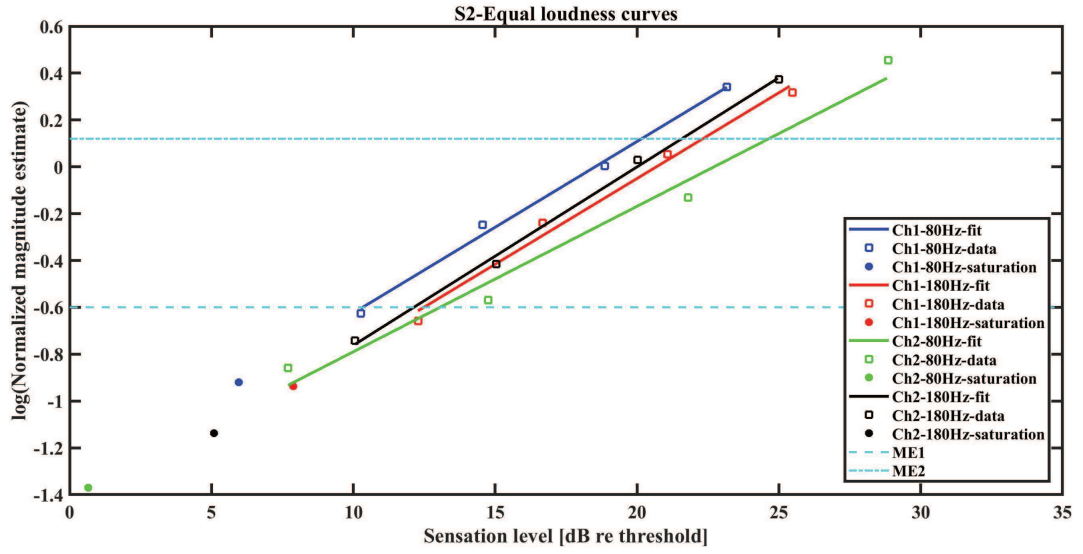


Figure B.4 Equal loudness curves for S2.

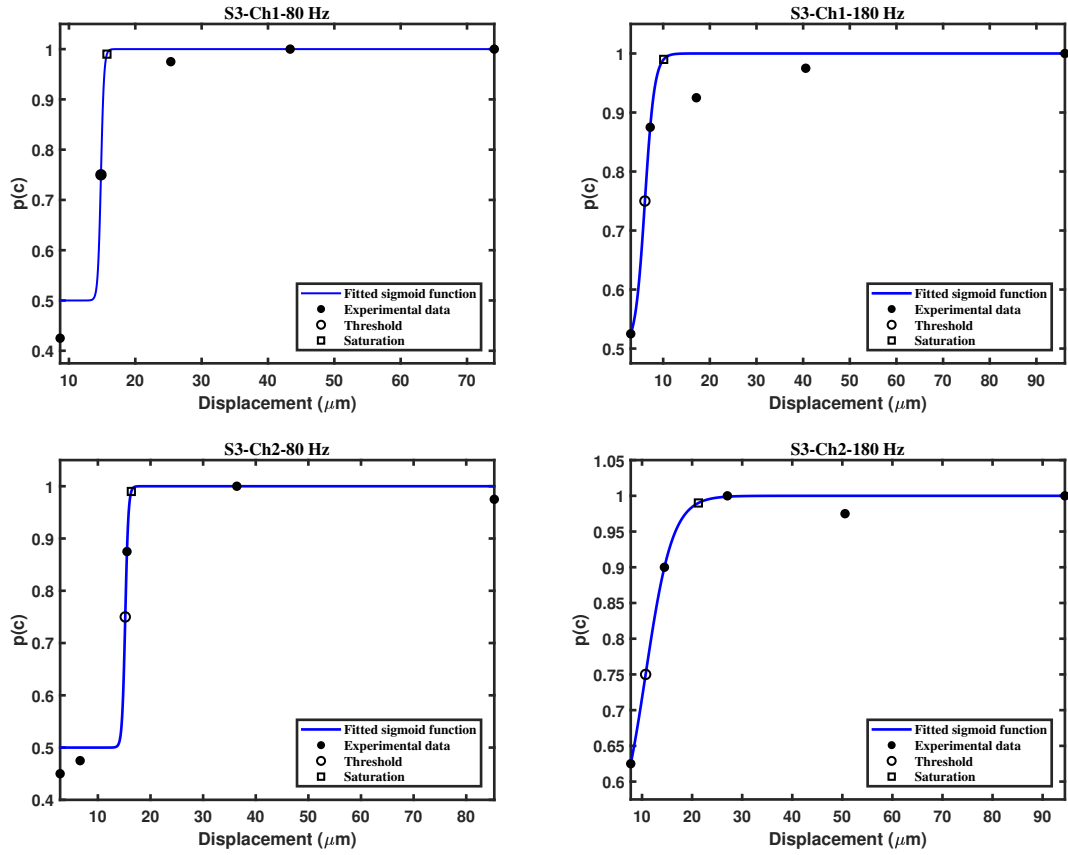


Figure B.5 Psychometric curves for S3.

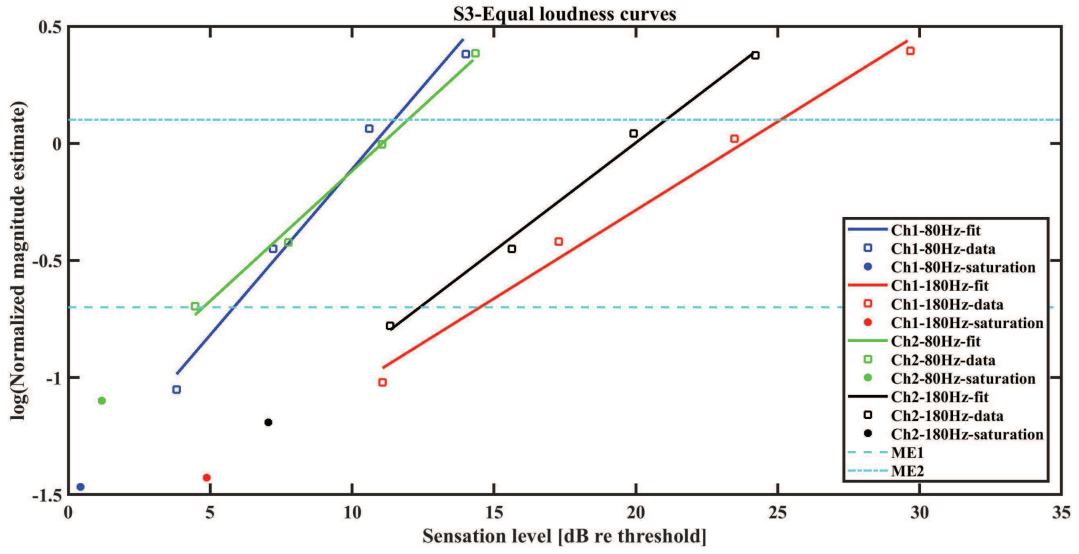


Figure B.6 Equal loudness curves for S3.

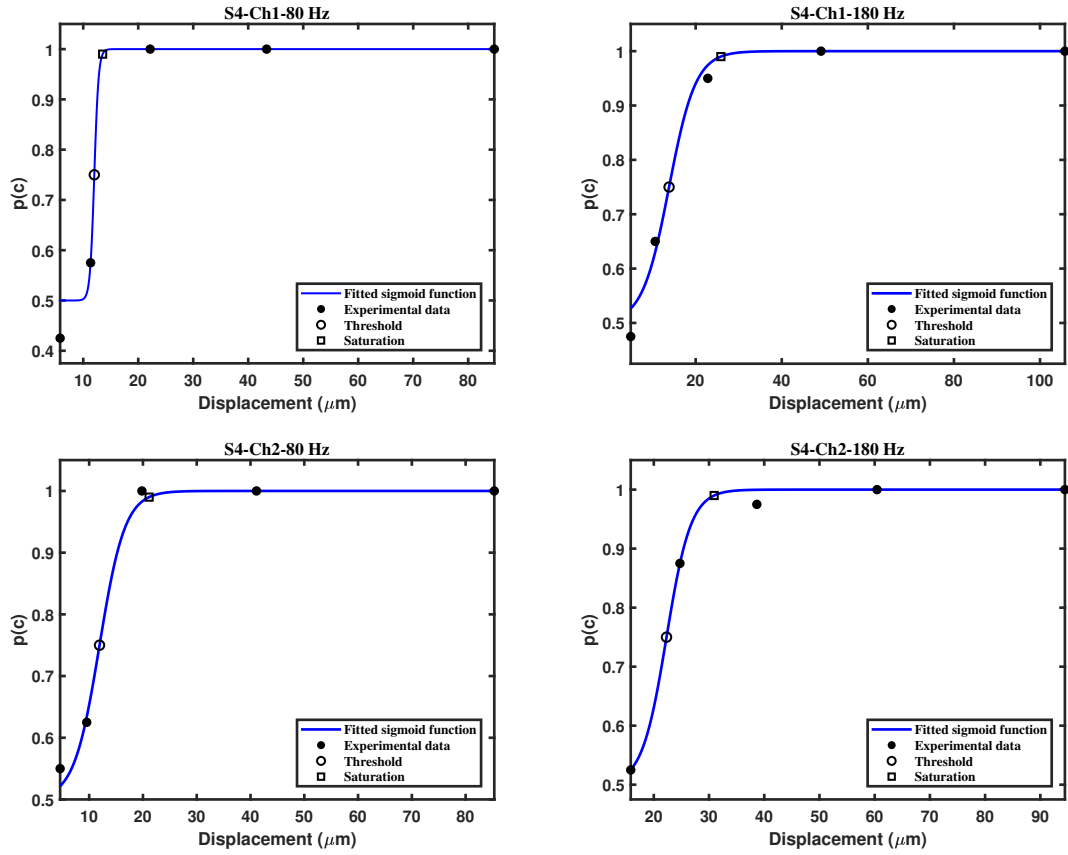


Figure B.7 Psychometric curves for S4.

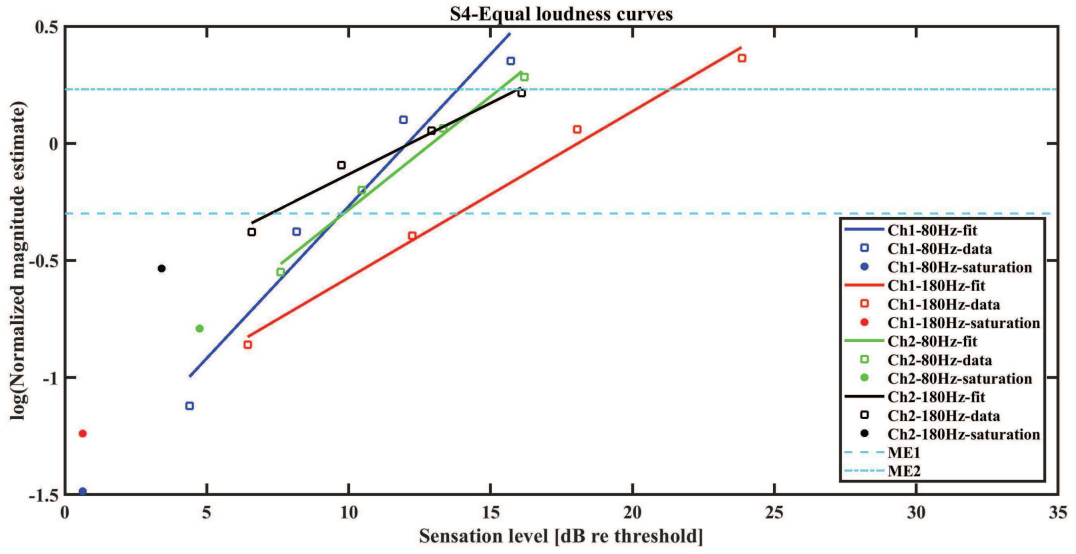


Figure B.8 Equal loudness curves for S4.

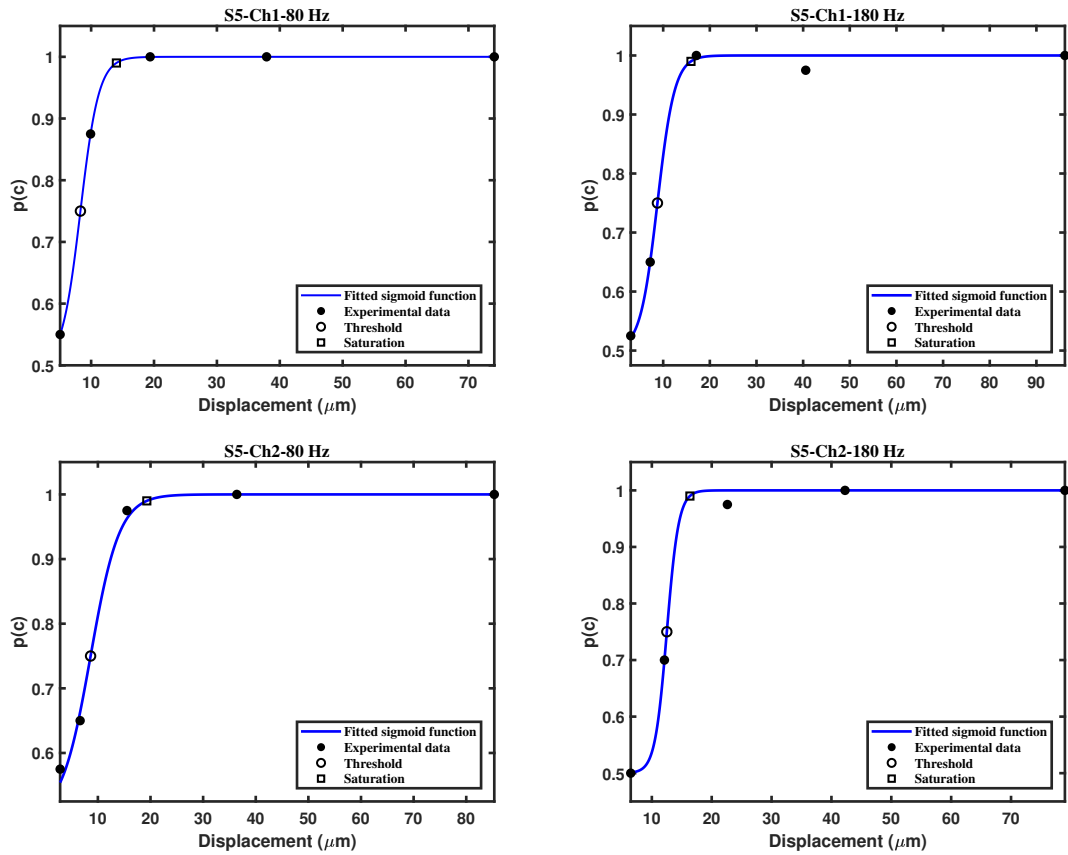


Figure B.9 Psychometric curves for S5.

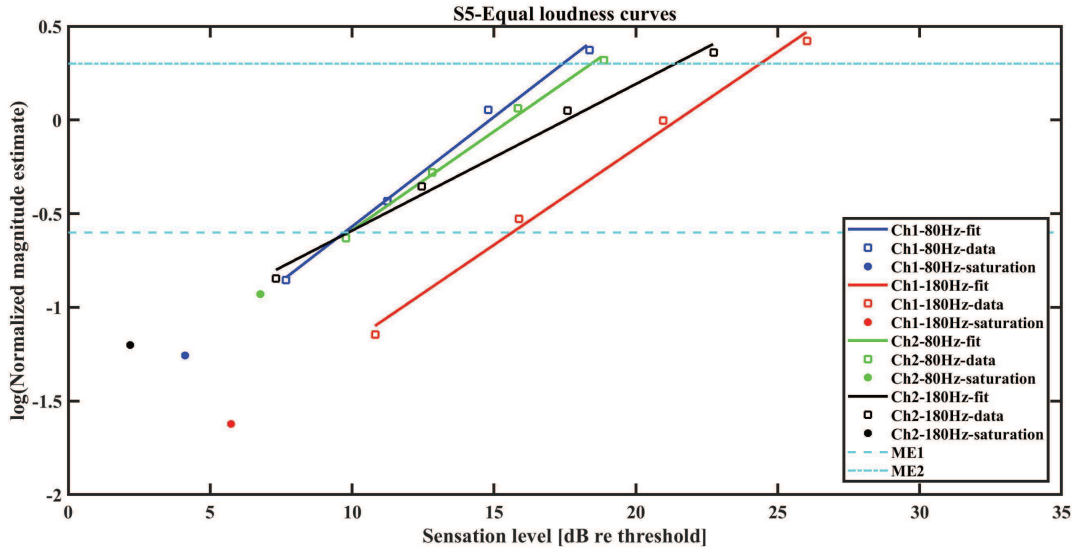


Figure B.10 Equal loudness curves for S5.

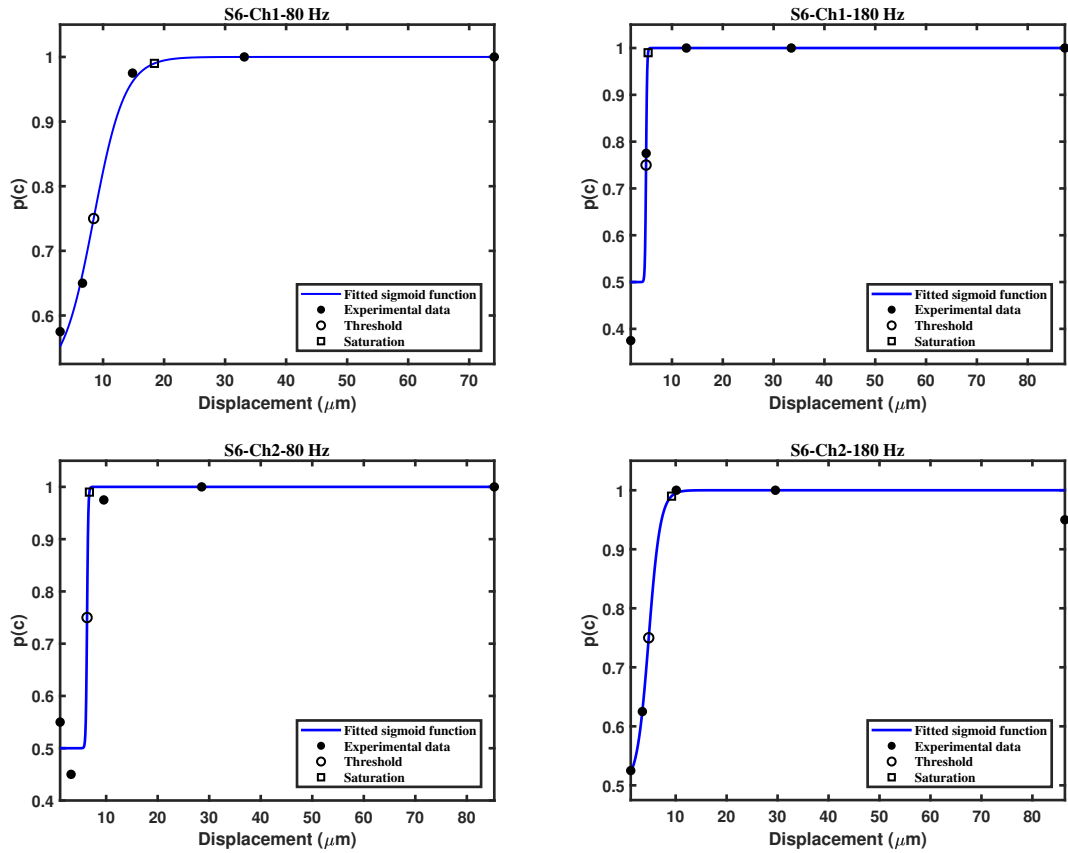


Figure B.11 Psychometric curves for S6.

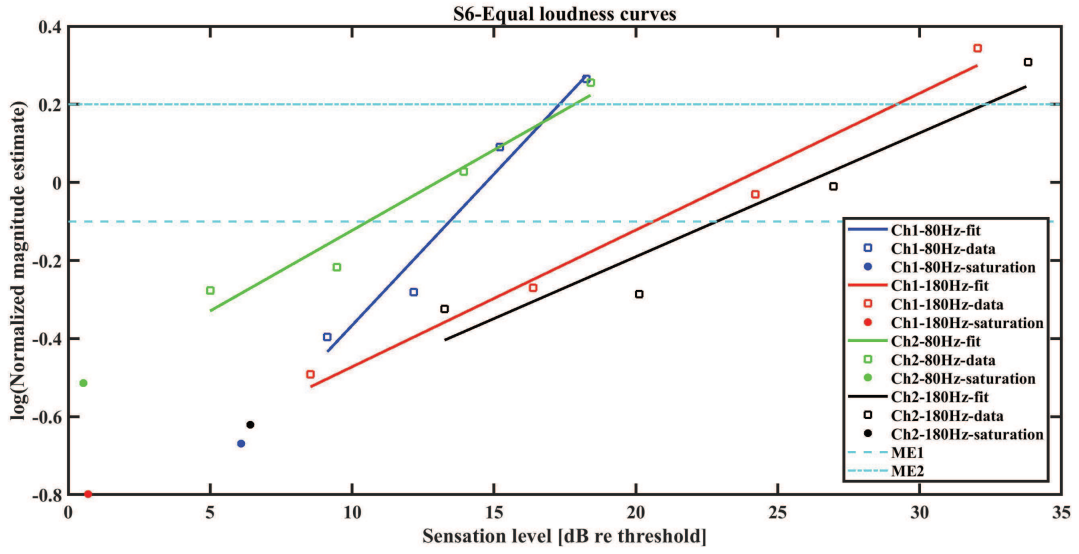


Figure B.12 Equal loudness curves for S6

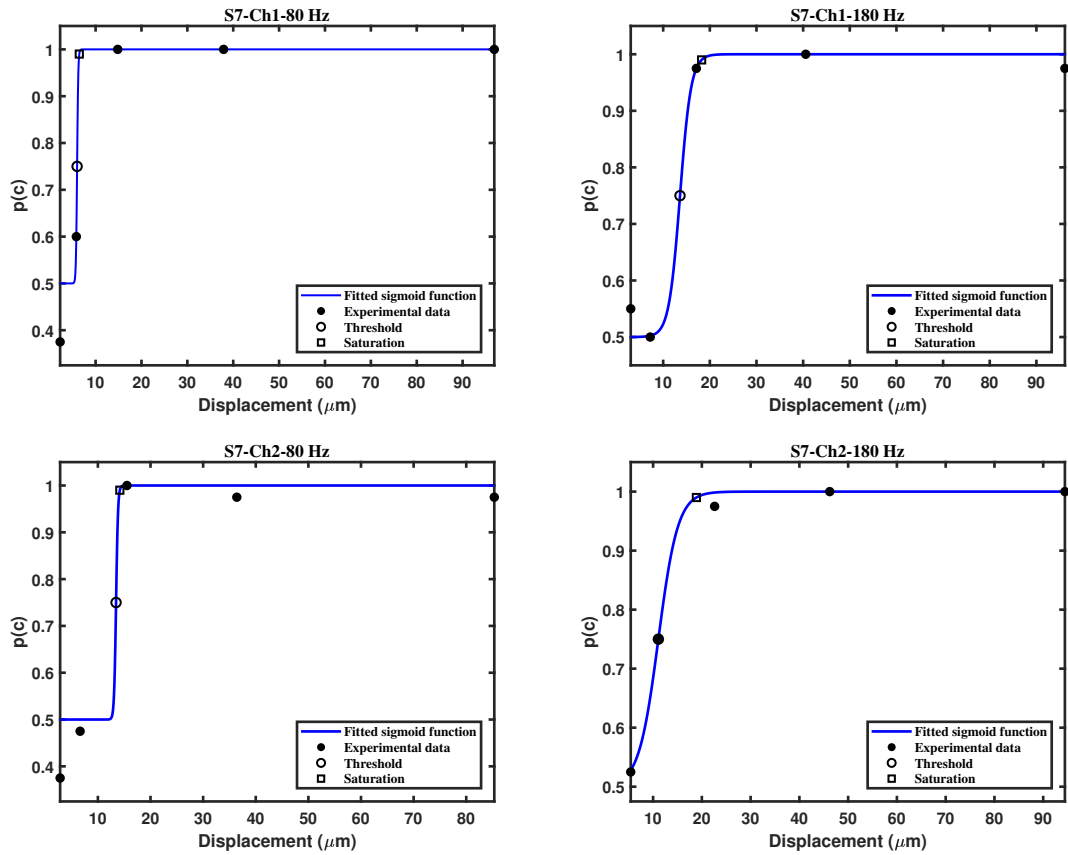


Figure B.13 Psychometric curves for S7.

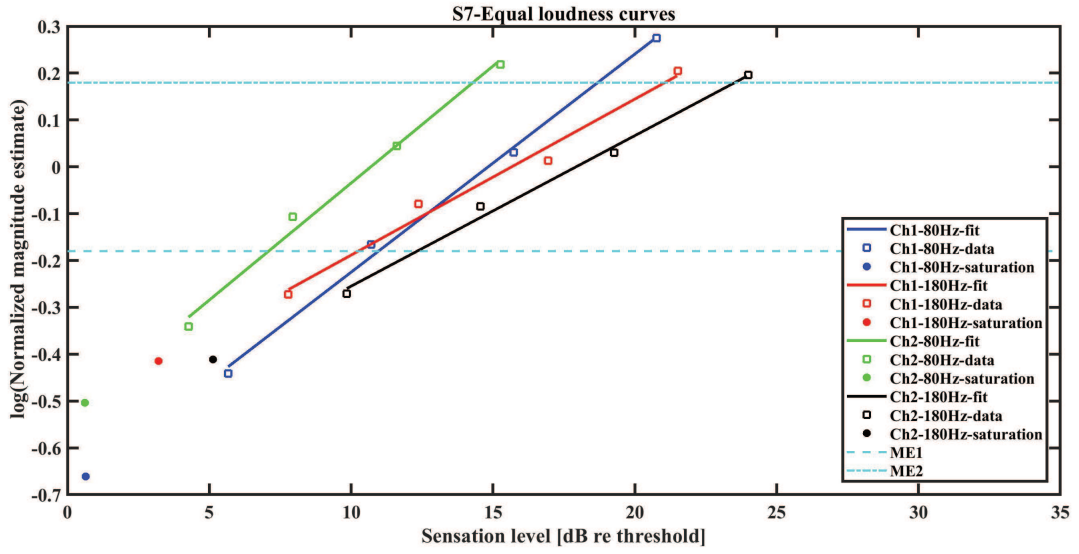


Figure B.14 Equal loudness curves for S7.

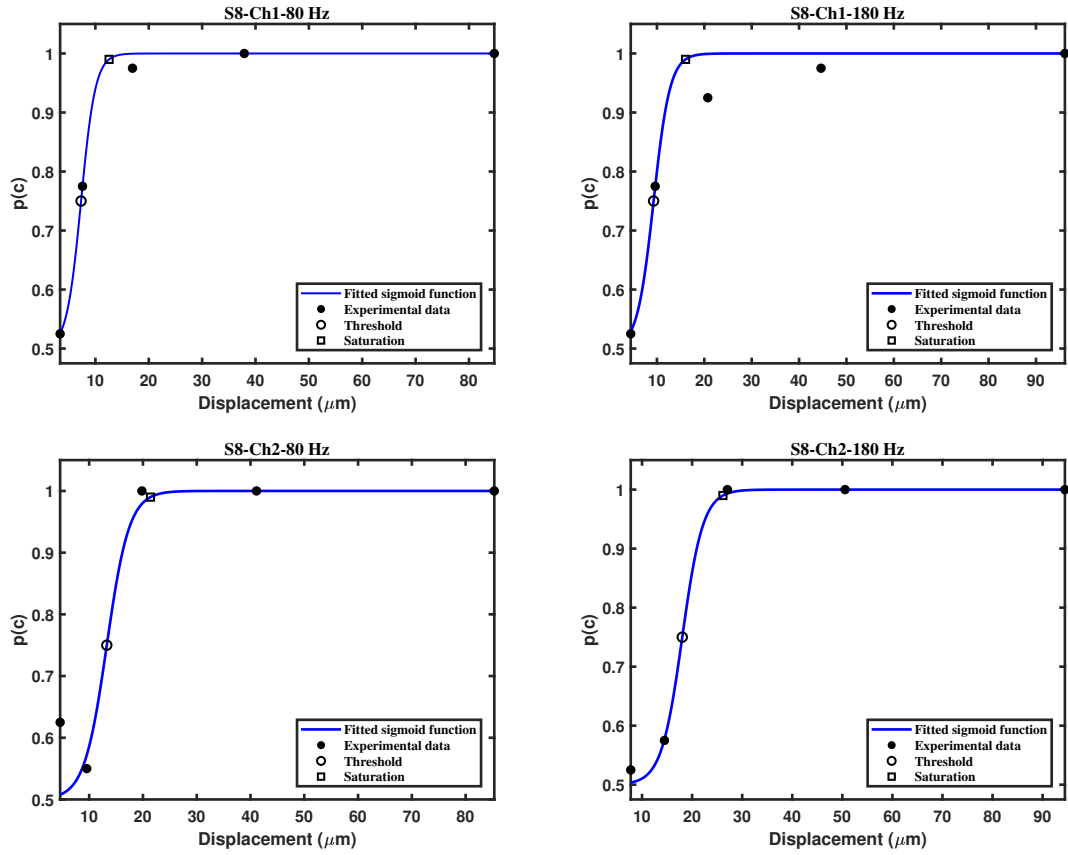


Figure B.15 Psychometric curves for S8.

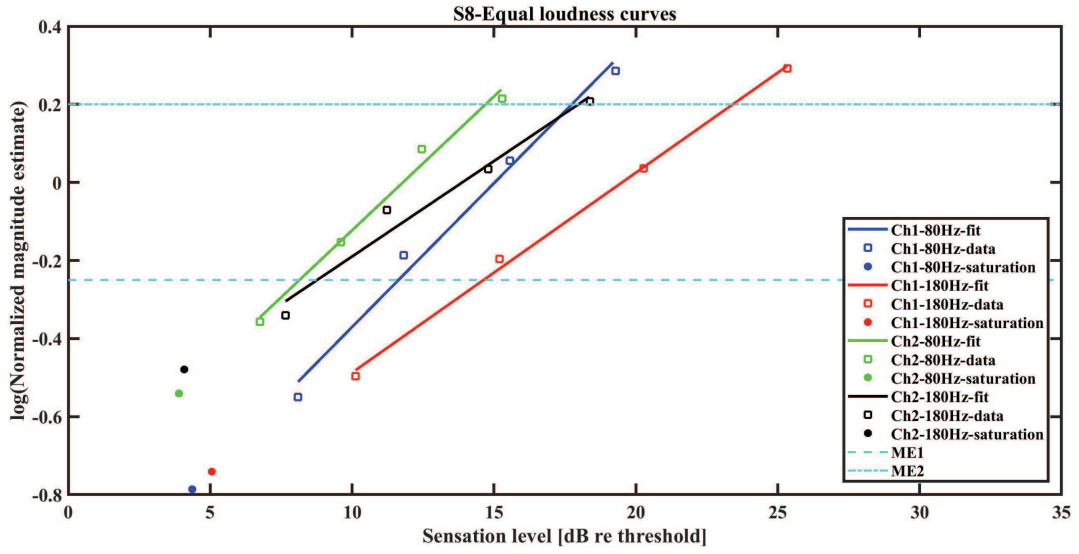


Figure B.16 Equal loudness curves for S8.

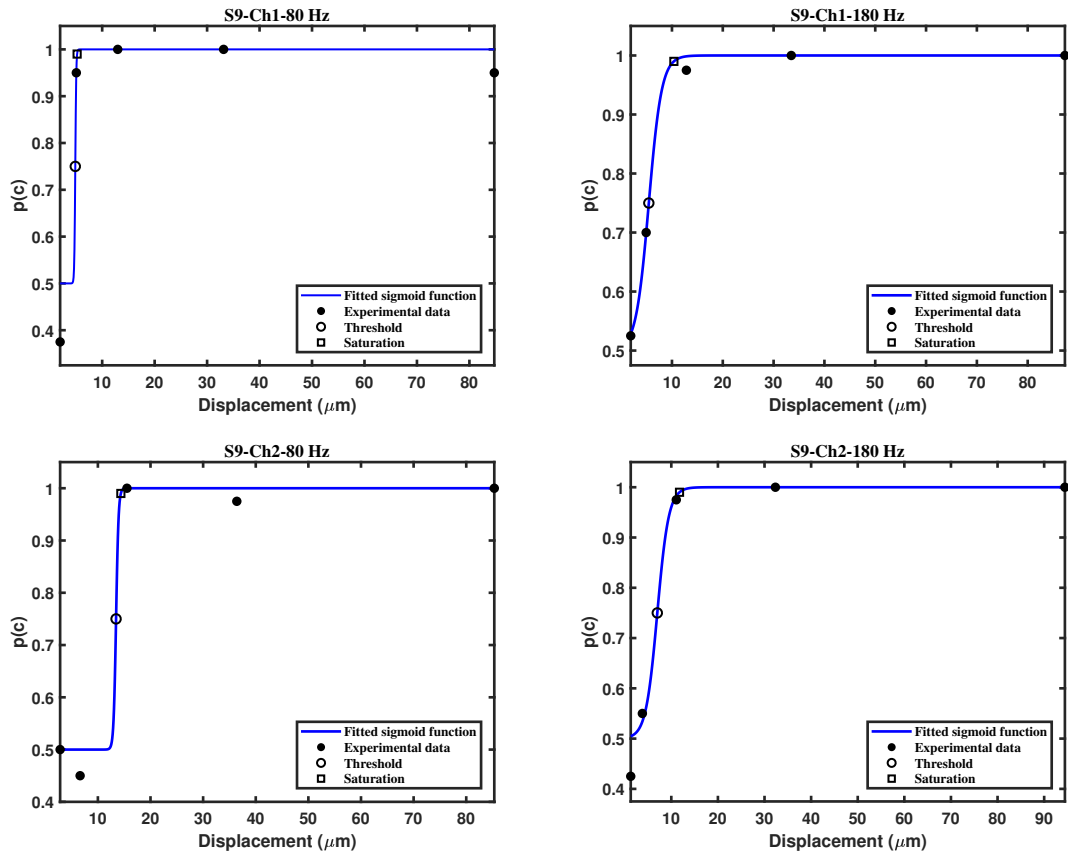


Figure B.17 Psychometric curves for S9.

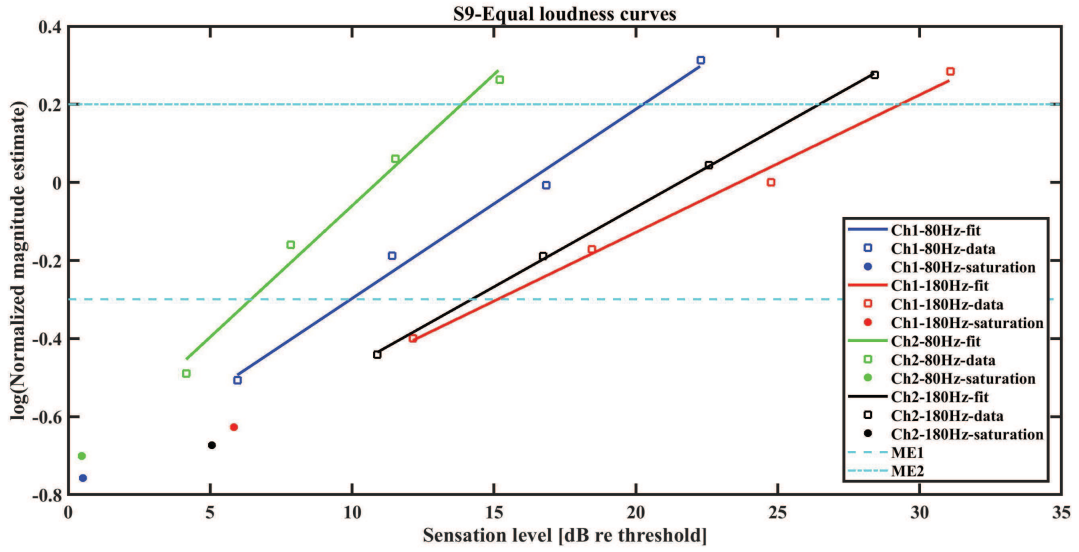


Figure B.18 Equal loudness curves for S9.

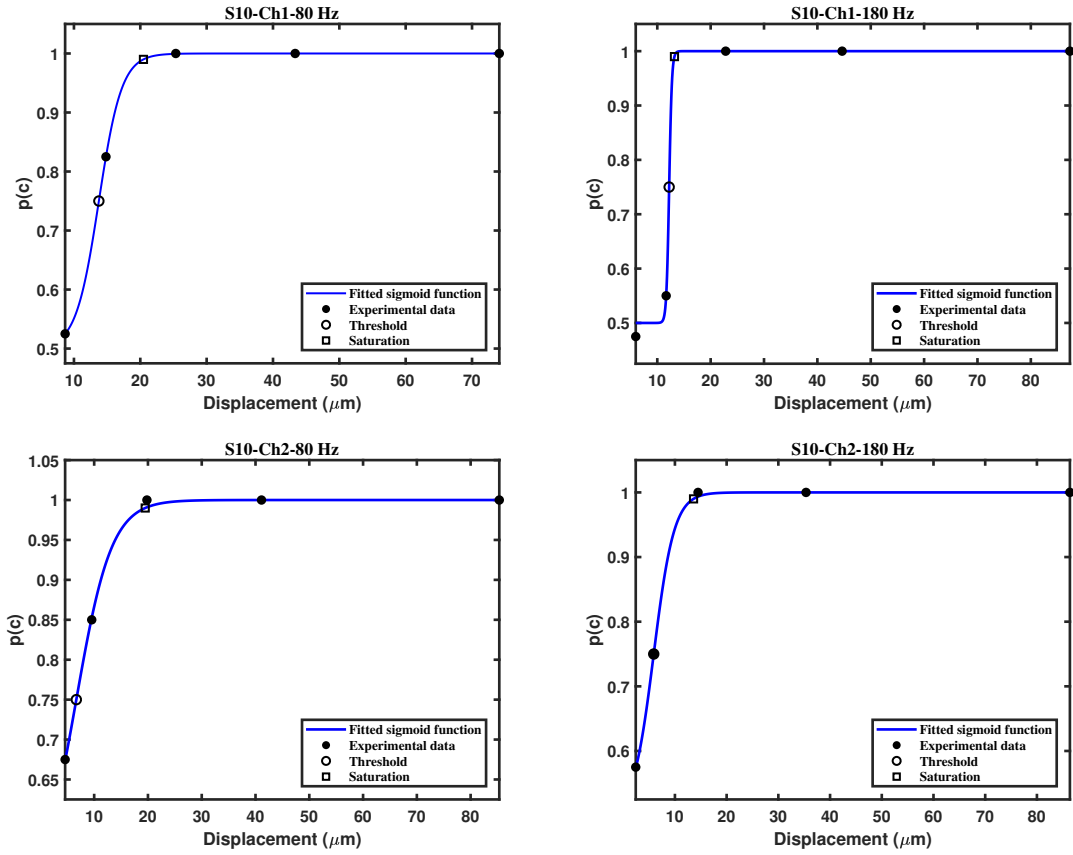


Figure B.19 Psychometric curves for S10.

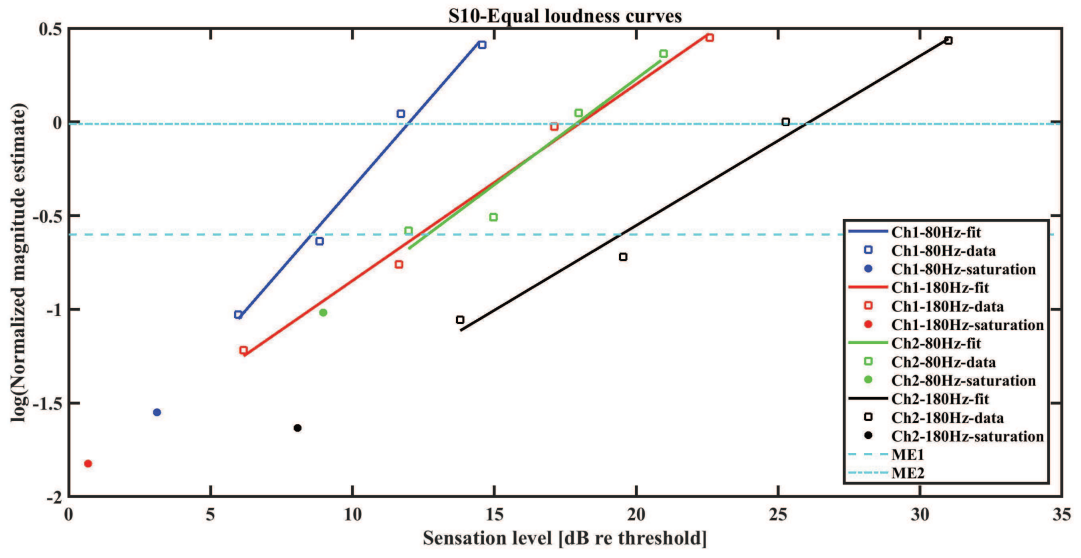


Figure B.20 Equal loudness curves for S10.

**APPENDIX C. INDIVIDUAL SUBJECT PERFORMANCE
IN DISCRETE EVENT-DRIVEN FEEDBACK
EXPERIMENTS**

Table C.1

List of sequences used in discrete event-driven feedback experiments.

No	Sequence	Stimuli
1	Flexion in air- Extension in air	AR-BR
2	Extension in air- Flexion in air	BR-AR
3	Flexion in air- Contact to soft object	AR-AL
4	Flexion in air- Contact to hard object	AR-BL
5	Flexion in air- Contact to soft object-Release from soft object	AR-AL-BR
6	Flexion in air- Contact to hard object-Release from hard object	AR-BL-BR
7	Flexion in air- Contact to soft object- Flexion in soft object	AR-AL-CR
8	Flexion in air- Contact to hard object- Flexion in hard object	AR-BL-CR
9	Contact to soft object- Flexion in soft object- Force increases in soft object	AL-CR-CL
10	Contact to hard object- Flexion in hard object- Force increases in hard object	BL-CR-DL
11	Contact to soft object- Flexion in soft object- Stationary in soft object	AL-CR-AL
12	Contact to hard object- Flexion in hard object- Stationary in hard object	BL-CR-BL
13	Contact to soft object- Flexion in soft object- Extension in soft object	AL-CR-DR
14	Contact to hard object- Flexion in hard object- Extension in hard object	BL-CR-DR

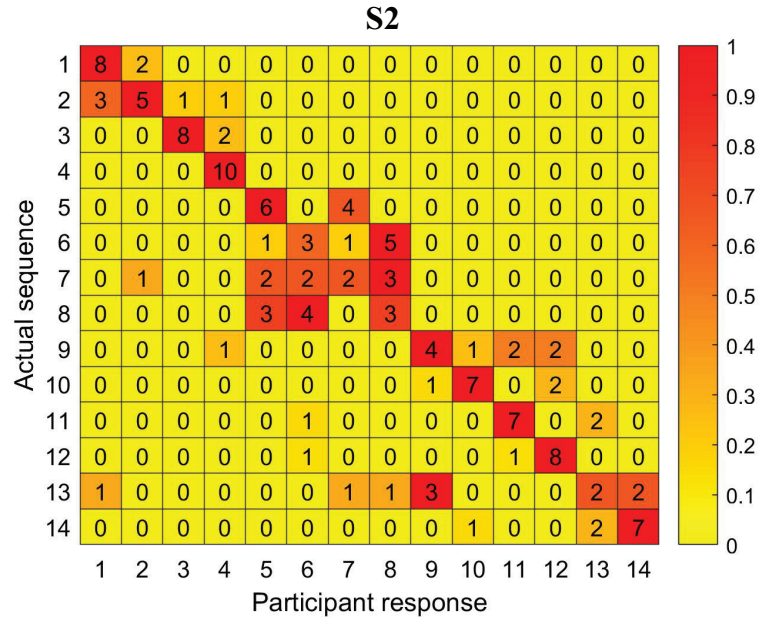


Figure C.1 Confusion matrix for S2's responses in discrete event driven feedback experiment.

Table C.2

Performance scores for S2's responses in discrete event-driven feedback experiment.

Sequence no	Recall	Precision	F1 Score
1	0.80	0.67	0.73
2	0.50	0.63	0.56
3	0.80	0.89	0.84
4	1.00	0.71	0.83
5	0.60	0.50	0.55
6	0.30	0.27	0.29
7	0.20	0.25	0.22
8	0.30	0.25	0.27
9	0.40	0.50	0.44
10	0.70	0.78	0.74
11	0.70	0.70	0.70
12	0.80	0.67	0.73
13	0.20	0.33	0.25
14	0.70	0.78	0.74

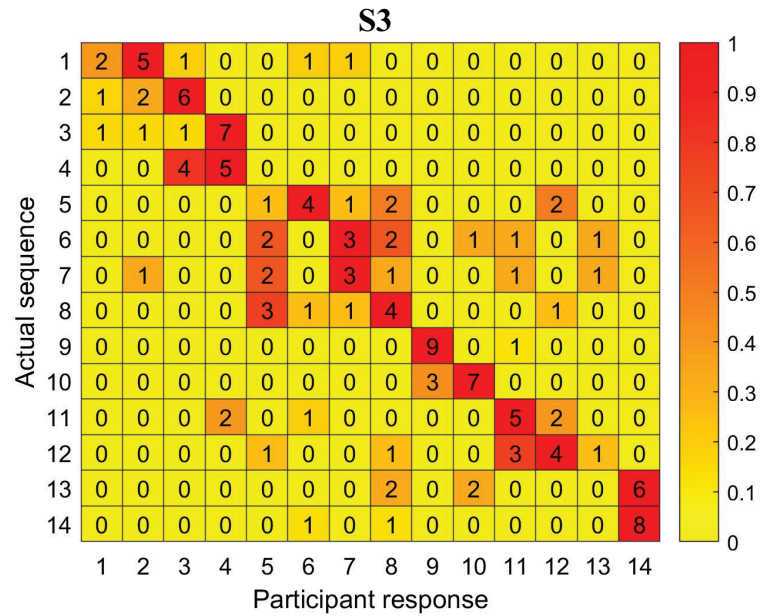


Figure C.2 Confusion matrix for S3's responses in discrete event driven feedback experiment.

Table C.3

Performance scores for S3's responses in discrete event-driven feedback experiment.

Sequence no	Recall	Precision	F1 Score
1	0.20	0.50	0.29
2	0.22	0.22	0.22
3	0.10	0.08	0.09
4	0.56	0.36	0.43
5	0.10	0.11	0.11
6	0.00	0.00	0.00
7	0.33	0.33	0.33
8	0.40	0.31	0.35
9	0.90	0.75	0.82
10	0.70	0.70	0.70
11	0.50	0.45	0.48
12	0.40	0.44	0.42
13	0.00	0.00	0.00
14	0.80	0.57	0.67

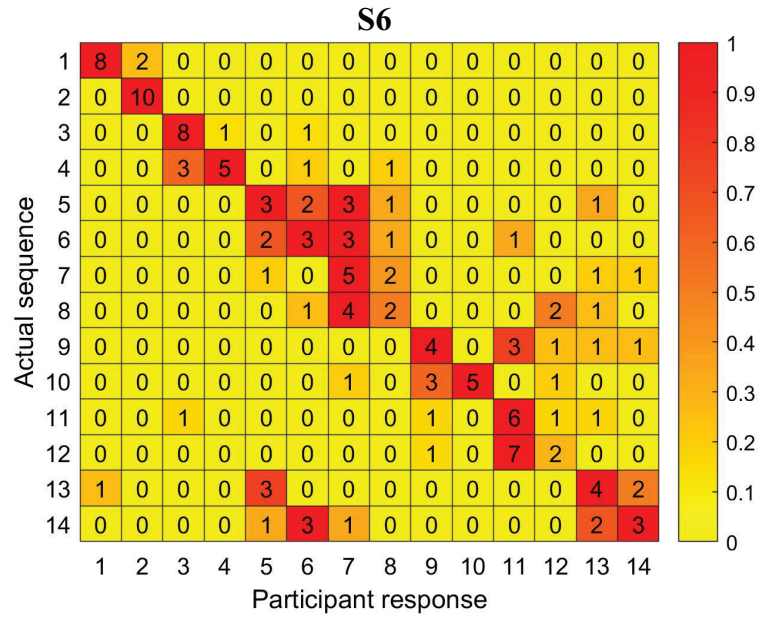


Figure C.3 Confusion matrix for S6's responses in discrete event driven feedback experiment.

Table C.4

Performance scores for S6's responses in discrete event-driven feedback experiment.

Sequence no	Recall	Precision	F1 Score
1	0.80	0.89	0.84
2	1.00	0.83	0.91
3	0.80	0.67	0.73
4	0.50	0.83	0.63
5	0.30	0.30	0.30
6	0.30	0.27	0.29
7	0.50	0.29	0.37
8	0.20	0.29	0.24
9	0.40	0.44	0.42
10	0.50	1.00	0.67
11	0.60	0.35	0.44
12	0.20	0.29	0.24
13	0.40	0.36	0.38
14	0.30	0.43	0.35

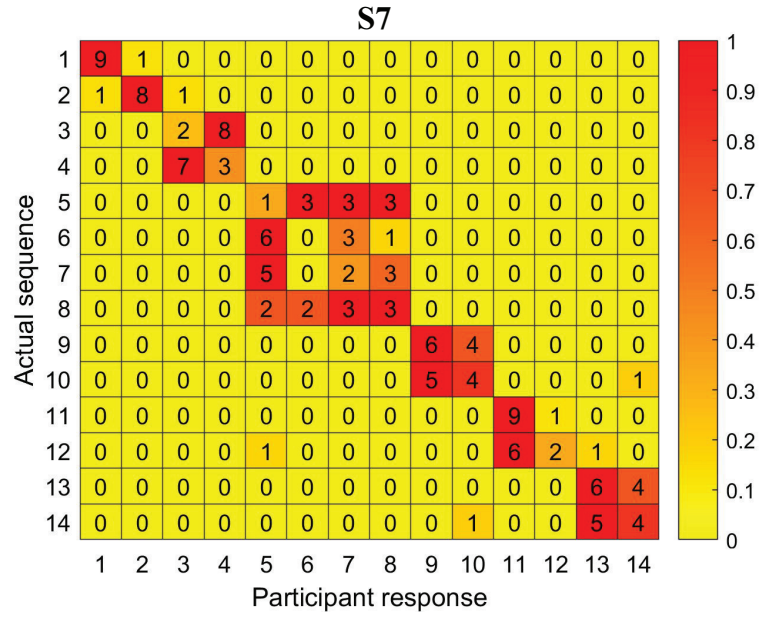


Figure C.4 Confusion matrix for S7's responses in discrete event driven feedback experiment.

Table C.5

Performance scores for S7's responses in discrete event-driven feedback experiment.

Sequence no	Recall	Precision	F1 Score
1	0.90	0.90	0.90
2	0.80	0.89	0.84
3	0.20	0.20	0.20
4	0.30	0.27	0.29
5	0.10	0.07	0.08
6	0.00	0.00	0.00
7	0.20	0.18	0.19
8	0.30	0.30	0.30
9	0.60	0.55	0.57
10	0.40	0.44	0.42
11	0.90	0.60	0.72
12	0.20	0.67	0.31
13	0.60	0.50	0.55
14	0.40	0.44	0.42

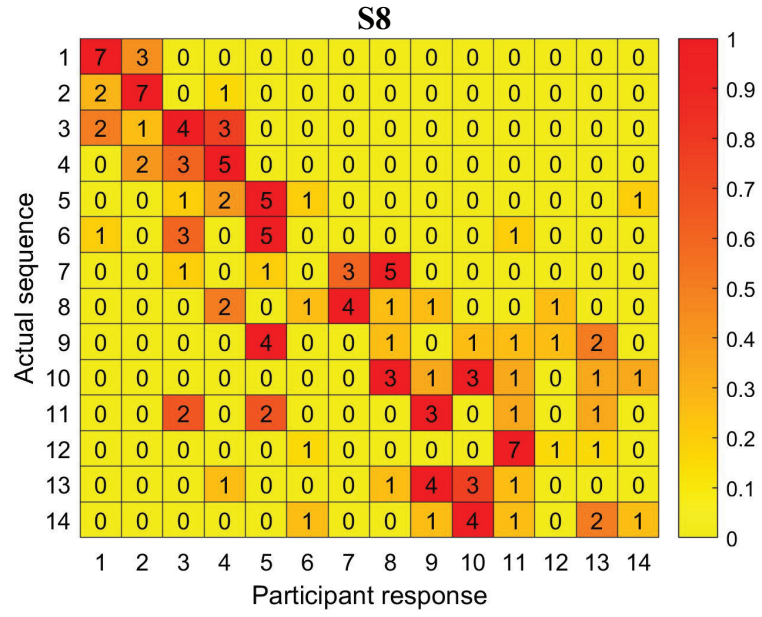


Figure C.5 Confusion matrix for S8's responses in discrete event driven feedback experiment.

Table C.6

Performance scores for S8's responses in discrete event-driven feedback experiment.

Sequence no	Recall	Precision	F1 Score
1	0.70	0.58	0.64
2	0.70	0.54	0.61
3	0.40	0.29	0.33
4	0.50	0.36	0.42
5	0.50	0.29	0.37
6	0.00	0.00	0.00
7	0.30	0.43	0.35
8	0.10	0.09	0.10
9	0.00	0.00	0.00
10	0.30	0.27	0.29
11	0.11	0.08	0.09
12	0.10	0.33	0.15
13	0.00	0.00	0.00
14	0.10	0.33	0.15

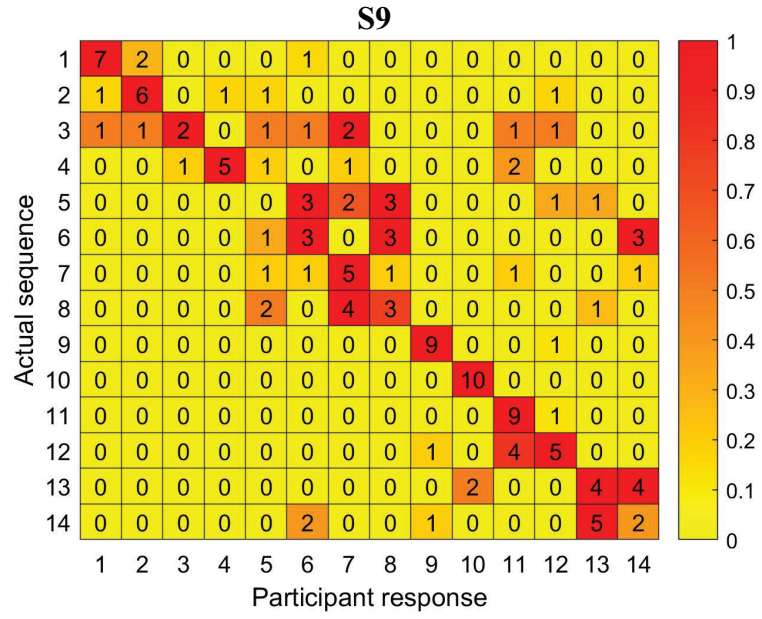


Figure C.6 Confusion matrix for S9's responses in discrete event driven feedback experiment.

Table C.7

Performance scores for S9's responses in discrete event-driven feedback experiment.

Sequence no	Recall	Precision	F1 Score
1	0.70	0.78	0.74
2	0.60	0.67	0.63
3	0.20	0.67	0.31
4	0.50	0.83	0.63
5	0.00	0.00	0.00
6	0.30	0.27	0.29
7	0.50	0.36	0.42
8	0.30	0.30	0.30
9	0.90	0.82	0.86
10	1.00	0.83	0.91
11	0.90	0.53	0.67
12	0.50	0.50	0.50
13	0.40	0.36	0.38
14	0.20	0.20	0.20

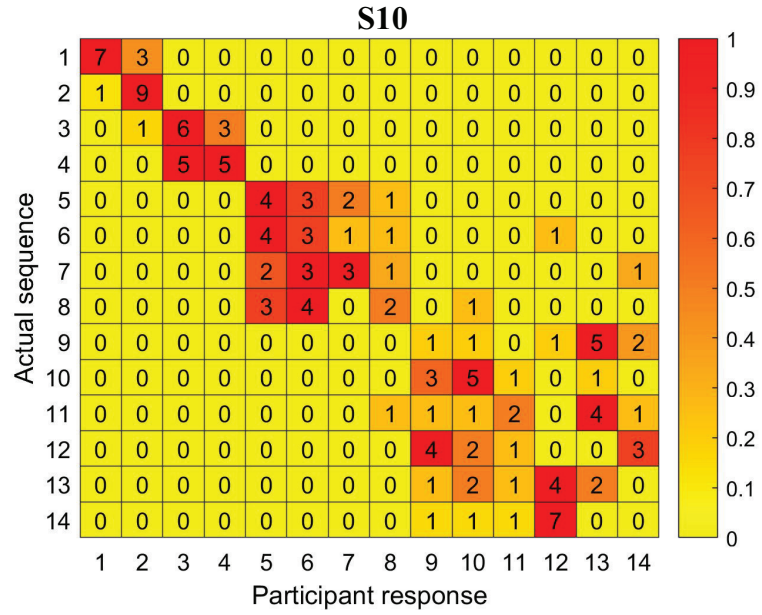


Figure C.7 Confusion matrix for S10’s responses in discrete event driven feedback experiment.

Table C.8

Performance scores for S10’s responses in discrete event-driven feedback experiment.

Sequence no	Recall	Precision	F1 Score
1	0.70	0.88	0.78
2	0.90	0.69	0.78
3	0.60	0.55	0.57
4	0.50	0.63	0.56
5	0.40	0.31	0.35
6	0.30	0.23	0.26
7	0.30	0.50	0.38
8	0.20	0.33	0.25
9	0.10	0.09	0.10
10	0.50	0.38	0.43
11	0.20	0.33	0.25
12	0.00	0.00	0.00
13	0.20	0.17	0.18
14	0.00	0.00	0.00

APPENDIX D. LIST OF PUBLICATIONS

Journal articles

- Yıldız, M. Z., **I. Toker**, F. B. Özkan, and B. Güçlü, "Effects of passive and active movement on vibrotactile detection thresholds of the pacinian channel and forward masking," *Somatosensory and Motor Research*, Vol. 32, no. 4, pp. 262-272, 2015.
- **Karakuş, I.**, B. Güçlü, "Psychophysical principles of discrete event-driven vibrotactile feedback for prostheses," *Somatosensory and Motor Research*. In Press, DOI: 10.1080/08990220.2020.1769055, Published online: 25 May 2020.
- **Karakuş, I.** A. Atasoy, E. Kaplanoğlu, M. Özkan, B. Güçlü, "Classification of somatosensory information from a robotic hand," *Frontiers in Neuroscience*, In Review.

Conference proceedings

- **Karakuş, I.**, E. Kaplanoğlu, M. Özkan, and B. Güçlü, "Characterization of a bend sensor for neuroprosthetic applications," in *Proceedings of Electric Electronics, Computer Science, Biomedical Engineerings' Meeting (EBBT)*, (Istanbul, Turkey), April 2017.
- **Karakuş, I.**, H. Şahin, A. Atasoy, E. Kaplanoğlu, M. Özkan, and B. Güçlü, "Evaluation of sensory feedback from a robotic hand: A preliminary study," in *EuroHaptics 2018: Haptics: Science, Technology, and Applications*, (Pisa, Italy), pp. 452-463, Springer, June 2018.

REFERENCES

1. Antfolk, C., M. D'Alonzo, B. Rosén, G. Lundborg, F. Sebelius, and C. Cipriani, "Sensory feedback in upper limb prosthetics," *Expert Review of Medical Devices*, Vol. 10, no. 1, pp. 45–54, 2013.
2. Biddiss, E., and T. Chau, "Upper-limb prosthetics: Critical factors in device abandonment," *American Journal of Physical Medicine and Rehabilitation*, Vol. 86, no. 12, pp. 977–987, 2007.
3. Carey, S. L., D. J. Lura, and M. J. Highsmith, "Differences in myoelectric and body-powered upper-limb prostheses: Systematic literature review," *Journal of Rehabilitation Research and Development*, Vol. 52, no. 3, pp. 247–262, 2015.
4. Dietrich, C., K. Walter-Walsh, S. Preißler, G. O. Hofmann, O. W. Witte, W. H. R. Miltner, and T. Weiss, "Sensory feedback prosthesis reduces phantom limb pain: Proof of principle," *Neuroscience Letters*, Vol. 507, no. 2, pp. 97–100, 2012.
5. Biddiss, E., D. Beaton, and T. Chau, "Consumer design priorities for upper limb prosthetics," *Disability and Rehabilitation: Assistive Technology*, Vol. 2, no. 6, pp. 346–357, 2007.
6. Raveh, E., S. Portnoy, and J. Friedman, "Adding vibrotactile feedback to a myoelectric-controlled hand improves performance when online visual feedback is disturbed," *Human Movement Science*, Vol. 58, pp. 32–40, 2018.
7. Raveh, E., J. Friedman, and S. Portnoy, "Evaluation of the effects of adding vibrotactile feedback to myoelectric prosthesis users on performance and visual attention in a dual-task paradigm," *Clinical Rehabilitation*, Vol. 32, no. 10, pp. 1308–1316, 2018.
8. Cuberovic, I., A. Gill, L. J. Resnik, D. J. Tyler, and E. L. Graczyk, "Learning of artificial sensation through long-term home use of a sensory-enabled prosthesis," *Frontiers in Neuroscience*, Vol. 13, no. 853, 2019.
9. Clemente, F., G. Valle, M. Controzzi, I. Strauss, F. Iberite, T. Stieglitz, G. Granata, P. M. Rossini, F. Petrini, S. Micera, and C. Cipriani, "Intraneural sensory feedback restores grip force control and motor coordination while using a prosthetic hand," *Journal of Neural Engineering*, Vol. 16, no. 2, 2019.
10. Shehata, A. W., M. Rehani, Z. E. Jassat, and J. S. Hebert, "Mechanotactile sensory feedback improves embodiment of a prosthetic hand during active use," *Frontiers in Neuroscience*, Vol. 14, no. 263, 2020.
11. *Vincent Evolution 2*, Vincent Systems. Available at: <https://vincentsystems.de/en/>. [Accessed: 26-May-2020].
12. Carrozza, M. C., G. Cappiello, S. Micera, B. B. Edin, L. Beccai, and C. Cipriani, "Design of a cybernetic hand for perception and action," *Biological Cybernetics*, Vol. 95, pp. 629–644, 2006.
13. Cipriani, C., M. Controzzi, and M. C. Carrozza, "The smarthand transradial prosthesis," *Journal of Neuroengineering and Rehabilitation*, Vol. 8, no. 29, 2011.

14. Resnik, L., S. L. Klinger, and K. Etter, "The deka arm: Its features, functionality, and evolution during the veterans affairs study to optimize the deka arm," *Prosthetics and Orthotics International*, Vol. 38, no. 6, pp. 492–504, 2014.
15. Controzzi, M., F. Clemente, D. Barone, A. Ghionzoli, and C. Cipriani, "The sssamyhand: a dexterous lightweight myoelectric hand prosthesis," *IEEE Transactions on Neural Systems and Rehabilitation Engineering*, Vol. 25, no. 5, pp. 459–468, 2016.
16. Controzzi, M., F. Clemente, D. Barone, L. B. Luciani, N. Pierotti, M. Bacchereti, and C. Cipriani, "Progress towards the development of the detop hand prosthesis: A sensorized transradial prosthesis for clinical use," in *Converging Clinical and Engineering Research on Neurorehabilitation III. ICNR 2018. Biosystems & Biorobotics* (Macia, L., S. Micera, M. Akay, and J. Pons, eds.), Vol. 21, pp. 103–106, Springer International Publishing, 2019.
17. Bach-y-Rita, P., and S. W. Kercel, "Sensory substitution and the human – machine interface," *Trends in Cognitive Sciences*, Vol. 7, no. 12, pp. 541–546, 2003.
18. Gonzalez, J., H. Soma, M. Sekine, and W. Yu, "Psycho-physiological assessment of a prosthetic hand sensory feedback system based on an auditory display: A preliminary study," *Journal of Neuroengineering and Rehabilitation*, Vol. 9, no. 33, 2012.
19. Kaczmarek, K. A., J. G. Webster, P. B. y Rita, and W. J. Tompkins, "Electrotactile and and vibrotactile displays for sensory substitution systems," *IEEE Transactions on Biomedical Engineering*, Vol. 38, no. 1, pp. 1–16, 1991.
20. Dhillon, G. S., and K. W. Horch, "Direct neural sensory feedback and control of a prosthetic arm," *IEEE Transactions on Neural Systems and Rehabilitation Engineering*, Vol. 13, no. 4, pp. 468–472, 2005.
21. Kim, S. S., A. P. Sripathi, R. J. Vogelstein, R. S. Armiger, A. F. Russell, and S. J. Bensmaia, "Conveying tactile feedback in sensorized hand neuroprostheses using a biofidelic model of mechanotransduction," *IEEE Transactions on Biomedical Circuits and Systems*, Vol. 3, no. 6, pp. 398–404, 2009.
22. Horch, K., S. Meek, T. G. Taylor, and D. T. Hutchinson, "Object discrimination with an artificial hand using electrical stimulation of peripheral tactile and proprioceptive pathways with intrafascicular electrodes," *IEEE Transactions on Neural Systems and Rehabilitation Engineering*, Vol. 19, no. 5, pp. 483–489, 2011.
23. Schiefer, M., D. Tan, S. M. Sidek, and D. J. Tyler, "Sensory feedback by peripheral nerve stimulation improves task performance in individuals with upper limb loss using a myoelectric prosthesis," *Journal of Neural Engineering*, Vol. 13, no. 1, 2016.
24. Oddo, C. M., S. Raspopovic, F. Artoni, A. Mazzoni, G. Spigler, F. Petrini, F. Giambattistelli, F. Vecchio, F. Miraglia, L. Zollo, G. D. Pino, D. Camboni, M. C. Carrozza, E. Guglielmelli, P. M. Rossini, U. Faraguna, and S. Micera, "Intraneural stimulation elicits discrimination of textural features by artificial fingertip in intact and amputee humans," *eLIFE Neuroscience*, Vol. 8, no. 5, 2016.
25. Schiefer, M. A., E. L. Graczyk, S. M. S. D. W. Tan, and D. J. Tyler, "Artificial tactile and proprioceptive feedback improves performance and confidence on object identification tasks," *PLoS ONE*, Vol. 13, no. 12, 2018.

26. D'Anna, E., G. Valle, A. Mazzoni, I. Strauss, F. Iberite, J. Patton, F. M. Petrini, S. Raspopovic, G. Granata, R. D. Iorio, M. Controzzi, C. Cipriani, T. Stieglitz, P. M. Rossini, and S. Micera, "A closed-loop hand prosthesis with simultaneous intraneural tactile and position feedback," *Science Robotics*, Vol. 4, no. 27, 2019.
27. Rohland, T. A., "Sensory feedback for powered limb prostheses," *Medical and Biological Engineering*, Vol. 13, no. 2, pp. 300–301, 1975.
28. Shannon, G. F., "A myoelectrically-controlled prosthesis with sensory feedback," *Medical & Biological Engineering & Computing*, Vol. 17, pp. 73–80, 1979.
29. Meek, S. G., S. C. Jacobsen, and P. P. Goulding, "Extended physiologic tactation: Design and evaluation of a proportional force feedback system," *Journal of Rehabilitation Research and Development*, Vol. 26, no. 3, pp. 53–62, 1989.
30. Antfolk, C., C. Balkenius, G. Lundborg, B. Rosen, and F. Sebelius, "Design and technical construction of a tactile display for sensory feedback in a hand prosthesis system," *BioMedical Engineering OnLine*, Vol. 9, no. 50, 2010.
31. Antfolk, C., A. Björkman, S.-O. Frank, F. Sebelius, G. Lundborg, and B. Rosén, "Sensory feedback from a prosthetic hand based on air-mediated pressure from the hand to the forearm skin," *Journal of Rehabilitation Medicine*, Vol. 44, no. 8, pp. 702–707, 2012.
32. Antfolk, C., M. D'Alonzo, M. Controzzi, G. Lundborg, B. Rosén, F. Sebelius, and C. Cipriani, "Artificial redirection of sensation from prosthetic fingers to the phantom hand map on transradial amputees: Vibrotactile versus mechanotactile sensory feedback," *IEEE Transactions on Neural Systems and Rehabilitation Engineering*, Vol. 21, no. 1, pp. 112–120, 2013.
33. Antfolk, C., C. Cipriani, M. C. Carrozza, C. Balkenius, A. Björkman, G. Lundborg, B. Rosén, and F. Sebelius, "Transfer of tactile input from an artificial hand to forearm: Experiments in amputee and able-bodied volunteers," *Disability and Rehabilitation: Assistive Technology*, Vol. 8, no. 3, pp. 249–254, 2013.
34. Witteveen, H. J. B., F. Luft, J. S. Rietman, and P. H. Veltink, "Stiffness feedback for myoelectric forearm prostheses using vibrotactile stimulation," *IEEE Transactions on Neural Systems and Rehabilitation Engineering*, Vol. 22, no. 1, pp. 53–61, 2014.
35. Clemente, F., M. D'Alonzo, M. Controzzi, B. B. Edin, and C. Cipriani, "Non-invasive, temporally discrete feedback of object contact and release improves grasp control of closed-loop myoelectric transradial prostheses," *IEEE Transactions on Neural Systems and Rehabilitation Engineering*, Vol. 24, no. 12, pp. 1314–1322, 2016.
36. Dosen, S., M. Markovic, M. Strbac, M. Belić, V. Kojić, G. Bijelić, T. Keller, and D. Farina, "Multichannel electrotactile feedback with spatial and mixed coding for closed-loop control of grasping force in hand prostheses," *IEEE Transactions on Neural Systems and Rehabilitation Engineering*, Vol. 25, no. 3, pp. 183–195, 2017.
37. Aboseria, M., F. Clemente, L. F. Engels, and C. Cipriani, "Discrete vibro-tactile feedback prevents object slippage in hand prostheses more intuitively than other modalities," *IEEE Transactions on Neural Systems and Rehabilitation Engineering*, Vol. 26, no. 8, pp. 1577–1584, 2018.
38. Svensson, P., U. Wijk, A. Björkman, and C. Antfolk, "A review of invasive and non-invasive sensory feedback in upper limb prostheses," *Expert Review of Medical Devices*, Vol. 14, no. 6, pp. 439–447, 2017.

39. Stephens-Fripp, B., G. Alici, and R. Mutlu, "A review of non-invasive sensory feedback methods for transradial prosthetic hands," *IEEE Access*, Vol. 6, pp. 6878–6899, 2018.
40. Dosen, S., M. Schaeffer, and D. Farina, "Time-division multiplexing for myoelectric closed-loop control using electrotactile feedback," *Journal of Neuroengineering and Rehabilitation*, Vol. 11, no. 138, 2014.
41. Patterson, P. E., and J. A. Katz, "Design and evaluation of a sensory feedback system that provides grasping pressure in a myoelectric hand," *Journal of Rehabilitation Research and Development*.
42. Poveda, A. R., "Myoelectric prostheses with sensorial feedback," in *2002 MyoElectric Controls/Powered Prosthetics Symposium*, (Fredericton, New Brunswick, Canada), August 2002.
43. Pylatiuk, C., A. Kargov, and S. Schulz, "Design and evaluation of a low-cost force feedback system for myoelectric prosthetic hands," *Journal of Prosthetics and Orthotics*, Vol. 18, no. 2, pp. 57–61, 2006.
44. Chatterjee, A., P. Chaubey, J. Martin, and N. Thakor, "Testing a prosthetic haptic feedback simulator with an interactive force matching task," *Journal of Prosthetics and Orthotics*, Vol. 20, no. 2, pp. 27–34, 2008.
45. Cipriani, C., F. Zaccone, S. Micera, and M. C. Carrozza, "On the shared control of an emg-controlled prosthetic hand: Analysis of user - prosthesis interaction," *IEEE Transactions on Robotics*, Vol. 24, no. 1, pp. 170–184, 2008.
46. Witteveen, H. J. B., E. A. Droog, J. S. Rietman, and P. H. Veltink, "Vibro- and electrotactile user feedback on hand opening for myoelectric forearm prostheses," *IEEE Transactions on Biomedical Engineering*, Vol. 59, no. 8, pp. 2219–2226, 2012.
47. Rombokas, E., C. E. Stepp, C. Chang, M. Malhotra, and Y. Matsuoka, "Vibrotactile sensory substitution for electromyographic control of object manipulation," *IEEE Transactions on Biomedical Engineering*, Vol. 60, no. 8, pp. 2226–2232, 2013.
48. Cipriani, C., J. L. Segil, F. Clemente, R. F. ff Weir, and B. Edin, "Humans can integrate feedback of discrete events in their sensorimotor control of a robotic hand," *Experimental Brain Research*, Vol. 232, no. 11, pp. 3421–3429, 2014.
49. Markovic, M., M. A. Schweisfurth, L. F. Engels, T. Bentz, D. WÄ¼stefeld, D. Farina, and S. Dosen, "The clinical relevance of advanced artificial feedback in the control of a multifunctional myoelectric prosthesis," *Journal of NeuroEngineering and Rehabilitation*, Vol. 15, no. 28, 2018.
50. Pena, A. E., L. Rincon-Gonzalez, J. J. Abbas, and R. Jung, "Effects of vibrotactile feedback and grasp interface compliance on perception and control of a sensorized myoelectric hand," *PLoS ONE*, Vol. 14, no. 1, pp. 1–21, 2019.
51. Engels, L. F., A. W. Shehata, E. J. Scheme, L. W. Sensinger, and C. Cipriani, "When less is more - discrete tactile feedback dominates continuous audio biofeedback in the integrated percept while controlling a myoelectric prosthetic hand," *Frontiers in Neuroscience*, Vol. 13, no. 578, 2019.

52. Choi, K., P. Kim, K. Kim, and S. Kim, "Mixed-modality stimulation to evoke two modalities simultaneously in one channel for electrocutaneous sensory feedback," *IEEE Transactions on Neural Systems and Rehabilitation Engineering*, Vol. 25, no. 12, pp. 2258–2269, 2017.
53. D'Alonzo, M., S. Dosen, C. Cipriani, and D. Farina, "Hyve — hybrid vibro-electrotactile stimulation — is an efficient approach to multi-channel sensory feedback," *IEEE Transactions on Haptics*, Vol. 7, no. 2, pp. 181–190, 2014.
54. Barone, D., M. D'Alonzo, M. Controzzi, F. Clemente, and C. Cipriani, "A cosmetic prosthetic digit with bioinspired embedded touch feedback," in *2017 International Conference on Rehabilitation Robotics (ICORR)*, (London, UK), pp. 1136–1141, July 2017.
55. Johansson, R. S., and B. B. Edin, "Predictive feed-forward sensory control during grasping and manipulation in man," *Biomedical Research*, Vol. 14, no. 4, pp. 95–106, 1993.
56. Flanagan, J. R., M. C. Bowman, and R. S. Johansson, "Control strategies in object manipulation tasks," *Current Opinion in Neurobiology*, Vol. 16, no. 6, pp. 650–659, 2006.
57. Johansson, R. S., and J. R. Flanagan, "Coding and use of tactile signals from the fingertips in object manipulation tasks," *Nature Reviews Neuroscience*, Vol. 10, no. 5, pp. 345–359, 2009.
58. Buma, D. G., J. R. Buitenweg, and P. H. Veltink, "Intermittent stimulation delays adaptation to electrocutaneous sensory feedback," *IEEE Transactions on Neural Systems and Rehabilitation Engineering*, Vol. 15, no. 3, pp. 435–441, 2007.
59. Pasluosta, C. F., H. Tims, and A. W. L. Chiu, "Slippage sensory feedback and nonlinear force control system for a low-cost prosthetic hand," *American Journal of Biomedical Sciences*, Vol. 1, no. 4, pp. 295–302, 2009.
60. Schweisfurth, M. A., M. Markovic, S. Dosen, F. Teich, B. Graimann, and D. Farina, "Electrotactile emg feedback improves the control of prosthesis grasping force," *Journal of Neural Engineering*, Vol. 13, no. 5, 2016.
61. Dosen, S., M. Markovic, K. Somer, B. Graimann, and D. Farina, "Emg biofeedback for online predictive control of grasping force in a myoelectric prosthesis," *Journal of Neuroengineering and Rehabilitation*, Vol. 12, no. 55, 2015.
62. Aziziaghdam, M., and E. Samur, "Providing contact sensory feedback for upper limb robotic prosthesis," in *2014 IEEE Haptics Symposium (HAPTICS)*, (Houston, TX), pp. 575–579, February 2014.
63. Aziziaghdam, M., and E. Samur, "Real-time contact sensory feedback for upper limb robotic prostheses," *IEEE/ASME Transactions on Mechatronics*, Vol. 22, no. 4, pp. 1786–1795, 2017.
64. Bandyopadhyaya, I., D. Babu, A. Kumar, and J. Roychowdhury, "Tactile sensing based softness classification using machine learning," in *2014 IEEE International Advance Computing Conference (IACC)*, (Gurgaon, India), pp. 1231–1236, February 2014.
65. Schmitz, A., Y. Bansho, K. Noda, H. Iwata, T. Ogata, and S. Sugano, "Tactile object recognition using deep learning and dropout," in *2014 IEEE-RAS International Conference on Humanoid Robots*, (Madrid, Spain), pp. 1044–1050, November 2014.

66. Spiers, A. J., M. V. Liarokapis, B. Calli, and A. M. Dollar, "Single-grasp object classification and feature extraction with simple robot hands and tactile sensors," *IEEE Transactions on Haptics*, Vol. 9, no. 2, pp. 207–220, 2016.
67. Su, Z., J. A. Fishel, T. Yamamoto, and G. E. Loeb, "Use of tactile feedback to control exploratory movements to characterize object compliance," *Frontiers in Neurobotics*, Vol. 6, no. 7, 2012.
68. Chitta, S., M. Piccoli, and J. Sturm, "Tactile object class and internal state recognition for mobile manipulation," in *2010 IEEE International Conference on Robotics and Automation*, (Anchorage, Alaska, USA), pp. 2342–2348, May 2010.
69. Fishel, J. A., and G. E. Loeb, "Bayesian exploration for intelligent identification of textures," *Frontiers in Neurobotics*, Vol. 6, no. 4, 2006.
70. Chu, V., I. McMahon, L. Riano, C. G. McDonald, Q. He, J. M. Perez-Tejada, M. Arrigo, N. Fitter, J. C. Nappo, T. Darrell, and K. J. Kuchenbecker, "Using robotic exploratory procedures to learn the meaning of haptic adjectives," in *2013 IEEE International Conference on Robotics and Automation*, (Karlsruhe, Germany), pp. 3048–3055, May 2013.
71. Edwards, A. L., M. R. Dawson, J. S. Hebert, C. Sherstan, R. S. Sutton, K. M. Chan, and P. M. Pilarski, "Application of real-time machine learning to myoelectric prosthesis control: A case series in adaptive switching," *Prosthetics and Orthotics International*, Vol. 40, no. 5, pp. 573–581, 2016.
72. Parker, A. S. R., A. L. Edwards, and P. M. Pilarski, "Exploring the impact of machine-learned predictions on feedback from an artificial limb," in *2019 IEEE 16th International Conference on Rehabilitation Robotics (ICORR)*, (Toronto, Canada), pp. 1239–1246, June 2019.
73. Murray, A. M., R. L. Klatzky, and P. K. Khosia, "Psychophysical characterization and testbed validation of a wearable vibrotactile glove for telemanipulation," *Presence*, Vol. 12, no. 2, pp. 156–182, 2003.
74. Geng, B., K. Yoshida, and W. Jensen, "Impacts of selected stimulation patterns on the perception threshold in electrocutaneous stimulation," *Journal of NeuroEngineering and Rehabilitation*, Vol. 8, no. 9, 2011.
75. Geng, B., J. Dong, W. Jensen, S. Dosen, D. Farina, and E. N. Kamavuako, "Psychophysical evaluation of subdermal electrical stimulation in relation to prosthesis sensory feedback," *IEEE Transactions on Neural Systems and Rehabilitation Engineering*, Vol. 26, no. 3, pp. 709–715, 2018.
76. Wilke, M. A., C. Niethammer, B. Meyer, D. Farina, and S. Dosen, "Psychometric characterization of incidental feedback sources during grasping with a hand prosthesis," *Journal of NeuroEngineering and Rehabilitation*, Vol. 16, no. 155, 2019.
77. Stephens-Fripp, B., R. Mutlu, and G. Alici, "A comparison of recognition and sensitivity in the upper arm and lower arm to mechanotactile stimulation," *IEEE Transactions on Medical Robotics and Bionics*, Vol. 2, no. 1, pp. 76–85, 2020.
78. Dong, J., B. Geng, I. K. Niazi, I. Amjad, S. Dosen, W. Jensen, and E. N. Kamavuako, "The variability of psychophysical parameters following surface and subdermal stimulation: A multiday study in amputees," *IEEE Transactions on Neural Systems and Rehabilitation Engineering*, Vol. 28, no. 1, pp. 174–180, 2020.

79. Karakuş, I., H. Şahin, A. Atasoy, E. Kaplanoğlu, M. Özkan, and B. Güçlü, "Evaluation of sensory feedback from a robotic hand: A preliminary study," in *Haptics: Science, Technology, and Applications. EuroHaptics 2018. Lecture Notes in Computer Science* (Prattichizzo, D., H. Shinoda, H. Tan, E. Ruffaldi, and A. Frisoli, eds.), (Pisa, Italy), pp. 452–463, Springer, June 2018.
80. Karakuş, I., and B. Güçlü, "Psychophysical principles of discrete event-driven vibrotactile feedback for prostheses," *Somatosensory and Motor Research*, Vol. Published online, 2020.
81. Güçlü, B., and S. J. Bolanowski, "Vibrotactile thresholds of the non-pacini channel: I. methodological issues," *Somatosensory & Motor Research*, Vol. 22, no. 1, pp. 49–56, 2005.
82. Güçlü, B., and Ç. Öztekin, "Tactile sensitivity of children : Effects of frequency , masking , and the non-pacini channel," *Journal of Experimental Child Psychology*, Vol. 98, no. 2, pp. 113–130, 2007.
83. Güçlü, B., "Deviation from weber's law in the non-pacini channel: A psychophysical and simulation study of intensity discrimination," *Neural Computation*, Vol. 19, no. 10, pp. 2638–2664, 2007.
84. Mikkelsen, M., J. He, M. Tommerdahl, R. A. E. Edden, S. H. Mostofsky, and N. A. J. Puts, "Reproducibility of flutter-range vibrotactile detection and discrimination thresholds," *Scientific Reports*, Vol. 10, no. 6528, 2020.
85. *Psychophysics: The Fundamentals*, Lawrence Erlbaum Associates, Mahwah, NJ, USA, 3rd ed., 1997.
86. Güçlü, B., and Ş. M. Dinçer, "Neural coding in the non-pacini channel: A psychophysical and simulation study of magnitude estimation," *Somatosensory & Motor Research*, Vol. 30, no. 1, pp. 1–15, 2013.
87. Verrillo, R. T., "Comparison of vibrotactile threshold and suprathreshold responses in men and women," *Perception & Psychophysics*, Vol. 26, no. 1, pp. 20–24, 1979.
88. Bernstein, L. E., M. B. Schechter, and J. M. H. Goldstein, "Child and adult vibrotactile thresholds for sinusoidal and pulsatile stimuli," *Journal of the Acoustical Society of America*, Vol. 80, no. 1, pp. 118–123, 1986.
89. Verrillo, R. T., and J. S. J. Bolanowski, "The effects of skin temperature on the psychophysical responses to vibration on glabrous and hairy skin," *The Journal of the Acoustical Society of America*, Vol. 80, no. 2, pp. 528–532, 1986.
90. Gescheider, G. A., S. J. Bolanowski, K. L. Hall, K. E. Hoffman, and R. T. Verrillo, "The effects of aging on information-processing channels in the sense of touch : I . absolute sensitivity," *Somatosensory & Motor Research*, Vol. 11, no. 4, pp. 345–357, 1994.
91. Yıldız, M. Z., and B. Güçlü, "Relationship between vibrotactile detection threshold in the pacini channel and complex mechanical modulus of the human glabrous skin," *Somatosensory & Motor Research*, Vol. 30, no. 1, pp. 37–47, 2013.
92. Maw, J., K. Y. Wong, and P. Gillespie, "Hand anatomy," *British Journal of Hospital Medicine*, Vol. 77, no. 3, pp. C34–3–C38–40, 2016.

93. Taylor, C. L., and R. J. Schwarz, "The anatomy and mechanics of the human hand," *Artificial Limbs*, Vol. 2, no. 2, pp. 22–35, 1955.
94. Schreuders, T. A. R., J. W. Brandsma, and H. J. Stam, "Functional anatomy and biomechanics of the hand, perceptual, and cognitive changes," in *Hand Function: A Practical Guide to Assessment* (Duruöz, M. T., ed.), ch. 1, pp. 3–22, Springer New York: Springer New York, 2014.
95. Kandel, E. R., J. H. Schwartz, T. M. Jessell, S. A. Siegelbaum, and A. J. Hudspeth, eds., *Principles of Neural Science*, McGraw-Hill, 5th ed., 2013.
96. Blausen, "Medical gallery of blausen medical 2014," *WikiJournal of Medicine*, Vol. 1, no. 2, 2014.
97. Kandel, E. R., J. H. Schwartz, and T. M. Jessell, eds., *Principles of Neural Science*, McGraw-Hill, 4th ed., 2000.
98. Alpaydm, E., *Introduction to Machine Learning*, MIT Press, 3rd ed., 2014.
99. Bishop, C., *Pattern Recognition and Machine Learning*, Springer-Verlag New Yorks, 1st ed., 2006.
100. Stuart Russell, P. N., *Artificial Intelligence : A Modern Approach*, Prentice Hall, 3rd ed., 2010.
101. Atasoy, A., E. Kaya, E. Toptas, S. Kuchimov, E. Kaplanoglu, and M. Ozkan, "24 dof emg controlled hybrid actuated prosthetic hand," in *38th Annual International Conference of the IEEE Engineering in Medicine and Biology Society (EMBC)*, (Orlando, FL), pp. 5059–5062, August 2016.
102. Saudabayev, A., and H. A. Varol, "Sensors for robotic hands: A survey of state of the art," *IEEE Access*, Vol. 3, pp. 1765–1782, 2015.
103. Martin, J., S. Beck, A. Lehmann, R. Mikut, C. Pylatiuk, S. Schulz, and G. Bretthauer, "Sensors, identification, and low level control of a flexible anthropomorphic robot hand," *International Journal of Humanoid Robotics*, Vol. 1, no. 3, pp. 517–532, 2004.
104. Borghetti, M., E. Sardini, and M. Serpelloni, "Sensorized glove for measuring hand finger flexion for rehabilitation purposes," *IEEE Transactions on Instrumentation and Measurement*, Vol. 62, no. 12, pp. 3308–3314, 2013.
105. Gücüyener, A., and E. Kaplanoğlu, "Wireless hand rehabilitation system (whrs)," *Balkan Journal of Electrical & Computer Engineering*, Vol. 5, no. 1, pp. 9–13, 2017.
106. Karakuş, I., E. Kaplanoğlu, M. Özkan, and B. Güçlü, "Characterization of a bend sensor for neuroprosthetic applications," in *2017 Electric Electronics, Computer Science, Biomedical Engineerings' Meeting (EBBT)*, (Istanbul, Turkey), April 2017.
107. Castro, M. C. F., and A. J. Cliquet, "A low-cost instrumented glove for monitoring forces during object manipulation," *IEEE Transactions on Rehabilitation Engineering*, Vol. 5, no. 2, pp. 140–147, 1997.
108. Hall, R. S., G. T. Desmoulin, and T. E. Milner, "A technique for conditioning and calibrating force-sensing resistors for repeatable and reliable measurement of compressive force," *Journal of Biomechanics*, Vol. 41, no. 16, pp. 3492–3495, 2008.

109. Cutkosky, M. R., "On grasp choice, grasp models, and the design of hands for manufacturing tasks," *IEEE Transactions on Robotics and Automation*, Vol. 5, no. 3, pp. 269–279, 1989.
110. Feix, T., J. Romero, H.-B. Schmiebmayer, A. M. Dollar, and D. Kragic, "The grasp taxonomy of human grasp types," *IEEE Transactions on Human-Machine Systems*, Vol. 46, no. 1, pp. 66–77, 2016.
111. Berg, J. A., J. F. 3rd Dammann, F. V. Tenore, G. A. Tabot, J. L. Boback, L. R. Manfredi, M. L. Peterson, K. D. Katyal, M. S. Johannes, A. Makhlin, R. Wilcox, R. K. Franklin, R. J. Vogelstein, N. G. Hatsopoulos, and S. J. Bensmaia, "Behavioral demonstration of a somatosensory neuroprosthesis," *IEEE Transactions on Neural Systems and Rehabilitation Engineering*, Vol. 21, no. 3, pp. 500–507, 2013.
112. Resnik, L., F. Acluche, M. Borgia, J. Cancio, G. Latlief, and N. Sasson, "Function, quality of life, and community integration of deka arm users after discharge from prosthetic training: Impact of home use experience," *Prosthetics and Orthotics International*, Vol. 42, no. 6, pp. 571–582, 2018.
113. Güçlü, B., and S. J. Bolanowski, "Tristate markov model for the firing statistics of rapidly-adapting mechanoreceptive fibers," *Journal of Computational Neuroscience*, Vol. 17, pp. 107–126, 2004.
114. Güçlü, B., E. A. Schepis, S. Yelke, C. A. Yucesoy, and S. J. Bolanowski, "Ovoid geometry of the pacinian corpuscle is not the determining factor for mechanical excitation," *Somatosensory & Motor Research*, Vol. 23, no. 3-4, pp. 119–126, 2006.
115. Güçlü, B., G. K. Mahoney, L. J. Pawson, A. K. Pack, R. L. Smith, and S. J. Bolanowski, "Localization of merkel cells in the monkey skin: An anatomical model," *Somatosensory & Motor Research*, Vol. 25, no. 2, pp. 123–138, 2008.
116. Greenspan, J. D., and S. J. Bolanowski, *The psychophysics of tactile perception and its peripheral physiological basis*, pp. 25–103. Academic Press, 1996.
117. Bear, M. F., B. W. Connors, and M. A. Paradiso, *Neuroscience : Exploring the Brain*, Lippincott Williams and Wilkins, 3rd ed., 2007.
118. Vallbo, A. B., and R. S. Johansson, "The tactile sensory innervation of the glabrous skin of the human hand," in *Active Touch* (Gordon, G., ed.), pp. 29–54, Oxford: Oxford:Pergamon Press, 1978.
119. Zwislocki, J. J., and E. M. Relkin, "On a psychophysical transformed-rule up and down method converging on a 75 % level of correct responses," *Proceedings of the National Academy of Sciences of the United States of America*, Vol. 98, no. 8, pp. 4811–4814, 2001.
120. Verrillo, R. T., "Effect of contactor area on the vibrotactile threshold," *The Journal of the Acoustical Society of America*, Vol. 35, no. 12, pp. 1962–1966, 1963.
121. Verrillo, R. T., "Effect of spatial parameters on the vibrotactile threshold," *Journal of Experimental Psychology*, Vol. 71, no. 4, pp. 570–575, 1966.
122. Verrillo, R. T., "Vibrotactile thresholds measured at the finger," *Perception & Psychophysics*, Vol. 9, no. 4, pp. 329–330, 1971.

123. Frisina, R. D., and G. A. Gescheider, "Comparison of child and adult vibrotactile thresholds as a function of frequency and duration," *Perception & Psychophysics*, Vol. 22, no. 1, pp. 100–103, 1977.
124. Bolanowski, S. J., G. A. Gescheider, R. T. Verrillo, and C. M. Checkosky, "Four channels mediate the mechanical aspects of touch," *The Journal of the Acoustical Society of America*, Vol. 84, no. 5, pp. 1680–1694, 1988.
125. Gescheider, G. A., S. J. Bolanowski, and R. T. Verrillo, "Some characteristics of tactile channels," *Behavioural Brain Research*, Vol. 148, no. 1-2, pp. 35–40, 2004.
126. Gescheider, G. A., J. H. Wright, and R. T. Verrillo, *Information-processing Channels in the Tactile Sensory System : A Psychophysical and Physiological Analysis*, Taylor and Francis Group, 2010.
127. Gescheider, G. A., S. J. Bolanowski, and K. R. Hardick, "The frequency selectivity of information-processing channels in the tactile sensory system," *Somatosensory & Motor Research*, Vol. 18, no. 3, pp. 191–201, 2001.
128. Gescheider, G. A., S. J. Bolanowski, J. V. Pope, and R. T. Verrillo, "A four-channel analysis of the tactile sensitivity of the fingertip : Frequency selectivity , spatial summation , and temporal summation," *Somatosensory & Motor Research*, Vol. 19, no. 2, pp. 114–124, 2002.
129. Verrillo, R. T., "Vibrotactile thresholds for hairy skin," *Journal of Experimental Psychology*, Vol. 72, no. 1, pp. 47–50, 1966.
130. Bolanowski, S. J., G. A. Gescheider, and R. T. Verrillo, "Hairy skin : Psychophysical channels and their physiological substrates," *Somatosensory & Motor Research*, Vol. 11, no. 3, pp. 279–290, 1994.
131. Schlereth, T., W. Magerl, and R.-D. Treede, "Spatial discrimination thresholds for pain and touch in human hairy skin," *Pain*, Vol. 92, no. 1-2, pp. 187–194, 2001.
132. Verrillo, R. T., "Psychophysics of vibrotactile stimulation," *The Journal of the Acoustical Society of America*, Vol. 77, no. 1, pp. 225–232, 1985.
133. Makous, J. C., G. A. Gescheider, and S. J. Bolanowski, "The effects of static indentation on vibrotactile threshold," *The Journal of the Acoustical Society of America*, Vol. 99, no. 5, pp. 3149–3153, 1996.
134. Gescheider, G. A., B. Güçlü, J. L. Sexton, S. Karalunas, and A. Fontana, "Spatial summation in the tactile sensory system: Probability summation and neural integration," *Somatosensory & Motor Research*, Vol. 22, no. 4, pp. 255–268, 2005.
135. Verrillo, R. T., "Temporal summation in vibrotactile sensitivity," *The Journal of the Acoustical Society of America*, Vol. 37, no. 5, pp. 843–846, 1965.
136. Verrillo, R. T., and G. A. Gescheider, "Enhancement and summation in the perception of two successive vibrotactile stimuli," *Perception & Psychophysics*, Vol. 18, no. 2, pp. 128–136, 1975.
137. Gescheider, G. A., and N. Migel, "The journal of the acoustical society of america," *Some temporal parameters in vibrotactile forward masking*, Vol. 98, no. 6, pp. 3195–3199, 1995.

138. Craig, J. C., “The role of onset in the perception of sequentially presented vibrotactile patterns,” *Perception & Psychophysics*, Vol. 34, no. 5, pp. 421–432, 1983.
139. Cholewiak, R. W., and J. C. Craig, “Vibrotactile pattern recognition and discrimination at several body sites,” *Perception & Psychophysics*, Vol. 35, no. 6, pp. 53–514, 1984.
140. Cholewiak, R. W., and A. A. Collins, “Vibrotactile pattern discrimination and communality at several body sites,” *Perception & Psychophysics*, Vol. 57, no. 5, pp. 724–737, 1995.
141. Mahns, D. A., N. M. Perkins, V. Sahai, L. Robinson, and M. J. Rowe, “Vibrotactile frequency discrimination in human hairy skin,” *Journal of Neurophysiology*, Vol. 95, no. 3, pp. 1442–1450, 2006.
142. Yıldız, M. Z., I. Toker, F. B. Özkan, and B. Güçlü, “Effects of passive and active movement on vibrotactile detection thresholds of the pacinian channel and forward masking,” *Somatosensory & Motor Research*, Vol. 32, no. 4, pp. 262–272, 2015.
143. Schofield, J. S., C. E. Shell, D. T. Beckler, Z. C. Thumser, and P. D. Marasco, “Long-term home-use of sensory-motor-integrated bidirectional bionic prosthetic arms promotes functional, perceptual, and cognitive changes,” *Frontiers in Neuroscience*, Vol. 14, no. 120, 2020.
144. Bark, K., E. Hyman, F. Tan, E. Cha, S. A. Jax, L. J. Buxbaum, and K. J. Kuchenbecker, “Effects of vibrotactile feedback on human learning of arm motions,” *IEEE Transactions on Neural Systems and Rehabilitation Engineering*, Vol. 23, no. 1, pp. 51–63, 2015.
145. Rajanna, V., P. Vo, J. Barth, M. Mjelde, T. Grey, C. Oduola, and T. Hammond, “Kinohaptics: An automated, wearable, haptic assisted, physio-therapeutic system for post-surgery rehabilitation and self-care,” *Journal of Medical Systems*, Vol. 40, no. 3, 2016.
146. Flores, G., S. Kurniawan, R. Manduchi, E. Martinson, L. Morales, and E. A. Sisbot, “Vibrotactile guidance for wayfinding of blind walkers,” *IEEE Transactions on Haptics*, Vol. 8, no. 3, pp. 306–317, 2015.
147. Szewczyk, T. H. J., “Improving precision in navigating laparoscopic surgery instruments toward a planar target using haptic and visual feedback,” *Frontiers in Robotics and AI*, Vol. 3, no. 37, 2016.
148. Abiri, A., Y.-Y. Juo, A. Tao, S. J. Askari, J. Pensa, J. W. Bisley, E. P. Datson, and W. S. Grundfest, “Artificial palpation in robotic surgery using haptic feedback,” *Surgical Endoscopy*, Vol. 33, no. 4, pp. 1252–1259, 2019.
149. Kapur, P., M. Jensen, L. J. Buxbaum, S. A. Jax, and K. J. Kuchenbecker, “Spatially distributed tactile feedback for kinesthetic motion guidance,” in *2010 IEEE Haptics Symposium*, (Waltham, MA, USA), pp. 519–526, March 2010.
150. Shionoiri, H., R. Sakuragi, R. Kodama, and H. Kajimoto, “Vibrotactile feedback to combine with swing presentation for virtual reality applications,” in *Haptics: Science, Technology, and Applications. EuroHaptics 2018. Lecture Notes in Computer Science* (Prattichizzo, D., H. Shinoda, H. Tan, E. Ruffaldi, and A. Frisoli, eds.), (Pisa, Italy), pp. 114–124, Springer, June 2018.
151. Maereg, A. T., A. Nagar, D. Reid, and E. L. Secco, “Wearable vibrotactile haptic device for stiffness discrimination during virtual interactions,” *Frontiers in Robotics and AI*, Vol. 4, no. 42, 2017.